LBNL-6930E

ECO2N V2.0: A TOUGH2 Fluid Property Module for Mixtures of Water, NaCl, and CO_2

Lehua Pan, Nicolas Spycher, Christine Doughty, and Karsten Pruess

Earth Sciences Division, Lawrence Berkeley National Laboratory
University of California, Berkeley, CA 94720

February 2015

This work was partly supported by TOUGH Royalty fund, the Director, Office of Science, Office of Basic Energy Sciences of the U.S. Department of Energy and by the Zero Emission Research and Technology project (ZERT) under Contract No. DE-AC03-76SF00098, and the Assistant Secretary for Energy Efficiency and Renewable Energy, Geothermal Technologies Program of the U.S. Department of Energy under Contract No. DE-AC02-05CH11231.

Summary

ECO2N V2.0 is a fluid property module for the TOUGH2 simulator (Version 2.1) that was designed for applications to geologic sequestration of CO_2 in saline aquifers and enhanced geothermal reservoirs. ECO2N V2.0 is an enhanced version of the previous ECO2N V1.0 module (Pruess, 2005). It expands the temperature range up to about 300^{o}C whereas V1.0 can only be used for temperatures below about 110^{o}C. V2.0 includes a comprehensive description of the thermodynamic and thermophysical properties of H_2O - NaCl - CO_2 mixtures, that reproduces fluid properties largely within experimental error for the temperature, pressure and salinity conditions 10 °C < T < 300 °C, P < 600 bar, and salinity up to halite saturation. This includes density, viscosity, and specific enthalpy of fluid phases as functions of temperature, pressure, and composition, as well as partitioning of mass components H_2O, NaCl and CO_2 among the different phases. In particular, V2.0 accounts for the effects of water on the thermophysical properties of the CO_2-rich phase, which was ignored in V1.0, using a model consistent with the solubility models developed by Spycher and Pruess (2005, 2010). In terms of solubility models, V2.0 uses the same model for partitioning of mass components among the different phases (Spycher and Pruess, 2005) as V1.0 for the low temperature range (<99^{o}C) but uses a new model (Spycher and Pruess, 2010) for the high temperature range (>109^{o}C). In the transition range (99-109^{o}C), a smooth interpolation is applied to estimate the partitioning as a function of the temperature. Flow processes can be modeled isothermally or non-isothermally, and phase conditions represented may include a single (aqueous or CO_2-rich) phase, as well as two-phase (brine-CO_2) mixtures. Fluid phases may appear or disappear in the course of a simulation, and solid salt may precipitate or dissolve. Note that the model cannot be applied to subcritical conditions that involves both liquid and gaseous CO_2 unless thermol process is ignored (i.e.,isothermal run). For those cases, a user may use the fluid property module ECO2M (Pruess, 2011) instead.

This report gives technical specifications of ECO2N V2.0 and includes instructions for preparing input data.

Table of Contents

1. Introduction

ECO2N V2.0 is a fluid property module for the general-purpose reservoir simulator TOUGH2 (Version 2.1) (Pruess et al., 2012; Pruess, 2004) that was designed for applications to geologic sequestration of CO_2 in saline aquifers and enhanced geothermal reservoirs. In geothermal reservoirs and many potential CO_2 storage sites, the temperature could well be beyond 110^{o}C (the upper limit implemented in the earlier fluid module ECO2N V1.0). ECO2N V2.0 is an enhanced version of ECO2N V1.0 that inherits all the capabilities of ECO2N V1.0 and expands the applicable temperature range up to about 300^{o}C by incorporating the newly developed mutual dissolution correlations for higher temperature of Spycher and Pruess (2010). The fluid property module can be used to model non-isothermal multiphase flow in the system H_2O – NaCl – CO_2. TOUGH2/ECO2N V2.0 represents fluids as consisting of two phases: a water-rich aqueous phase, hereafter referred to as "liquid," and a CO_2-rich phase, hereafter referred to as "gas." In addition, solid salt may also be present. The only chemical reactions modeled by ECO2N V2.0 are equilibrium phase partitioning of water and carbon dioxide between the liquid and gaseous phases, and precipitation and dissolution of solid salt. The partitioning of H_2O and CO_2 between liquid and gas phases is modeled as a function of temperature, pressure, and salinity, using the recently developed correlations of Spycher and Pruess (2005, 2010). Dissolution and precipitation of salt is treated by means of local equilibrium solubility. Associated changes in fluid porosity and permeability may also be modeled. All phases - gas, liquid, solid - may appear or disappear in any grid block during the course of a simulation. Thermodynamic conditions covered include a temperature range from about 10 to 300 °C (approximately), pressures up to 600 bar, and salinity up to NaCl (halite) saturation. Note that the model cannot be applied to subcritical conditions that involves both liquid and gaseous CO_2 unless thermol process is ignored (i.e.,isothermal run). For those cases, a user may use the fluid property module ECO2M (Pruess, 2011) instead.

ECO2N V2.0 is written in Fortran 77 and is "plug-compatible" with TOUGH2, Version 2.1[1].

The source code files[1] are CO2Proper_new.f, CO2Proper_old.f, and ECO2N_V20.f. The following compiler options are required: real*8, integer*4, an no array bound checking.

---

[1] The code for the more accurate effective thermal conductivity models that accounts for the effects of CO2 saturation, salt content, etc. (thcondsubs.f90) is written following Fortran 90 standard. Although it is included in the distribution package, it is actually not a part of ECO2N. The interested users should compile it with TOUGH2 core code following the instructions in Appendix D.

As an example, we list the linking instruction that would be used on a typical Linux/Unix system using Intel Fortran.

```
ifort -o xco2n t2cg22.o meshm.o ECO2N_V20.o CO2Property_new.o CO2Property_old.o t2f.o t2solv.o ma28.o
```

Execution of TOUGH2 with an input file “rcc3.inp” to create an output file “rcc3.out” would be made with the command

```
xco2n <rcc3.inp >rcc3.out
```

The file CO2TAB need to be copied to the working directory when run TOUGH2/ECO2N V2.0 since this file contains the PVT data of pure CO_2 within the proper ranges of pressure and temperature. If the user had CO2TAB come with previous version of ECO2N, he or she should replace it with the new one come with ECO2N V2.0.

The present report is a user's guide for the TOUGH2/ECO2N V2.0 simulator. Information provided in the TOUGH2 users' guide (Pruess et al., 2012) is not duplicated here. In order to make this report self-contained, however, we include much of the material that was covered in the earlier ECO2N V1.0 user’s guide (Pruess, 2005). We begin with a discussion of phase conditions and thermodynamic variables in the system H_2O – NaCl – CO_2. This is followed by a discussion of our thermophysical property model, and guidance for preparing input data. Several sample problems are provided which document code performance and serve as a tutorial for applications.

2. Fluid Phases and Thermodynamic Variables in the System of Water-NaCl-CO_2

In the two-component system water-CO_2, at temperatures above the freezing point of water and not considering hydrate phases, three different fluid phases may be present: an aqueous phase that is mostly water but may contain some dissolved CO_2, a liquid CO_2-rich phase that may contain some water, and a gaseous CO_2-rich phase that also may contain some water. Altogether there may be seven different phase combinations (Fig. 2.1). If NaCl ("salt") is added as a third fluid component, the number of possible phase combinations doubles, because in each of the seven phase combinations depicted in Fig. 2.1 there may or may not be an additional phase consisting of solid salt. Liquid and gaseous CO_2 may coexist along the saturated vapor pressure curve of CO_2, which ends at the critical point (T_{crit}, P_{crit}) = (30.978°C and 73.773 bar, Span and Wagner, 1996; 31.06°C and 73.825 bar, Angus et al., 1976; 31.04 ˚C, 73.82 bar, Vargaftik, 1975). In calculation of thermophysical properties of pure CO_2, ECO2N uses the critical point as suggested by Vargaftik (1975), see Fig. 2.2. Above supercritical temperatures or pressures, there is just a single CO_2-rich phase.

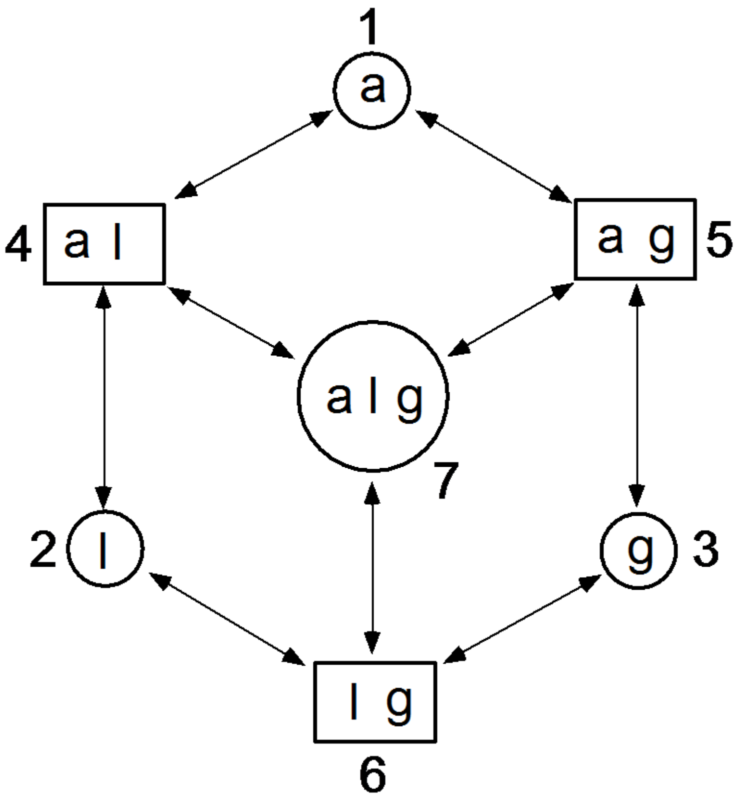

Figure 2.1. Possible phase combinations in the system water-CO_2. The phase designations are a - aqueous, l - liquid CO_2, g - gaseous CO_2. Separate liquid and gas phases exist only at subcritical conditions. ECO2N V2.0 can represent conditions 1, 2 (or 3), and 4 (or 5) but not 6 nor 7.

It should be noted that in this report we refer to “subcritical” and “supercritical” conditions in reference to pure CO_2. Technically, the CO_2-H_2O system remains subcritical below the critical curve for this system, which is located at much higher temperatures and pressures (e.g., P > 500 bar at 300°C, Takenouchi and Kennedy, 1964) than the critical point for pure CO_2. However, because the three-phase line and its critical end point for the CO_2-H_2O system lies very close to the two-phase (vapor saturation) curve for pure CO_2 (Wendland et al., 1999), it is most practical to refer to “subcritical” and “supercritical” conditions in reference to pure CO_2 (Figure 2.2).Like ECO2N V1.0, the present version of ECO2N V2.0 can only represent a limited subset of the phase conditions depicted in Fig. 2.1. Thermophysical properties are accurately calculated for gaseous as well as for liquid CO_2, but no distinction between gaseous and liquid CO_2 phases is made in the treatment of flow, and no phase change between liquid and gaseous CO_2 is treated. Accordingly, of the seven phase combinations shown in Fig. 2.1, ECO2N V2.0 can represent the ones numbered 1 (single-phase aqueous with or without dissolved CO_2 and salt), 2 and 3 (a single CO_2-rich phase that may be either liquid or gaseous CO_2, and may include dissolved water), and 4 and 5 (two-phase conditions consisting of an aqueous and a single CO_2-rich phase, with no distinction being made as to whether the CO_2-rich phase is liquid or gas). ECO2N V2.0 cannot represent conditions 6 (two-phase mixture of liquid and gaseous CO_2) and 7 (three-phase conditions). All sub- and super-critical CO_2 is considered as a single non-wetting phase that will henceforth be referred to as "gas." ECO2N V2.0 may be applied to sub- as well as super-critical temperature and pressure conditions, but applications that involve subcritical conditions are limited to systems in which there is no change of phase between liquid and gaseous CO_2, and in which no mixtures of liquid and gaseous CO_2 coexist. For those cases, a user may use the fluid property module ECO2M (Pruess, 2011) instead.

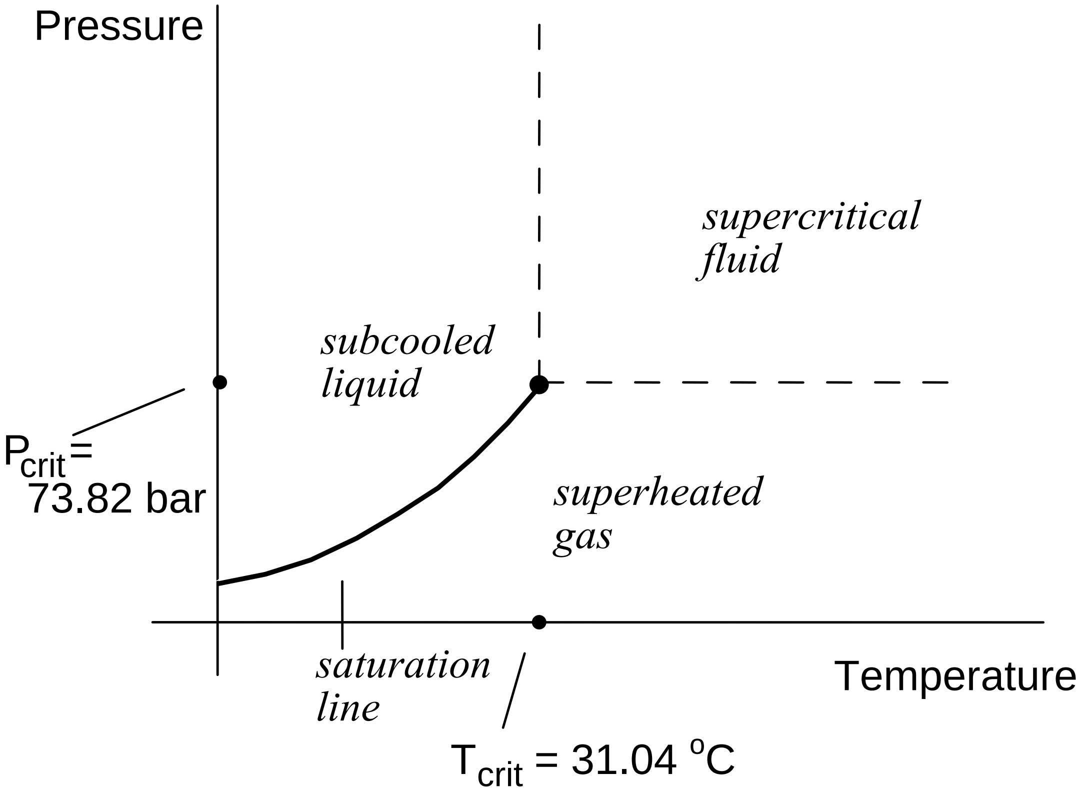

Figure 2.2. Phase states of pure CO_2.

In the numerical simulation of brine-CO_2 flows, we will be concerned with the fundamental thermodynamic variables that characterize the brine-CO_2 system, and their change with time in different subdomains (grid blocks) of the flow system. Four "primary variables" are required to define the state of water-NaCl-CO_2 mixtures, which according to conventional TOUGH2 usage are denoted by X1, X2, X3, and X4. A summary of the fluid components and phases modeled by ECO2N V2.0, and the choice of primary thermodynamic variables, appears in Table 2.1. Different variables are used for different phase conditions, but two of the four primary variables are the same, regardless of the number and nature of phases present. This includes the first primary variable X1, denoting pressure, and the fourth primary variable X4, which is temperature. The second primary variable pertains to NaCl salt and is denoted X_{sm}. Depending upon whether or not a precipitated NaCl salt phase is present, the variable X_{sm} has different meanings. When no solid NaCl salt is present, X_{sm} denotes X_s, the salt mass fraction defined on the basis of the two-component system water and dissolved NaCl salt. When solid salt is present, X_s is no longer an independent variable, as it is determined by the equilibrium solubility of NaCl, which is primarily a function of temperature (the pressure effect can be neglected). In the presence of solid salt, for reasons that are explained below, we use as second primary variable the quantity "solid saturation plus ten," $X_{sm} = S_s + 10$. Here, S_s is defined in analogy to fluid saturations and denotes the fraction of void space occupied by solid salt. The physical range of both X_s and S_s is (0, 1); the reason for defining X_{sm} by adding a number 10 to S_s is to enable the presence or absence of solid salt to be recognized simply from the numerical value of the second primary variable. As had been mentioned above, the salt concentration variable X_s is defined with respect to the two-component system H_2O – NaCl (i.e., on a CO_2-free basis). This choice makes the salt concentration variable independent of CO_2 concentration, which simplifies the calculation of the partitioning of the H_2O and CO_2 components between the aqueous and gas phases (see below). In the three-component system H_2O - NaCl - CO_2, the true NaCl mass fraction in the aqueous phase is also a function of CO_2 concentration. Therefore, the dissolved NaCl mass fraction X_s (expressed on a CO_2-free basis) can be related to NaCl molality as follows:

$$X_s = \frac{m_{NaCl} M_{NaCl}}{1000 + m_{NaCl} M_{NaCl}} \qquad (2.1)$$

Here m_{NaCl} is the molality of NaCl (moles of NaCl per kg of water), M_{NaCl} = 58.448 is the molecular weight of NaCl, and the number 1000 appears in the denominator because molality is defined as moles per 1000 g of water. For convenience we also list the inverse of Eq. (2.1).

$$m_{NaCl} = \frac{1000 X_s / M_{NaCl}}{1 - X_s} \qquad (2.2)$$

Table 2.1. Summary of ECO2N V2.0

Components	# 1: water # 2: NaCl # 3: CO_2
Parameter choices (NK, NEQ, NPH, NB) =	(3, 4, 3, 6) water, NaCl, CO_2, nonisothermal (default) (3, 3, 3, 6) water, NaCl, CO_2, isothermal molecular diffusion can be modeled by setting NB = 8
Primary Variables	

single fluid phase (only aqueous, or only gas)# (P, X_{sm}, X3, T)

P – pressure (Pa)

X_{sm} – NaCl salt mass fraction X_s (on the basis of a two-component, CO_2-free water-salt system), or solid NaCl saturation S_s+10

X3 - CO_2 (true) mass fraction in the aqueous phase, or in the gas phase, in the three-component system water-salt-CO_2

T – temperature (°C)

two fluid phases (aqueous and gas)# (P, X_{sm}, S_g+10, T)

P – pressure (Pa)

X_{sm} – NaCl salt mass fraction X_s (on the basis of a two-component, CO_2-free water-salt system), or solid saturation S_s+10

S_g - gas phase saturation

T – temperature (°C)

\# When discussing fluid phase conditions, we refer to the potentially mobile (aqueous and gas) phases only; in all cases solid salt may precipitate or dissolve, adding another active phase to the system.

The third primary variable X3 is CO_2 mass fraction for single-phase conditions (onlyaqueous, or only gas) and is "gas saturation plus ten" (Sg + 10) for two-phase (aqueous and gas) conditions. The reason for adding 10 to Sg is analogous to the conventions adopted for the second primary variable, namely, to be able to distinguish single-phase conditions ($0 < X3 < 1$) from two phase conditions ($10 < X3 < 11$). In single-phase conditions, the CO_2 mass fraction is a "free" variable, i.e., it can vary continuously within certain parameter ranges, while in two-phase aqueous-gas conditions, it has a fixed value that is a function of temperature, pressure, and salinity (see below). Accordingly, for single-phase conditions the CO_2 mass fraction is included among the independent primary variables (= X3), while for two-phase conditions, the CO_2 mass fraction becomes a "secondary" parameter that is dependent upon primary variables (T, P, X_s). "Switching" primary variables according to phase conditions present provides a very robust and stable technique for dealing with changing phase compositions; see Section 2.2 below.

Initialization of a simulation with TOUGH2/ECO2N V2.0 would normally be made with the internally used primary variables as listed in Table 2.1. For convenience of the user, additional choices are available for initializing a flow problem; see Section 4.1 below.

2.1 Phase Composition

The partitioning of H_2O and CO_2 among co-existing aqueous and gas phases is calculated based on the correlations developed by Spycher and Pruess (2005) for the low temperature range (<99^{o}C) and Spycher and Pruess (2010) for the high temperature range (109 to ~300^{o}C). These correlations were derived from the requirement that chemical potentials of all components must be equal in different phases. For two-phase conditions, they predict the equilibrium composition of liquid (aqueous) and gas (CO_2-rich) phases as functions of temperature, pressure, and salinity, and are valid in the temperature range $12\ °C < T < 300\ °C$, for pressures up to 600 bar, and salinity up to saturated NaCl brines. In the indicated parameter range, mutual solubilities of H_2O and CO_2 are calculated with accuracy typically within experimental uncertainties.

At temperatures between 99 and 109^{o}C, we use a cubic function to interpolate both the equilibrium mass fraction of CO_2 in the aqueous phase and the equilibrium mass fraction of H_2O in the gas (CO_2 rich) phase. The interpolation function makes use of four parameters that are determined by the function values and the function's first derivatives at the two end points of the interpolation range (99 and 109^{o}C). This approach guarantees a smooth transition between the low temperature and the high temperature ranges such that both the function and its first derivative are continuous. It was found that the current approach performs better than the model parameter blending approach suggested in Spycher and Pruess (2010) in terms of numerical stability and convergence, probably because this approach avoids the troublesome calculation of the mutual solubility near 100^{o}C for both models. Figure 2.1.1 shows the curves of dissolved CO_2 mass fraction at saturation as a function of temperature between 80 to 120^{o}C and the corresponding derivatives. As shown in the figure, the model implemented in ECO2N V2.0 has a smooth transition in terms of both the function and its derivative. It effectively removes the troublesome bumps in the derivative, especially at T = 100^{o}C.

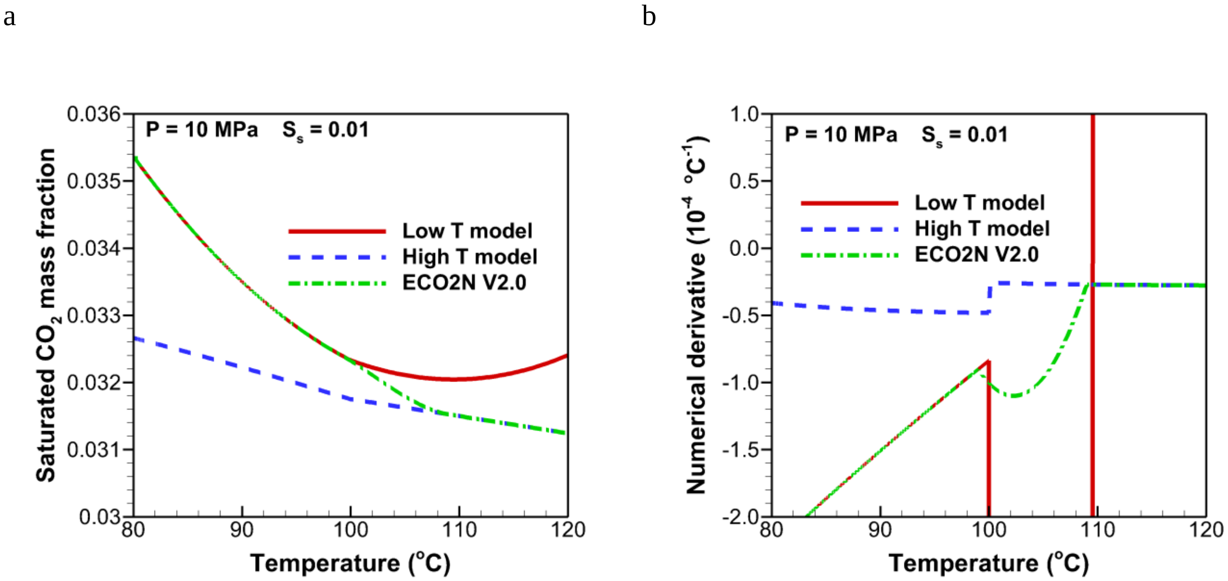

Figure 2.1.1. Transition between low temperature model (<99°C) and high temperature model (>109°C). a) Computed dissolved CO_2 mass fraction (at saturation) as a function of temperature; b) the numerical derivative of the dissolved CO_2 mass fraction with respect to temperature (ΔT = 1E-8 $^oC^{-1}$). "Low T model" indicates the mutual solubility model developed by Spycher and Pruess (2005), whereas "High T model" indicates the mutual solubility model for higher temperatures by Spycher and Pruess (2010). "ECO2N V2.0" indicates the combined model implemented in ECO2N V2.0.

In the previous version of ECO2N (V1.0), for the mutual solubility calculations, the CO_2 molar volumes are calculated using a tabular EOS based on Altunin's correlation (1975), instead of the Redlich-Kwong equation of state used in Spycher and Pruess (2005, 2010). Altunin's correlations yield slightly different molar volumes than the Redlich-Kwong EOS whose parameters were fit by Spycher and Pruess (2005) to obtain the best overall match between observed and predicted CO_2 concentrations in the aqueous phase. The (small) differences in Altunin's molar volumes cause predictions for the mutual solubility of water and CO_2 to be somewhat different also. This practice is no longer used in the new version of ECO2N (V2.0). However, for users who want to exactly match the solubility model in the low temperature range with ECO2N V1.0, we offer an option to do so by setting IE(16)=1 in the SELEC block of the input file. In this case, the exact same model implemented in ECO2N V1.0 will be used to calculate the mutual solubility in the low temperature range (<99°C). Note that this option should not be used if the temperature can go higher because it would result in inconsistency in calculation of the mutual solubility between low and high temperature ranges.

Two equilibrium CO_2 mass fractions, $X_{CO2,eq}$ (the equilibrium CO_2 mass fraction in the aqueous phase) and $Y_{CO2,eq}$ (the equilibrium CO_2 mass fraction in the gas phase), are used to determine the phase conditions based on the CO_2 mass fraction, X3. The relationship between CO_2 mass fraction X3 and phase composition of the fluid mixture is as follows (see Fig. 2.1.2)

- $X3 < X_{CO2,eq}$ corresponds to single-phase liquid conditions;
- $X3 > Y_{CO2,eq}$ corresponds to single-phase gas;
- intermediate values ($X_{CO2,eq} \leq X3 \leq Y_{CO2,eq}$) correspond to two-phase conditions with different proportions of aqueous and gas phases.

Dissolved NaCl concentrations may for typical sequestration conditions range as high as 6.25 molal. This corresponds to mass fractions of up to X_{sm} = 26.7% in the two-component system water-salt. Phase conditions as a function of X_{sm} are as follows.

- $X_{sm} \leq XEQ$ corresponds to dissolved salt only;
- $X_{sm} > XEQ$ corresponds to conditions of a saturated NaCl brine and solid salt.

Here XEQ denotes the equilibrium solubility of NaCl, which in ECO2N is evaluated as in EWASG (Battistelli et al., 1997) as a function of temperature, using an equation by Potter cited in Chou (1987). No dependence of XEQ on CO_2 concentration is taken into account.

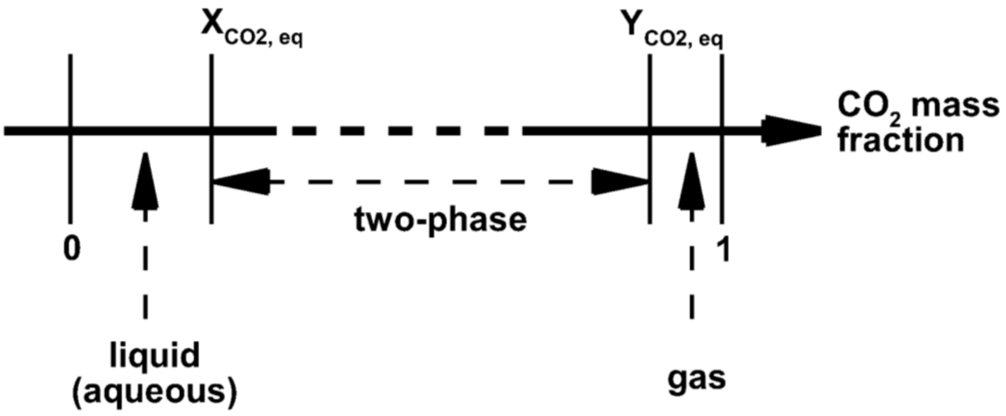

Figure 2.1.2. CO_2 phase partitioning in the system H_2O - NaCl - CO_2. The CO_2 mass fraction in brine-CO_2 mixtures can vary in the range from 0 (no CO_2) to 1 (no brine). $X_{CO2,eq}$ and $Y_{CO2,eq}$ denote, respectively, the CO_2 mass fractions in aqueous and gas phases corresponding to equilibrium phase partitioning in two-phase conditions. Mass fractions less than $X_{CO2,eq}$ correspond to conditions in which only an aqueous phase is present, while mass fractions larger than $Y_{CO2,eq}$ correspond to single-phase gas conditions. Mass fractions intermediate between $X_{CO2,eq}$ and $Y_{CO2,eq}$ correspond to two-phase conditions with different proportions of aqueous and gas phases.

2.2 Phase Change

In single-phase (aqueous or gas) conditions, the third primary variable X3 is the CO_2 mass fraction in that phase. In single-phase aqueous conditions, we must have $X3 \leq X_{CO2,eq}$, while in single-phase gas conditions, we must have $X3 \geq Y_{CO2,eq}$. The possibility of phase change is evaluated by monitoring X3 in each grid block. The criteria for phase change from single-phase to two-phase conditions may be written as follows.

- single-phase aqueous conditions: a transition to two-phase conditions (evolution of a gas phase) will occur when $X3 > X_{CO2,eq}$;
- single-phase gas conditions: a transition to two-phase conditions (evolution of an aqueous phase) will occur when $X3 < Y_{CO2,eq}$.

When two-phase conditions evolve in a previously single-phase grid block, the third primary variable is switched to $X3 = S_g+10$. If the transition occurred from single-phase liquid conditions, the starting value of S_g is chosen as 10^{-6}; if the transition occurred from single-phase gas, the starting value is chosen as $1 - 10^{-6}$.

In two-phase conditions, the third primary variable is $X3 = S_g+10$. For two-phase conditions to persist, X3 must remain in the range $(10, 11 - S_s)$. Transitions to single-phase conditions are recognized as follows:

- if $X3 < 10$ (i.e., $S_g < 0$): gas phase disappears; make a transition to single-phase liquid conditions;
- if $X3 > 11 - S_s$ (i.e., $S_g > 1 - S_s$): liquid phase disappears; make a transition to single-phase gas conditions.

Phase change involving (dis-)appearance of solid salt is recognized as follows. When no solid salt is present, the second primary variable X_{sm} is the concentration (mass fraction referred to total water plus salt) of dissolved salt in the aqueous phase. The possibility of precipitation starting is evaluated by comparing X_{sm} with XEQ, the equilibrium solubility of NaCl at prevailing temperature. If $X_{sm} \leq XEQ$ no precipitation occurs, whereas for $X_{sm} > XEQ$ precipitation starts. In the latter case, variable X_{sm} is switched to S_s+10, where solid saturation S_s is initialized with a small non-zero value (10^{-6}). If a solid phase is present, the variable $X_{sm} = S_s+10$ is monitored. Solid phase disappears if $X_{sm} < 10$, in which case primary variable X_{sm} is switched to salt concentration, and is initialized as slightly below saturation, $X_{sm} = XEQ - 10^{-6}$.

2.3 Conversion of Units

The Spycher and Pruess (2005, 2010) model for phase partitioning in the system H_2O–NaCl–CO_2 is formulated in molar quantities (mole fractions and molalities), while TOUGH2/ECO2N V2.0 describes phase compositions in terms of mass fractions. This section presents the equations and parameters needed for conversion between the two sets of units. The conversion between various concentration variables (mole fractions, molalities, mass fractions) does not depend upon whether or not concentrations correspond to equilibrium between liquid and gas phases; accordingly, the relations given below are valid regardless of the magnitude of concentrations.

Let us consider an aqueous phase with dissolved NaCl and CO_2. If the modals of NaCl and CO_2 are m_{NaCl} and m_{CO2}, respectively, total mass per kg of water is

$$M = 1000\left(g\,H_2O\right) + m_{NaCl}\,M_{NaCl}\left(g\,NaCl\right) + m_{CO2}\,M_{CO2}\left(g\,CO_2\right) \qquad (2.3.1)$$

where M_{NaCl} and M_{CO2} are the molecular weights of NaCl and CO_2, respectively (see Table 2.3.1). Assuming NaCl to be completely dissociated, the total moles per kg of water are

$$m_T = \frac{1000}{M_{H2O}} + 2m_{NaCl} + m_{CO2} \qquad (2.3.2)$$

For a given CO_2 mole fraction, x_{CO2}, because $m_{CO2} = x_{CO2}\, m_T$, we obtain using Eq. (2.3.2)

$$m_{CO2} = \frac{x_{CO2}\left(2m_{NaCl} + 1000/M_{H2O}\right)}{1 - x_{CO2}} \qquad (2.3.3)$$

CO_2 mass fraction X3 in the aqueous phase is obtained by dividing the CO_2 mass in m_{CO2} moles by the total mass,

$$X3 = \frac{m_{CO2}M_{CO2}}{1000 + m_{NaCl}M_{NaCl} + m_{CO2}M_{CO2}} \qquad (2.3.4)$$

Water mass fraction Y_{H2O} in the CO_2-rich phase is simply

$$Y_{H2O} = \frac{y_{H2O}M_{H2O}}{y_{H2O}M_{H2O} + \left(1 - y_{H2O}\right)M_{CO2}} \qquad (2.3.5)$$

where y_{H2O} is the mole fraction of water in the gas phase, and the molecular weights of the various species are listed in Table 2.3.1 (Evans, 1982).

Table 2.3.1. Molecular weights in the system H_2O–NaCl–CO_2.

species	mol. weight
H_2O	18.015
Na	22.991
Cl	35.457
NaCl	58.448
CO_2	44.01

3. Thermophysical Properties of Water-NaCl-CO_2 Mixtures

Thermophysical properties needed to model the flow of water-NaCl-CO_2 mixtures in porous media include density, viscosity, and specific enthalpy of the fluid phases as functions of temperature, pressure, and composition, and partitioning of components among the fluid phases. Many of the needed parameters are obtained from the same correlations as were used in the EWASG property module of TOUGH2 (Battistelli et al., 1997). EWASG was developed for geothermal applications, and consequently considered conditions of elevated temperatures > 100 ˚C, and modest CO_2 partial pressures on the order of 1-10 bar. Unlike the ECO2N V1.0 module, which targets the opposite end of the temperature and pressure range, namely, modest temperatures below 110 ˚C, and high CO_2 pressures up to several hundred bars, ECO2N V2.0 includes an expanded range of temperature and pressure (10-300^{o}C and up to 600 bars).

Water properties in TOUGH2/ECO2N V2.0 are calculated, as in other members of the TOUGH family of codes, from the steam table equations as given by the International Formulation Committee (1967). Properties of pure CO_2 are obtained from correlations developed by Altunin (1975). We began using Altunin's correlations in 1999 when a computer program implementing them was conveniently made available to us by Victor Malkovsky of the Institute of Geology of Ore Deposits, Petrography, Mineralogy and Geochemistry (IGEM) of the Russian Academy of Sciences, Moscow. Altunin's correlations were subsequently extensively cross-checked against experimental data and alternative PVT formulations, such as Span and Wagner (1996). They were found to be very accurate (García, 2003).

Altunin's correlations are not used directly in the code, but are used ahead of a TOUGH2/ECO2N V2.0 simulation to tabulate density, viscosity, and specific enthalpy of pure CO_2 on a regular grid of (T, P)-values. These tabular data are provided to the ECO2N V2.0 module in a file called "CO2TAB," and property values are obtained during the simulation by means of bivariate interpolation. Fig. 3.1 shows the manner in which CO_2 properties are tabulated, intentionally showing a coarse (T, P)-grid so that pertinent features of the tabulation may be better seen. (For actual calculations, we use finer grid spacings; the CO2TAB data file distributed with ECO2N V2.0 covers the range 3.04 ˚C $\leq$ T $\leq$ 303.04 ˚C with $\Delta T = 2$ ˚C and 1 bar $\leq$ P $\leq$ 800 bar with $\Delta P \leq 4$ bar in most cases.) As shown in Fig. 3.1, the tabulation is made in such a way that for sub-critical conditions the saturation line is given by diagonals of the interpolation quadrangles. On the saturation line, two sets of data are provided, for liquid and gaseous CO_2, respectively, and in quadrangles that include points on both sides of the saturation line, points on the "wrong" side are excluded from the interpolation (i.e., 3-point interpolation). This scheme provides for an efficient and accurate determination of thermophysical properties of CO_2.

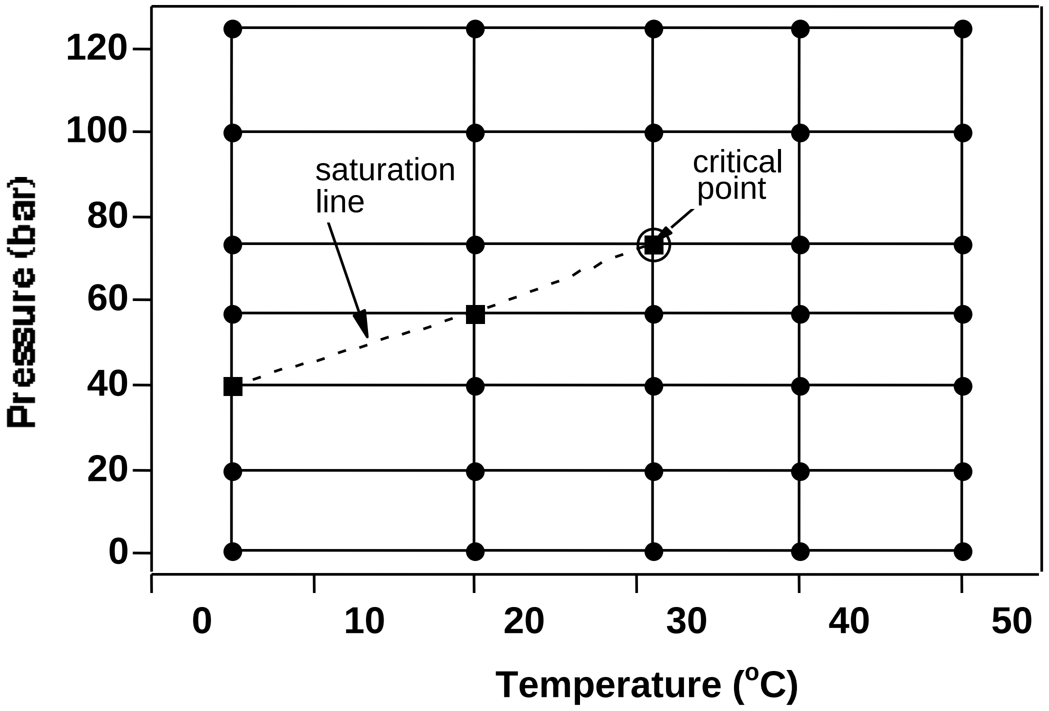

Figure 3.1. Schematic of the temperature-pressure tabulation of CO_2 properties. The saturation line (dashed) is given by the diagonals of interpolation rectangles.

Note that, unlike V1.0, the specific enthalpy of CO_2 calculated using Altunin's correlations in V2.0 is now shifted by a constant (-302192 J/kg) to make sure it has the same reference state as NIST webbook (i.e., the internal energy of saturated liquid water equals zero at the triple point of pure water at T=0.06°C and P=611.65Pa). Therefore, the change in thermal energy caused by composition change can be accounted for more consistently in case that other form of energy, e.g., kinetic energy, is included in the energy balance equation. As a result, users should pay attention to the specific enthalpy associated to the CO_2 injection in GENER section of TOUGH2 input file with this shaft in mind, especially using old input files.

We have implemented an alternative model for calculating the density and specific enthalpy of the CO_2-rich phase which is based on the cubic EOS summarized in Spycher and Pruess (2010), with departure functions discussed in Spycher and Pruess (2011). The interested user can invoke this model by setting IE(16)=2 in the input file. Spycher and Pruess (2011) have described the details of the model and its limitations, which will not be duplicated here. Note that the reference state for the specific enthalpy has been adjusted to be the same as NIST webbook (i.e., add 21390 J/mol and 42785.21984 J/mol to the calculated CO_2 enthalpy and water vapor enthalpy, respectively).). The alternative model is only applied for the density and the specific enthalpy of the gas phase (IE(16)=2), including the pure CO_2 or pure H_2O vapor phase. The liquid water properties and the properties of dissolved CO_2 are still calculated using steam table equations and Altunin's correlations, respectively. So is the viscosity of the gas phase.

Figures 3.2-3.4 compare the thermophysical properties of pure H_2O (liquid phase) calculated by ECO2N against the NIST web book (NIST, 2011) at certain pressure and temperature conditions. Figures 3.5-3.9 compare the thermophysical properties of pure H_2O (vapor) and CO_2 calculated by ECO2N against the NIST web book at certain pressure and temperature conditions. As shown in these comparisons, the calculated thermophysical properties of pure H_2O and CO_2 are consistent with NIST data except for the specific enthalpy of pure H_2O vapor calculated using the cubic EOS-based model, because the cubic EOS is not intended for pure water and cannot accurately predict the water saturation pressure curve (Spycher and Pruess, 2011). However, in most reservoir conditions that ECO2N would be applied, the gas phase is rarely expected to be pure H_2O vapor.

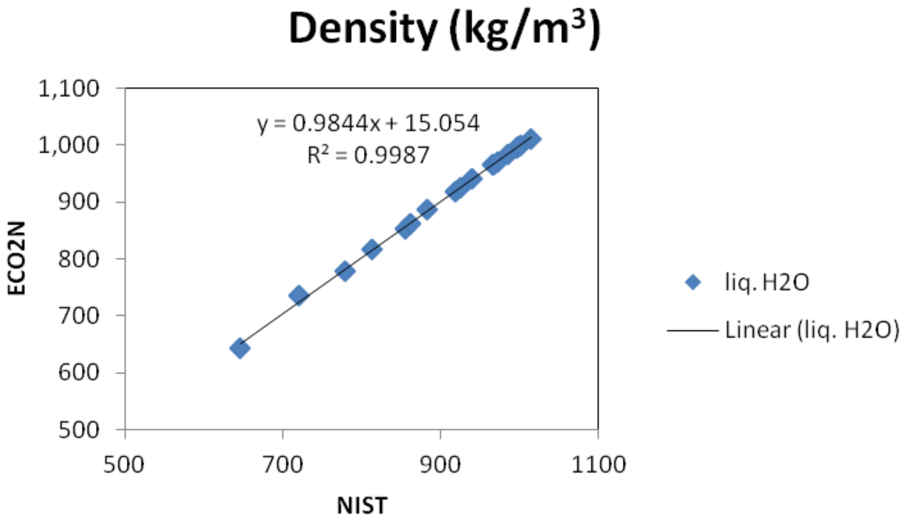

Figure 3.2. Density of pure water (liqud phase) at various P (0.4 – 44 MPa) and T (30 – 330°C) calculated by ECO2N and NIST (webbook).

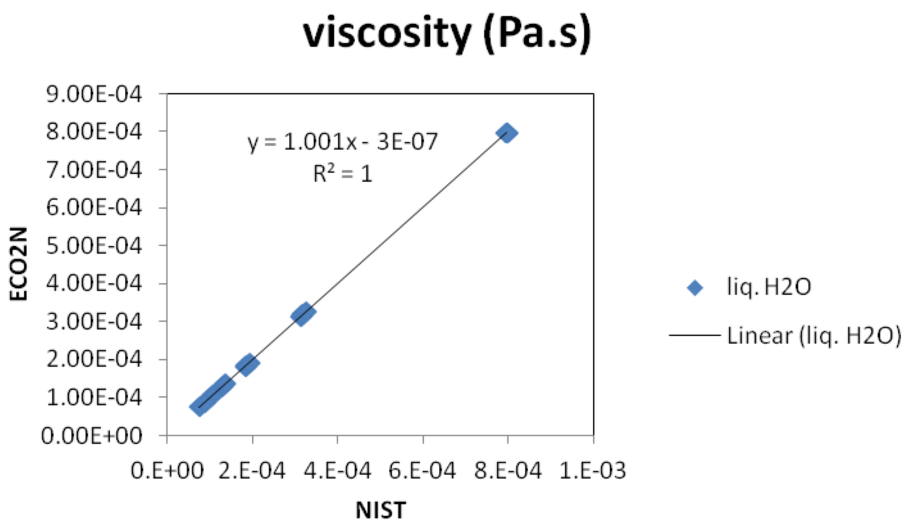

Figure 3.3. Viscosity of pure water (liquid phase) at various P (0.4 – 44 MPa) and T (30 – 330°C) calculated by ECO2N and NIST (web book).

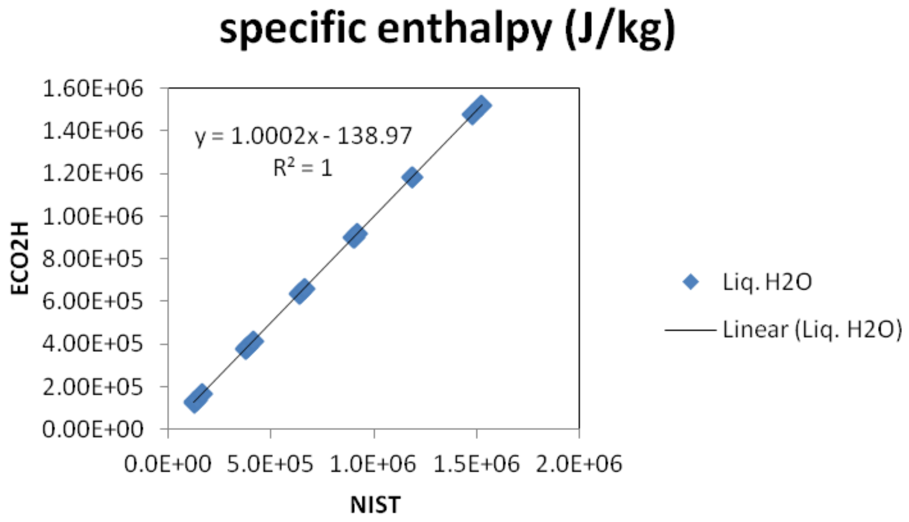

Figure 3.4. Specific enthalpy of pure water (liquid phase) at various P (0.4 – 44 MPa) and T (30 – 330°C) calculated by ECO2N and NIST (web book).

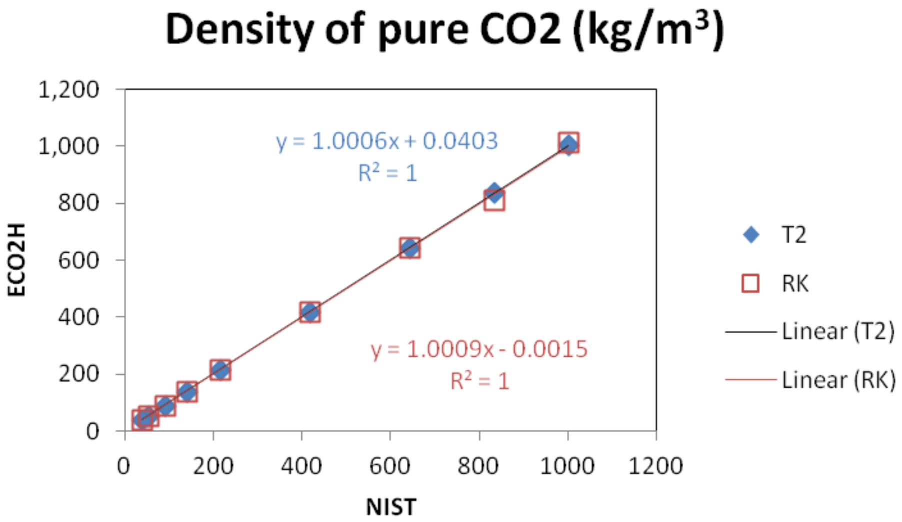

Figure 3.5. **Density of pure CO_2 at various P and T calculated by ECO2N and NIST (web book). Pressure varies from 4 to 44 MPa and temperature varies from 30 to 280°C. "T2" indicates the default Altunin (1975) model for gas phase density implemented in ECO2N whereas "RK" indicates the alternative model based on the cubic EOS.**

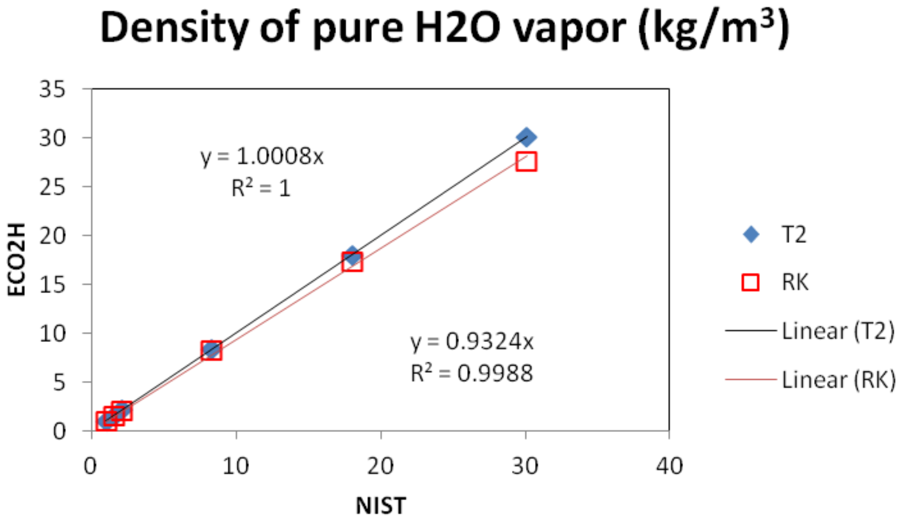

Figure 3.6. **Density of pure water (vapor) at various P and T calculated by ECO2N and NIST (web book). Pressure ranges are 2-6 MPa at 280°C and 0.2-0.4 MPa at 150°C, respectively. "T2" indicates the default steam-table model for gas phase density implemented in ECO2N whereas "RK" indicates the alternative model based on the cubic EOS.**

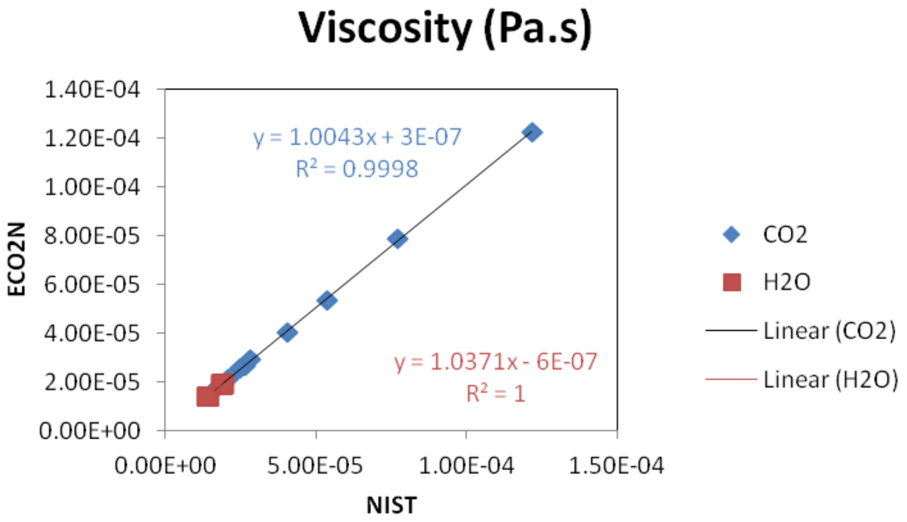

Figure 3.7. Viscosity of pure water (vapor) and CO_2 at various P and T calculated by ECO2N and NIST (web book). Pressure ranges are 2-6 MPa at 280°C and 0.2-0.4 MPa at 150°C, respectively, for pure H_2O vapor. For pure CO_2, pressure varies from 4 to 44 MPa and temperature varies from 30 to 280°C.

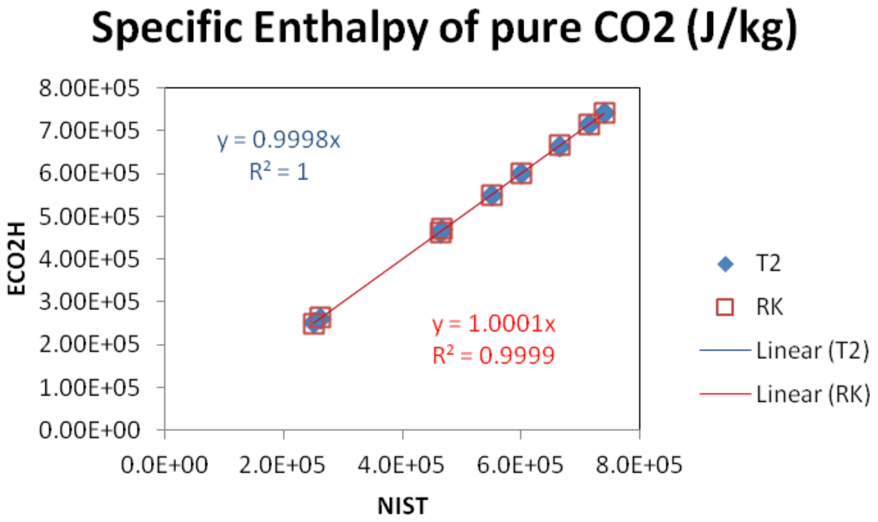

Figure 3.8. Specific enthalpy of pure CO2 at various P and T calculated by ECO2N and NIST (web book). Pressure varies from 4 to 44 MPa and temperature varies from 30 to 280°C. "T2" indicates the default Altunin (1975) model for gas phase specific enthalpy implemented in ECO2N whereas "RK" indicates the alternative model based on the cubic EOS.

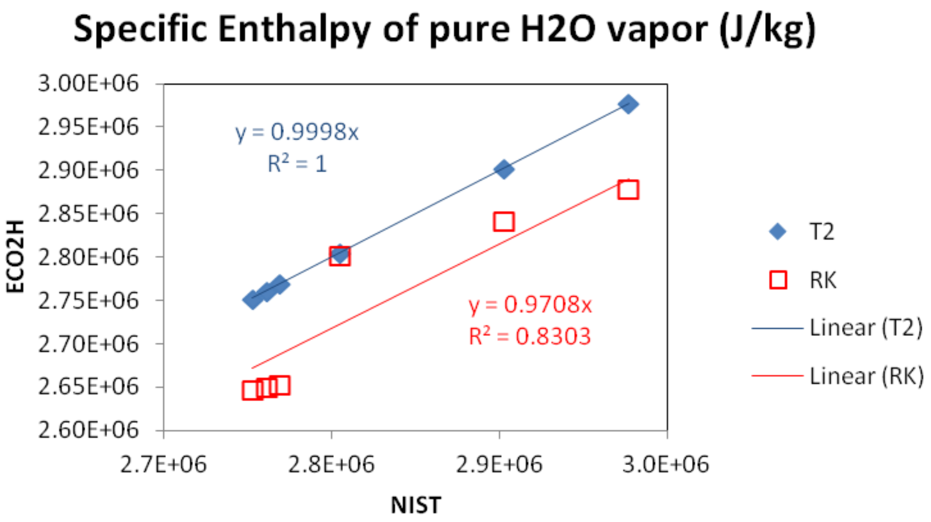

Figure 3.9. **Specific enthalpy of pure H2O (vapor) at various P (<Psat) and T calculated by ECO2N and NIST (web book). There are two sets of data points. The first set is corresponding to T = 280°C (P = 2, 4, or 6 MPa) while the second set is T = 150°C (P = 0.2, 0.3, or 0.4 MPa), respectively. "T2" indicates the default steam-table model for gas phase density implemented in ECO2N whereas "RK" indicates the alternative model based on the cubic EOS.**

The following sections describe the method implemented to calculate the thermophysical properties of the mixture in each phase which is consistent with the mutual solubility model.

3.1 Density of Aqueous Phase

Brine density ρ_b for the binary system water-salt is calculated as in Battistelli et al. (1997) from the correlations of Haas (1976) and Andersen et al. (1992). The calculation starts from aqueous phase density without salinity at vapor-saturated conditions, which is obtained from the correlations given by the International Formulation Committee (1967). Corrections are then applied to account for effects of salinity and pressure. The density of the aqueous phase with dissolved CO_2 is calculated assuming additivity of the volumes of brine and dissolved CO_2.

$$\frac{1}{\rho_{aq}} = \frac{1-X3}{\rho_b} + \frac{X3}{\rho_{CO2}} \tag{3.1.1}$$

where X3 is the mass fraction of CO_2 in the aqueous phase. The density of dissolved CO_2, ρ_{CO2}, is calculated as a function of temperature from the correlation for molar volume of dissolved CO_2 at infinite dilution developed by García (2001).

$$V_\phi = a + bT + cT^2 + dT^3 \tag{3.1.2}$$

In Eq. (3.1.2), molar volume of CO_2 is in units of cm^3 per gram-mole, temperature T is in ˚C, and *a* through *d* are fitting parameters given in Table 3.1.1.

Table 3.1.1. Parameters for molar volume of dissolved CO_2 (Eq. 3.1.2)

a	37.51
b	-9.585e-2
c	8.740e-4
d	-5.044e-7

Partial density of dissolved CO_2 in units of kg/m^3 is then

$$\rho_{CO2} = \frac{M_{CO2}}{V_\phi} * 10^3 \qquad (3.1.3)$$

where M_{CO2} is the molecular weight of CO_2.

Dissolved CO_2 amounts at most to a few percent of total aqueous density. Accordingly, dissolved CO_2 is always dilute, regardless of total fluid pressure. It is then permissible to neglect the pressure dependence of partial density of dissolved CO_2, and to use the density corresponding to infinite dilution.

3.2 Viscosity of Aqueous Phase

Brine viscosity is obtained as in EWASG from a correlation presented by Phillips et al. (1981), which reproduces experimental data in the temperature range from 10–350˚C for salinities up to 5 molal and pressures up to 500 bar within 2%. No allowance is made for the dependence of brine viscosity on the concentration of dissolved CO_2.

3.3 Specific Enthalpy of Aqueous Phase

Specific enthalpy of brine is calculated from the correlations developed by Lorenz et al. (2000), which are valid for all salt concentrations in the temperature range from $25^\circ\mathrm{C} \le T \le 300^\circ\mathrm{C}$. The enthalpy of the aqueous phase with dissolved CO_2 is obtained by adding the enthalpies of the CO_2 and brine (pseudo-) components, and accounting for the enthalpy of dissolution of CO_2.

$$h_{aq} = (1 - X3)h_b + X3h_{CO2,aq} \qquad (3.3.1)$$

$h_{CO2,aq} = h_{CO2} + h_{dis}$ is the specific enthalpy of aqueous (dissolved) CO_2, which includes heat of dissolution effects that are a function of temperature and salinity. For gas-like (low pressure) CO_2, the specific enthalpy of dissolved CO_2 is

$$h_{CO2,aq}(T,P,X_s) = h_{CO2,g}(T,P) + h_{dis,g}(T,X_s) \qquad (3.3.2)$$

where $h_{dis,g}$ is obtained as in Battistelli et al. (1997) from an equation due to Himmelblau (1959). For geologic sequestration we are primarily interested in liquid-like (high-pressure) CO_2, for which the specific enthalpy of dissolved CO_2 may be written as

$$h_{CO2,aq}(T,P,X_s) = h_{CO2,l}(T,P) + h_{dis,l}(T,X_s) \qquad (3.3.3)$$

Here $h_{dis,l}$ is the specific heat of dissolution for liquid-like CO_2, which can be calculated as shown below. Along the CO_2 saturation line, liquid and gaseous CO_2 phases may co-exist, and the expressions Eqs. (3.3.2, 3.3.3) must be equal there. We obtain

$$h_{dis,l}(T,X_s) = h_{dis,g}(T,X_s) + h_{CO2,gl}(T) \qquad (3.3.4)$$

where $h_{CO2,gl}(T) = h_{CO2,g}(T,P_s) - h_{CO2,l}(T,P_s)$ is the specific enthalpy of vaporization of CO_2, and $P_s = P_s(T)$ is the saturated vapor pressure of CO_2 at temperature T. Depending upon whether CO_2 is in gas or liquid conditions, we use Eq. (3.3.2) or (3.3.3) in Eq. (3.3.1) to calculate the specific enthalpy of dissolved CO_2. At the temperatures of interest here, $h_{dis,g}$ is a negative quantity, so that dissolution of low-pressure CO_2 is accompanied by an increase in temperature. $h_{CO2,gl}$ is a positive quantity, which will reduce or cancel out the heat-of-dissolution effects. This indicates that dissolution of liquid CO_2 will produce less temperature increase than dissolution of gaseous CO_2 and may even cause a temperature decline if $h_{CO2,gl}$ is sufficiently large.

Application of Eq. (3.3.1) is straightforward for single-phase gas and two-phase conditions, where h_{CO2} is obtained as a function of temperature and pressure through bivariate interpolation from a tabulation of Altunin's correlation (1975). A complication arises in evaluating h_{CO2} for single-phase aqueous conditions. Previously, in ECO2N V1.0, we made the assumption that $h_{CO2}(P, X_S, X3, T)$ for single-phase aqueous is identical to the value in a two-phase system with the same composition of the aqueous phase. To determine h_{CO2}, it was then necessary to invert the Spycher and Pruess (2005) phase partitioning relation $X3 = X_{CO2,eq}(P; T, X_S)$, in order to obtain the pressure P_{X3} in a two-phase aqueous-gas system that would correspond to a dissolved CO_2 mass fraction X3 in the aqueous phase, $P_{X3} = P(X3{=}X_{CO2,eq}; X_S, T)$. The inversion was accomplished by Newtonian iteration, using a starting guess P_0 for P_{X3} that was obtained from Henry's law. The specific enthalpy of dissolved CO_2 in ECO2N V1.0 for the entire range of X3 can be summarized (the subscript g or l was dropped for simplicity) as:

$$h_{CO2,aq}(T,P,X_s) = \begin{cases} h_{CO2}(T,P)+h_{dis}(T,X_s) & X3 \geq X_{CO2,eq} \\ h_{CO2}(T,P_{X3})+h_{dis}(T,X_s) & X3 < X_{CO2,eq} \end{cases} \qquad (3.3.5)$$

However, the resulting specific enthalpy of dissolved CO_2 does not have a continuous first derivative at the phase partition line, which could damage the Jacobi matrix and cause convergence problems when the system is close to a phase change. Figure 3.3.1 shows a contour map of the specific enthalpy of the dissolved CO_2 (excluding h_{dis} for simplicity) at given temperature (40˚C) and salinity (0.01). Above the phase partition line, the specific enthalpy only depends on the pressure. Below the phase partition line, it only depends on the mass fraction X3 because P_{X3} is actually a function of X3 which is defined by the phase partition line (the dashed line). Although h_{CO2} is continuous across the phase partition line, the partial derivative of h_{CO2} with respective to X3 is non-zero when approaching the line from below but is zero when approaching the line from above. Similar discontinuities can be found in the partial derivative with respect to other variables (e.g., P, T, or X_s). In ECO2N V2.0, we slightly modify the approach to make sure that all partial derivatives will be continuous across the phase partition line, which will be described in detail below.

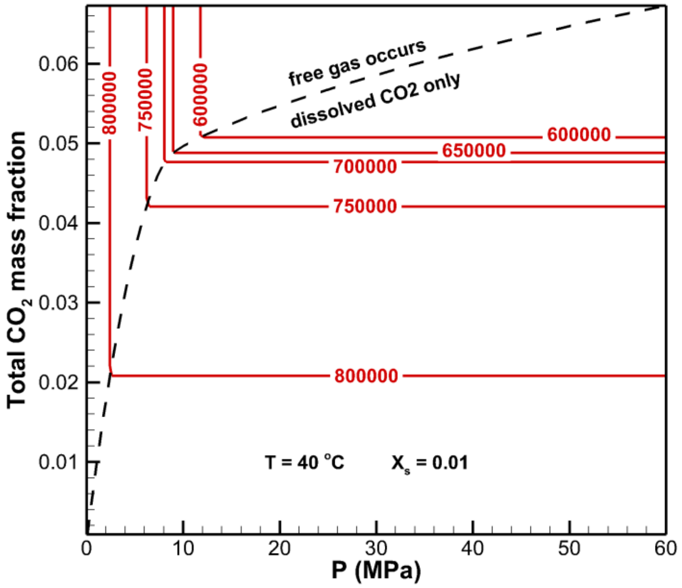

Figure 3.3.1. Contours of the specific enthalpy, $h_{CO2,\,aq}$-$h_{\neg dis}$, (J/kg) of the dissolved CO_2 (red lines) as a function of total CO_2 mass fraction X3 and pressure at a given temperature (40°C) and salt mass fraction (0.01) as calculated in ECO2N V1.0. The phase partition line (black dashed line) is calculated using the correlations developed by the Spycher and Pruess (2005). The specific enthalpy is continuous at the phase partition line, but its partial derivative with respective to either pressure or CO_2 mass fraction is not.

In TOUGH2, each element of the Jacobian matrix is a partial derivative of the equation residual R_i with respect to a primary variable X_j (Pruess, 1999). For the current issue, the related equation is the energy balance equation, in which the contribution of the dissolved CO_2 is the second term on the right hand side of equation (3.3.1), the dissolved CO_2 enthalpy. Therefore, we can examine the partial derivative of this term with respect to each primary variable. For example, the partial derivatives of the term with respective to P and X3 at X3=$X_{CO2,\,eq}$ can be written as (3.3.6a) and (3.3.6b), respectively.

$$\frac{\partial\left(X3h_{CO2,aq}\right)}{\partial P}=\begin{cases} X_{CO2,eq}\dfrac{\partial h_{CO2}(T,P)}{\partial P} & X3=X^{+}_{CO2,eq} \\ 0 & X3=X^{-}_{CO2,eq} \end{cases} \qquad (3.3.6a)$$

$$\frac{\partial\left(X3\,h_{CO2,aq}\right)}{\partial X3} = \begin{cases} h_{CO2}\left(T,P\right)+h_{dis}\left(T,X_s\right) & X3=X^{+}_{CO2,eq} \\ h_{CO2}\left(T,P\right)+h_{dis}\left(T,X_s\right)+X_{CO2,eq}\dfrac{\partial h_{CO2}\left(T,P_{X3}\right)}{\partial P_{X3}}\dfrac{\partial P_{X3}}{\partial X3} & X3=X^{-}_{CO2,eq} \end{cases} \qquad (3.3.6b)$$

where, the superscript of $X_{CO2,eq}$ indicates the side of the phase partition line. Both partial derivatives are not continuous across the phase partition line.

In ECO2N V2.0, we use a modified approach to calculate the dissolved CO_2 enthalpy so that its derivatives with respect to either primary variable are continuous across the phase partition line. We evaluate the specific enthalpy of the dissolved CO_2 for single-phase aqueous conditions as a nonlinearly scaled value of its counterpart under two-phase conditions.

$$h_{CO2,aq}\left(T,P,X_s\right)=\begin{cases} h_{CO2}\left(T,P\right)+h_{dis}\left(T,X_s\right) & X3\geq X_{CO2,eq} \\ h_{CO2}\left(T,P\right)f\left(X3\right)+h_{dis}\left(T,X_s\right) & X3<X_{CO2,eq} \end{cases} \qquad (3.3.7)$$

Where the scaling function f(X3) is defined as follow:

$$f\left(X3\right)=2-\cos\left[3\pi\left(X_{CO2,eq}-X3\right)\right] \qquad (3.3.8)$$

Note that the scaling function has the nice property at $X3=X_{CO2,eq}$:

$$\begin{gathered} f\left(X_{CO2,eq}\right)=1 \\ \left.\frac{df}{dX3}\right|_{X_{CO2,eq}}=3\pi\sin\left[3\pi\left(X_{CO2,eq}-X_{CO2,eq}\right)\right]=0 \end{gathered} \qquad (3.3.9)$$

As a result, the partial derivatives of the dissolved CO_2 enthalpy at $X3 = X^{-}_{CO2,\,eq}$ become:

$$\frac{\partial\left(X3h_{CO2,aq}\right)}{\partial P}=X_{CO2,eq}\frac{\partial h_{CO2}\left(T,P\right)}{\partial P} \qquad (3.3.10a)$$

$$\frac{\partial\left(X3h_{CO2,aq}\right)}{\partial X3}=h_{CO2}\left(T,P\right)+h_{dis}\left(T,X_s\right) \qquad (3.3.10b)$$

Both derivatives are continuous across the phase line. Although the modification alters the behavior near the phase partition line, the calculated enthalpies of the dissolved CO_2 are practically identical in ECO2N V2.0 and ECO2N V1.0 (Figure 3.3.2).

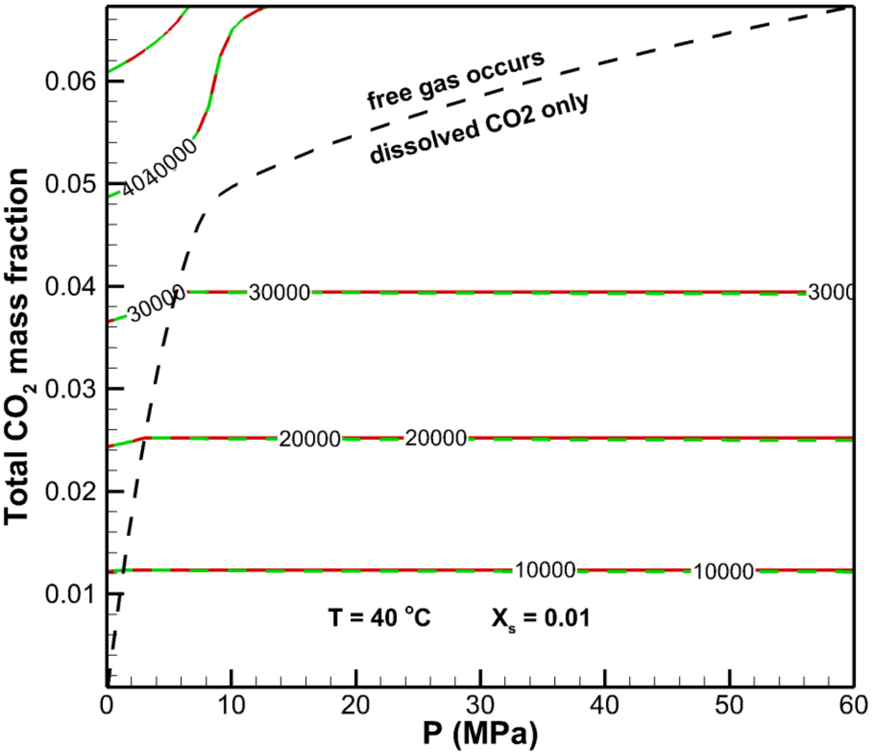

Figure 3.3.2. Contours of enthalpy, min(X3,$X_{CO2,\ eq}$)($h_{CO2,\ aq}$-h_{dis}), (J) of dissolved CO_2 (ECO2N V1.0, red lines; ECO2N V2.0, green dashed lines) as a function of total CO_2 mass fraction and pressure at a given temperature (40°C) and salt mass fraction (0.01). The phase partition line (black dashed line) is calculated using the correlations developed by Spycher and Pruess (2005).

3.4 Density of gas (CO_2-rich) phase

The “gas” phase modeled by ECO2N is a two-component CO_2-rich compressed “gas” phase, in which the CO_2 behaves either as a liquid, gas, or supercritical fluid. The water in this CO_2-rich phase could be considered as water vapor; however, its properties tend to deviate from “vapor-like” and approach “liquid-like” values as the gas phase pressure increases (Spycher and Pruess, 2011). At elevated pressures, the H_2O partial pressure in the gas phase can be well above the saturation pressure of pure H_2O, P_{sat}(T). This complexity makes the calculation of the density or other properties not as straightforward as in the case of ideal mixing. To properly model the effects of H_2O on the properties of the CO_2-rich phase, two approaches can be followed:

(1) The use of simple, smooth mixing functions of pure component properties (default option)
(2) The direct use of the cubic EOS implemented for solubility calculations (invoked by setting IE(16)=2 in the input file)

Both approaches present advantages and disadvantages. The first approach is more advantageous in terms of computational speed, but is empirical in nature and thus not fully accurate. The second approach relies on a rigorous thermodynamic basis, but suffers from the fact that cubic EOSs are typically not very accurate near phase boundaries, and much less accurate at reproducing volumetric data than solubility data. Therefore, both approaches are not expected to be fully accurate.

With approach (1), the gas phase properties for a given condition of pressure (P), temperature (T), and mass fraction of H_2O in the gas phase (Y_{H2O}) are estimated by interpolation between pure-component properties. While P and T are two primary variables in ECO2N, Y_{H2O} can be either the third primary variable (1-X3 in single-phase gas condition) or the equilibrium water mass fraction ($Y_{H2O,eq}$ in two-phase condition) calculated by the mutual solubility model (Spycher and Pruess, 2005, 2010):

$$Y_{H2O} = \begin{cases} Y_{H2O,eq} & \text{twophase} \\ 1 - X_3 & \text{single gas phase} \end{cases} \tag{3.4.1}$$

We can calculate the partial pressures of H_2O and CO_2 in the gas phase as follow:

$$\begin{aligned} P_{H2O} &= y_{H2O} P \\ P_{CO2} &= P - P_{H2O} \end{aligned} \tag{3.4.2}$$

Where y_{H2O} is the mole fraction of H_2O in the gas phase, which can be converted from the mass fraction of H_2O in the gas phase, Y_{H2O}:

$$y_{H2O} = \frac{Y_{H2O}/M_{H2O}}{Y_{H2O}/M_{H2O} + (1 - Y_{H2O})/M_{CO2}} \tag{3.4.3}$$

The density of the gas phase at a given grid cell with a gas phase volume of V_{gas} is defined as the ratio of the total mass of the mixture over the gas phase volume:

$$\rho_{gas} = \frac{n_{H2O} M_{H2O} + n_{CO2} M_{CO2}}{V_{gas}} \tag{3.4.4}$$

We assume that the compressibility factor of CO_2 in the mixture is the same as that in pure CO_2 under the same pressure and temperature. Therefore, the mass of CO_2 in the mixture can be simply estimated as :

$$n_{CO2} M_{CO2} = (1 - y_{H2O})\rho_a(P,T)V_{gas} \tag{3.4.5}$$

where ρ_a is obtained through bivariate interpolation from a tabulation of CO_2 densities at given temperature and pressure that is based on the correlations developed by Altunin (1975).

If the water partial pressure, P_{H2O}, is less or equals to the saturated vapor pressure, P_{sat}, the water in the gas mixture is in form of vapor. Therefore, the mass of water in the gas mixture, $n_{H2O}M_{H2O}$, is the mass of water vapor, n_vM_{H2O}, which can be directly calculated from the vapor density as:

$$n_v M_{H2O} = \rho_{sv}(P_v,T)V_{gas} \tag{3.4.6}$$

where , P_v is the vapor pressure (<=P_{sat}) and ρ_{SV} is the partial density of water vapor calculated using the steam table equations as given by the International Formulation Committee (1967). A complexity araises, however, when $P_{H2O} > P_{sat}$, in which the water in the CO_2-rich phase would tend to be more like liquid (Spycher and Pruess, 2005, 2010). As a result, we no longer can directly use the steam table equations to estimate the partial density of water in the mixture because P_{H2O} is beyond the defined domain of those equations and the water in the CO_2-rich phase is somewhat like a sub-mixture of “vapor-like” and “liquid-like” water. To quantify this sub-mixture of water in the CO_2-rich phase, we define a factor, X_L, as the mole fraction of “liquid-like” water in the sub-mixture:

$$X_L = \begin{cases} 0 & \text{if} \quad P_{H2O} \le P_{sat} \\ 1 - P_{sat}/P_{H2O} & \text{if } P_{H2O} > P_{sat} \end{cases} \tag{3.4.7}$$

Consequently, the mole fraction of “liquid-like” water in the CO_2-rich phase is $X_L y_{H2O}$, which can be used to scale the liquid water density into the partial density just like what did for CO_2. The mass of “liquid-like” water, n_LM_{H2O}, can be calculated as follow:

$$n_L M_{H2O} = X_L\, y_{H2O} f(X_L) \rho_{sL}(P\ ,T)V_{gas} \tag{3.4.8}$$

where ρ_{sL} is the calculated water density (liquid) at given P and T using steam table equations and $f(X_L)$ is the adjustment function to relate the density of liquid water to the density of “liquid-like” water. We found that a fraction power of X_L is the best fit to the available density data:

$$f(X_L) = X_L^{0.8} \tag{3.4.9}$$

Finally, the mass of water in the CO_2-rich phase can be calculated as the sum of “vapor-like” and “liquid-like” water:

$$n_{H2O} M_{H2O} = n_v M_{H2O} + n_L M_{H2O} \tag{3.4.10}$$

Note that the effect of "liquid-like" behavior will diminish if P_{H2O} is below P_{sat}, because X_L =1.

The density of the gas phase calculated by Eq. (3.4.4) will reduce to the pure CO_2 density calculated using the Altunin (1975) correlation if y_{H2O} approaches zero, or the pure H_2O vapor density calculated from the steam table equation if y_{H2O} approaches one (e.g., in case $P \leq P_{sat}$).

Approach (2), and its deviations in computed density for the CO_2-rich "gas" phase, are discussed in detail by Spycher and Pruess (2010 and 2011). Except close to the liquid-vapor phase boundary, this approach yields reasonable "gas"-phase compressibility factors for the CO_2-H_2O system, typically within a few percent of experimental volumetric data (reported for temperatures up ~300ºC and pressures ~200 bar). It should be noted that at temperatures below about 100ºC, the use of pure CO_2 properties (i.e., those tabulated in the CO2TAB file, using the accurate EOS of Altunin et al., 1975) is probably the best approach because the concentration of H_2O in compressed CO_2 below 100ºC is very small (typically < 1 mol%). Therefore, Approach (2) should be reserved for simulations at temperatures above 100ºC and pressures significantly above the pure H_2O saturation curve.

Figure 3.4.1 shows comparisons between the calculated densities of the gas phase against the experimental data published in the literature. Both models reproduce the experimental data reasonably well.

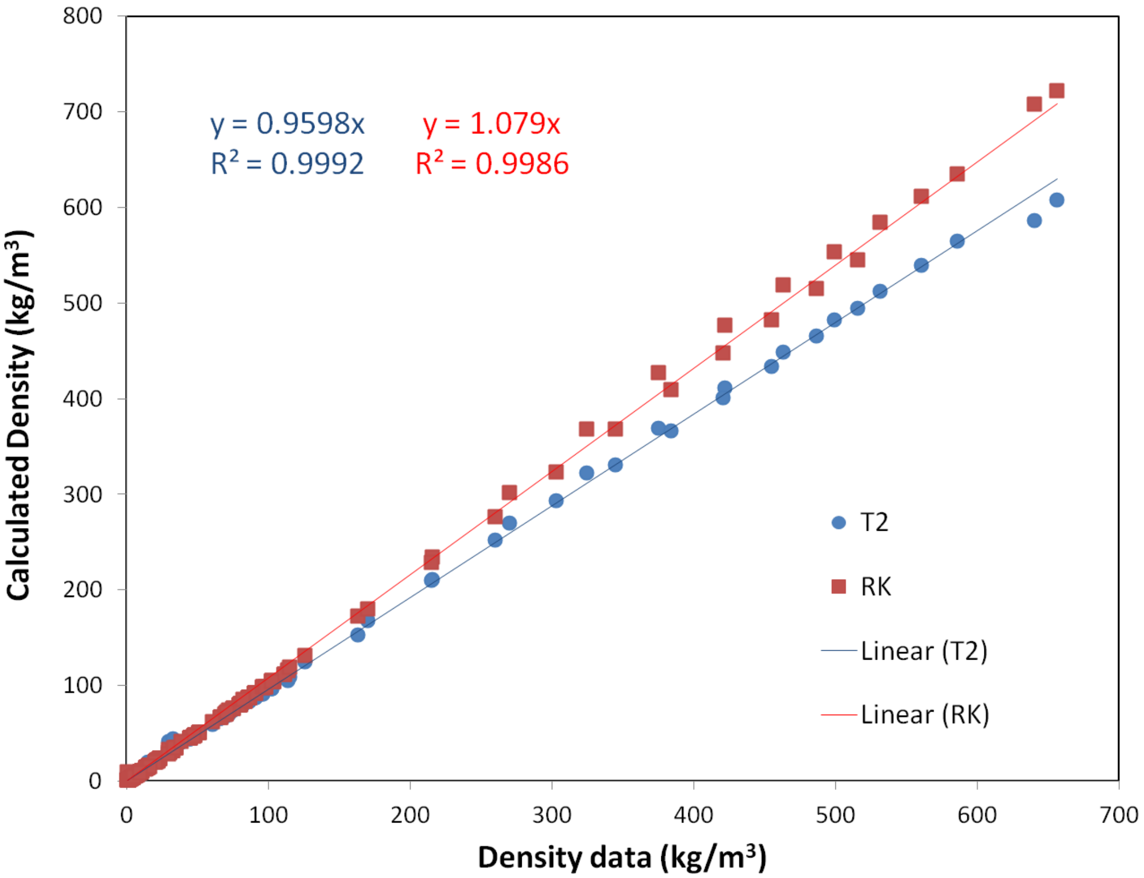

Figure 3.4.1 Comparison of computed densities of the gas phase against the experimental data reported in the literature (Fenghour et al., 1996; Patel et al., 1987; Patel and Eubank, 1988; Zawisza and Malesnska, 1981; Zakirov, 1984). "T2" indicates the default model (Eqs. 3.4.4-3.4.10) while "RK" indicates the alternative model (IE(16)=2).

3.5 Viscosity of Gas (CO_2-rich) Phase

The viscosity of the gas phase is calculated based on the method proposed by Davidson (1993), which relates the fluidity, f_{gas}, as the reciprocal of the viscosity, μ_{gas}:

$$\mu_{gas} = \frac{1}{f_{gas}} \qquad (3.5.1)$$

Because the gas phase here is a binary mixture of H_2O and CO_2, the fluidity of the gas phase can be calculated as:

$$f_{gas} = \frac{z_{H2O}^2}{\mu_{H2O}} + 2\frac{z_{H2O}z_{CO2}}{\sqrt{\mu_{H2O}\mu_{CO2}}}E_{12}^A + \frac{z_{CO2}^2}{\mu_{CO2}} \qquad (3.5.2)$$

where z_{H2O} and z_{CO2} are momentum fractions of H_2O and CO_2, respectively, and are calculated as follows:

$$z_{H2O} = \frac{y_{H2O}\sqrt{M_{H2O}}}{y_{H2O}\sqrt{M_{H2O}} + (1 - y_{H2O})\sqrt{M_{CO2}}} \qquad (3.5.3)$$

$$z_{CO2} = 1 - z_{H2O}$$

The empirical exponent A of 0.375 as suggested by Davidson (1993) is used, and the mean efficiency of momentum transfer E_{12} is calculated as follows:

$$E_{12} = \frac{2\sqrt{M_{H2O}M_{CO2}}}{M_{H2O} + M_{CO2}} \qquad (3.5.4)$$

μ_{CO2} is the viscosity of pure CO_2 at the given P and T, obtained through bivariate interpolation from a tabulation of CO_2 viscosity as a function of temperature and pressure that is based on the correlations developed by Altunin (1975). As mentioned above, the H_2O in the CO_2-rich phase behaves somewhat like a mixture of “vapor-like” and “liquid-like” components. The viscosity of H_2O in the gas phase is calculated as a sub-mixture in a similar way:

$$\mu_{H2O} = \frac{1}{f_{H2O}} \qquad (3.5.5)$$

Because the molecular weights of two water components are the same, the mean efficiency of the momentum transfer becomes unity. The fluidity of H_2O is calculated as follows:

$$f_{H2O} = \frac{z_v^2}{\mu_v} + 2\frac{z_v z_L}{\sqrt{\mu_v \mu_L}} + \frac{z_L^2}{\mu_L} \qquad (3.5.6)$$

The corresponding momentum fractions are calculated as follows:

$$z_L = \frac{X_L\sqrt{M_{H2O}}}{X_L\sqrt{M_{H2O}} + (1 - X_L)\sqrt{M_{H2O}}} = X_L \qquad (3.5.7)$$

$$z_v = 1 - z_L$$

where X_L is the mole fraction of “liquid-like” H_2O among the water in the gas phase calculated according to Eq. (3.4.7). μ_v and μ_L are viscosities of vapor and liquid H_2O, respectively, calculated from the steam table equations as given by the International Formulation Committee (1967).

3.6 Specific Enthalpy of Gas (CO_2-rich) Phase

As for density calculations, the specific enthalpy of the gas phase can be computed following two approaches:

(1) The use of smooth mixing functions of pure component properties (default option)

(2) The use of departure functions of the cubic EOS implemented for solubility calculations (invoked by setting IE(16)=2 in the input file)

With Approach (1), the specific enthalpy of the gas phase is simply calculated as mass-fraction weighted average plus a term representing mixing heat:

$$h_{gas} = Y_{H2O} h_{H2O} + (1 - Y_{H2O}) h_{CO2} + Y_{H2O} \left(\frac{P}{\rho_{gas}} - \frac{P_{H2O}}{\rho_{H2O}} \right) \tag{3.6.1}$$

h_{CO2} is the specific enthalpy of pure CO_2 at the given P and T, obtained through bivariate interpolation from a tabulation of CO_2 specific enthalpy as a function of temperature and pressure, which is based on the correlations developed by Altunin (1975). The last term of Eq. (3.6.1) represents the mixing heat, which is proportional to the mass fraction of water in the gas phase and the difference in the PV terms for the mixture and the H_2O component. This term will vanish if the gas phase consists of either pure CO_2 ($Y_{H2O}=0$) or pure H_2O ($P=P_{H2O}$), as expected. Consequently, the specific enthalpy of the gas phase calculated by Eq. (3.6.1) will reduce to the specific enthalpy of the pure CO_2 calculated using the Altunin (1975) correlation if Y_{H2O} approaches zero, or to the specific enthalpy of pure H_2O vapor calculated from the steam table equation if Y_{H2O} approaches one.

The specific enthalpy of H_2O is calculated as a weighted average of “vapor-like” and “liquid-like” internal energies plus a PV term for the sub-mixture of “vapor-like” and “liquid-like”water in the gas phase:

$$h_{H2O} = (1 - X_L) u_{sv} + X_L u_{sL} + \frac{P_{H2O}}{\rho_{H2O}} \tag{3.6.2}$$

Here, u_{sv} and u_{sL} are the internal energies of “vapor-like” and “liquid-like” H_2O, respectively, calculated from the steam table equations as given by the International Formulation Committee (1967). Note that, as mentioned above, the calculated specific enthalpy of pure CO_2 is shifted by a constant in ECO2N V2.0 to make sure the reference state is the same as that used by the NIST web book.

Approach (2) makes use of the departure functions of the cubic EOS implemented into ECO2N V2.0. Spycher and Pruess (2011) have described the details of the model and its limitations, which are not repeated here. Note that Spycher and Pruess’s original model adapted a different reference state for the water and CO_2 enthalpy calculations. We have modified it to match the reference state used by NIST (i.e., the internal energy of saturated liquid water equals zero at the triple point of pure water, T=0.06°C and P=611.65 Pa). The deviations in computed enthalpy for CO_2-H_2O mixtures at elevated temperatures and pressures are difficult to assess because of the paucity of experimental enthalpy data under these conditions. The results reported by Spycher and Pruess (2011) suggest that computed enthalpies of H_2O-CO_2 mixtures using their cubic EOS are likely reasonable at elevated pressures when water dissolved into the compressed CO_2 is expected to behave more “liquid-like” than “gas-like”. However, no experimental data are available to estimate enthalpy deviations at pressures above about 120 bar and elevated temperatures conducive to high H_2O concentrations in CO_2. It should be noted that under conditions of lower pressures, closer to the pure water saturation P-T curve, with high H_2O concentrations in CO_2, significant deviations may occur because the cubic EOS cannot accurately reproduce the enthalpy of pure H_2O vapor (see Figure 3.9).

Figure 3.6.1 shows comparisons between the calculated specific enthalpy of the gas phase against the experimental data published in literature for various pressures, temperatures, and mass fractions. The various forms of the experimental data have been converted to the total specific enthalpy at the same reference state accordingly. Both models reproduced the experimental data well.

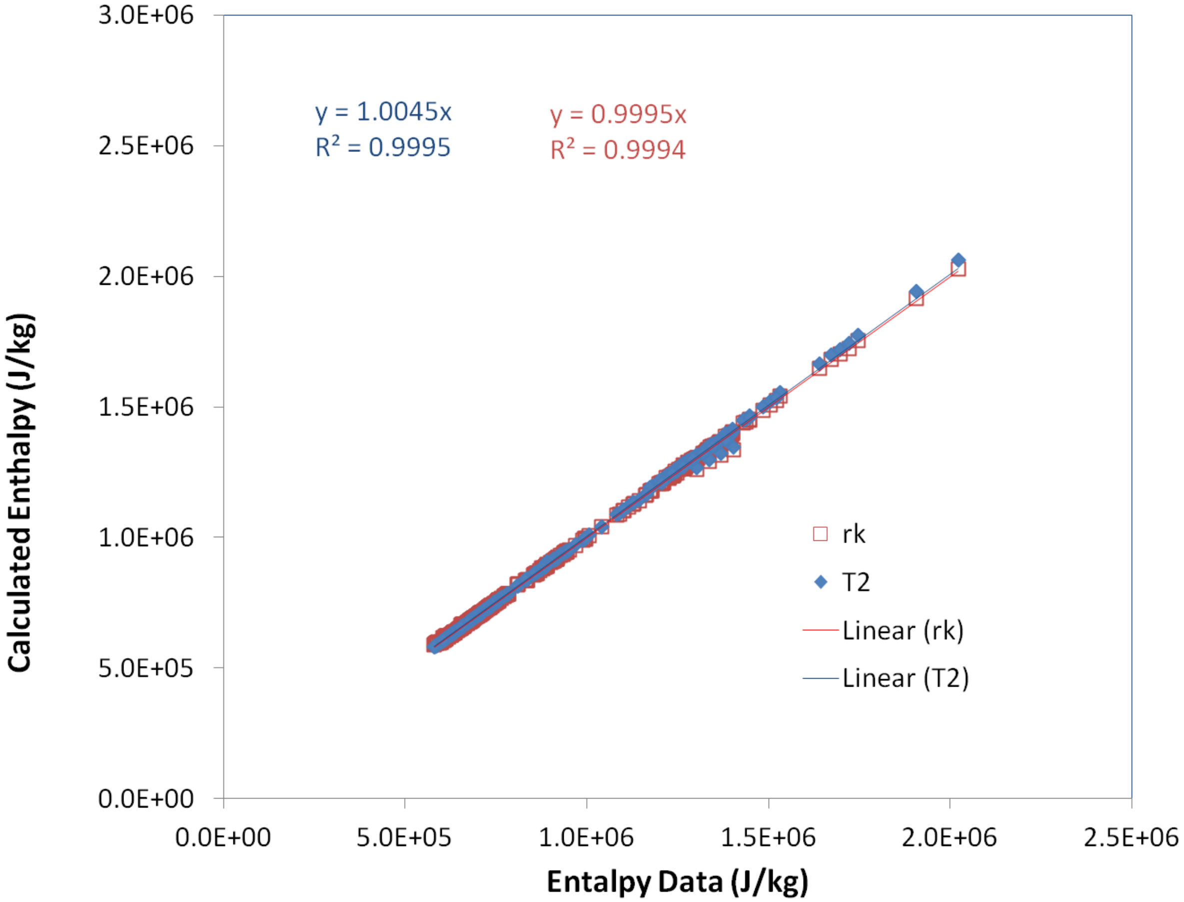

Figure 3.6.1 Comparison of computed specific enthalpy of the gas phase against the experimental data reported in the literature (Patel and Eubank, 1988; Bottini and Salville, 1985; Wormald et al. 1986). “T2” indicates the default model (Eqs. 3.6.1-3.6.2) while “RK” indicates the alternative model (IE(16)=2). The same reference state as used by NIST (i.e., the internal energy of saturated liquid water equals zero at the triple point of pure water, T=0.06°C and P=611.65 Pa) are used.

4. Preparation of Input Data

Most of TOUGH2/ECO2N V2.0 input specifications correspond to the general TOUGH2 input formats as given in the TOUGH2 user's guide (Pruess et al., 2012). This information is not duplicated in the present report; here we discuss only parameter choices specific to ECO2N V2.0.

4.1 Initialization Choices

Flow problems in TOUGH2/ECO2N V2.0 will generally be initialized with the primary thermodynamic variables as used in the code, but some additional choices are available for the convenience of users. The internally used variables are (P, X_{sm}, X3, T) for grid blocks in single-phase (liquid or gas) conditions and (P, X_{sm}, S_g+10, T) for two-phase (liquid and gas) grid blocks (see Table 2.1). Here X3 is the mass fraction of CO_2 in the fluid. As has been discussed above, for conditions of interest to geologic sequestration of CO_2, X3 is restricted to small values $0 \leq X3 \leq X_{CO2,eq}$ (a few percent) for single-phase liquid conditions, or to values near 1 ($Y_{CO2,eq} \leq X3 \leq 1$, with $Y_{CO2,eq} > 0.99$ typically) for single-phase gas (Fig. 2.1.2). Intermediate values $X_{CO2,eq} < X3 < Y_{CO2,eq}$ correspond to two-phase conditions, and thus should be initialized by specifying S_g+10 as the third primary variable. As a convenience to users, ECO2N V2.0 allows initial conditions to be specified using X3 in the full range $0 \leq X3 \leq 1$. During the initialization phase of a simulation, a check is made whether X3 is in fact within the range of mass fractions that correspond to single-phase (liquid or gas) conditions. If this is found not to be the case, the conditions are recognized as being two-phase, and the corresponding gas saturation is calculated from the phase equilibrium constraint.

$$X3\left(S_l\rho_l + S_g\rho_g\right) = S_l\rho_l X_{CO2,eq} + S_g\rho_g Y_{CO2,eq} \qquad (4.1.1)$$

Using $S_l = 1 - S_g - S_s$, with S_s the "solid saturation" (fraction of pore space occupied by solid salt), we obtain

$$S_g \quad = \quad A \times \left(1 - S_s\right) \qquad (4.1.2)$$

and the third primary variable is reset internally to X3 = S_g+10. Here the parameter A is given by

$$A = \frac{\left(X3 - X_{CO2,eq}\right)\rho_l}{\left(X3 - X_{CO2,eq}\right)\rho_l + \left(Y_{CO2,eq} - X3\right)\rho_g} \qquad (4.1.3)$$

Users may think of specifying single-phase liquid (aqueous) conditions by setting X3 = 10 (corresponding to $S_g = 0$), and single-phase gas conditions by setting X3 = 11 - S_s (corresponding to $S_l = 0$). Strictly speaking, this is not permissible, because two-phase initialization requires that both $S_g > 0$ and $S_l > 0$. Single-phase states should instead be initialized by specifying primary variable X3 as CO_2 mass fraction. However, as a user convenience, ECO2N V2.0 accepts initialization of single-phase liquid conditions by specifying X3 = 10 (S_g = 0). Such specification will be converted internally to two-phase in the initialization phase by adding a small number (10^{-11}) to the third primary variable, changing conditions to two-phase with a small gas saturation $S_g = 10^{-11}$.

Salt concentration or saturation of solid salt, if present, is characterized in ECO2N V2.0 by means of the second primary variable X_{sm}. When no solid phase is present, X_{sm} denotes X_s, the mass fraction of NaCl in the two-component system water-NaCl. This is restricted to the range $0 \le X_{sm} \le XEQ$, where XEQ = XEQ(T) is the solubility of salt. For $X_{sm} > 10$ this variable means $S_s + 10$, solid saturation plus 10. Users also have the option to specify salt concentration by means of molality m by assigning $X_{sm} = -m$. Such specification will in the initialization phase be internally converted to X_s by using Eq. (2.1). When salt concentration (as a fraction of total H_2O + NaCl mass) exceeds XEQ, this corresponds to conditions in which solid salt will be present in addition to dissolved salt in the aqueous phase. Such states should be initialized with a second primary variable $X_{sm} = S_s+10$. However, ECO2N V2.0 accepts initialization with $X_{sm} > XEQ$, recognizing this as the presence of solid salt, and converting the second primary variable internally to the appropriate solid saturation that will result in the total salt mass fraction in the binary system water-salt being equal to X_{sm}. The conversion starts from the following equation:

$$X_{sm} = \frac{XEQ \times S_l \rho_l (1 - X2) + S_s \rho_s}{S_l \rho_l (1 - X2) + S_s \rho_s} \qquad (4.1.4)$$

where the numerator gives the total salt mass per unit volume, in liquid and solid phases, while the denominator gives the total mass of salt plus water. Substituting $S_l = 1 - S_g - S_s$, this can be solved for S_s to yield

$$S_s = \frac{B \times (1 - S_g)}{1 + B} \qquad (4.1.5)$$

where the parameter B is given by

$$B = \frac{(X_{sm} - XEQ)\rho_l (1 - X2)}{\rho_s (1 - X_{sm})} \tag{4.1.6}$$

The most general conditions arise when both the second and third primary variables are initialized as mass fractions, nominally corresponding to single-phase fluid conditions with no solid phase present, but both mass fractions are in the range corresponding to two-phase fluid conditions with precipitated salt. Under these conditions, Eqs. (4.1.2) and (4.1.5) are solved simultaneously in ECO2N V2.0 for S_S and S_g, yielding

$$S_g = \frac{A}{1 + B - A \times B} \tag{4.1.7}$$

and

$$S_s = \frac{B \times (1 - A)}{1 + B - A \times B} \tag{4.1.8}$$

Then both the second and third primary variables are converted to phase saturations, S_S + 10 and S_g + 10, respectively. Examples of different initialization choices are given in sample problem 1 below.

4.2 Permeability Change from Precipitation and Dissolution of Salt

ECO2N offers several choices for the functional dependence of relative change in permeability, k/k_0, on relative change in active flow porosity, ϕ_f/ϕ_0:

$$\frac{k}{k_0} = f\left(\frac{\phi_f}{\phi_0}\right) \equiv f(1 - S_s) \tag{4.2.1}$$

The simplest model that can capture the converging-diverging nature of natural pore channels consists of alternating segments of capillary tubes with larger and smaller radii, respectively; see Figure 4.2.1. While in straight capillary tube models permeability remains finite as long as porosity is non-zero, in models of tubes with different radii in series, permeability is reduced to zero at a finite porosity.

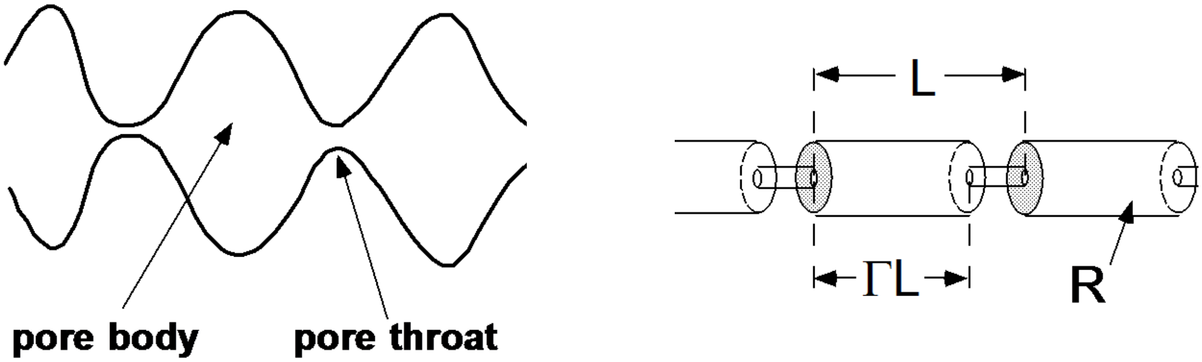

(a) conceptual model (b) tubes-in-series

Figure 4.2.1. Model for converging-diverging pore channels.

From the tubes-in-series model shown in Figure 4.2.1, the following relationship can be derived (Verma and Pruess, 1988):

$$\frac{k}{k_0} = \theta^2 \frac{1-\Gamma+\Gamma/\omega^2}{1-\Gamma+\Gamma\left[\theta/(\theta+\omega-1)\right]^2} \qquad (4.2.2)$$

Here

$$\theta = \frac{1-S_s-\phi_r}{1-\phi_r} \qquad (4.2.3)$$

depends on the fraction 1-S_s of original pore space that remains available to fluids, and on a parameter ϕ_r, which denotes the fraction of original porosity at which permeability is reduced to zero. Γ is the fractional length of the pore bodies, and the parameter ω is given by

$$\omega = 1+\frac{1/\Gamma}{1/\phi_r-1} \qquad (4.2.4)$$

Therefore, Eq. (4.2.2) has only two independent geometric parameters that need to be specified, ϕ_r and Γ. As an example, Figure 4.2.2 shows the permeability reduction factor from Eq. (4.2.2), plotted against $\phi/\phi_0 \equiv (1-S_s)$, for parameters of $\phi_r = \Gamma = 0.8$.

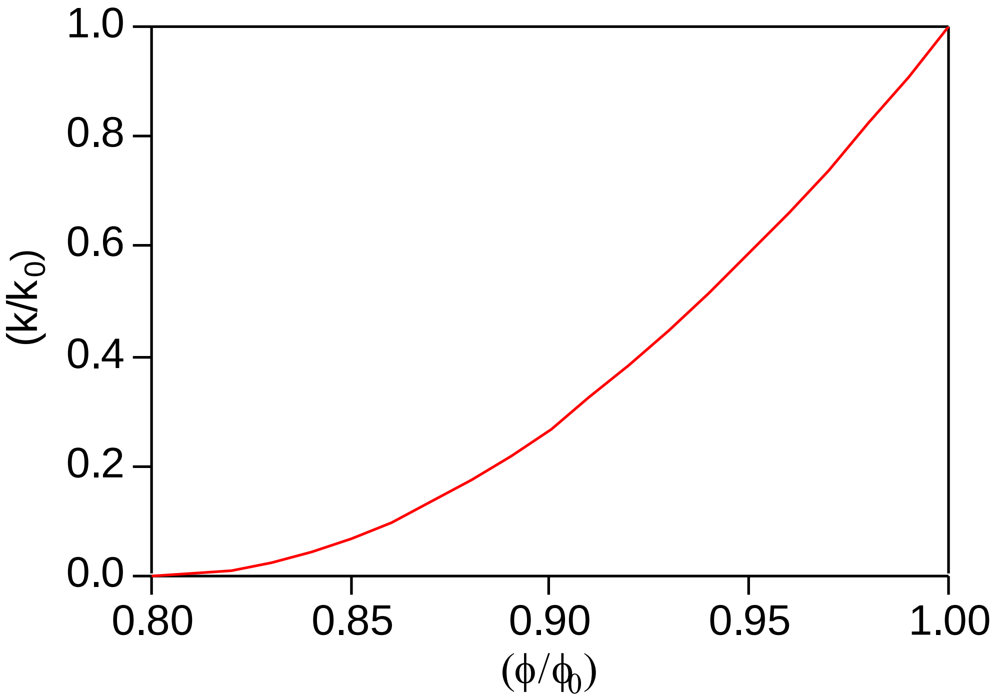

Figure 4.2.2. Porosity-permeability relationship for tubes-in-series model, after Verma and Pruess (1988).

For parallel-plate fracture segments of different aperture in series, a relationship similar to Eq. (4.2.2) is obtained, the only difference being that the exponent 2 is replaced everywhere by 3 (Verma and Pruess, 1988). If only straight capillary tubes of uniform radius are considered, we have $\phi_r = 0$, $\Gamma = 0$, and Eq. (4.2.2) simplifies to

$$k/k_0 = (1 - S_s)^2 \tag{4.2.5}$$

4.3 Program Options

Various options for ECO2N V2.0 can be selected through parameter specifications in data block SELEC. Default choices corresponding to various selection parameters set equal to zero provide the most comprehensive thermophysical property model. Certain functional dependencies can be turned off or replaced by simpler and less accurate models, as discussed below. These options are offered to enable users to identify the role of different effects in a flow problem, and to facilitate comparison with other simulation programs that may not include full dependencies of thermophysical properties.

SELEC keyword to introduce a data block with parameters for ECO2N V2.0.

Record SELEC.1

Format(16I5)
IE(I), I=1,16

IE(1) set equal to 1, to read one additional data record.

IE(10) allows choice of thermal conductivity models as a function of saturation and type of the fluid. This option requires to modify the TOUGH2 core code i.e., the subroutine MUILTI. See Appendix D for details about the models and the instructions of code modifications as well as input set up.

IE(11) selects dependence of permeability on the fraction $\phi_f/\phi_0 = (1-S_s)$ of original pore space that remains available to fluids when salt precipitates.

0: permeability does not vary with ϕ_f.
1: $k/k_0 = (1-S_s)^\gamma$, with γ = FE(9) (record SELEC.2).
2: fractures in series, i.e., Eq. (4.2.2) with exponent 2 replaced by 3.
3: tubes-in-series model, i.e., Eq. (4.2.2).

IE(12) allows choice of model for water solubility in CO_2

0: after Spycher and Pruess (2005).

1: evaporation model; i.e., water density in the CO_2-rich phase is calculated as density of saturated water vapor at prevailing temperature and salinity.

IE(13) allows choice of dependence of brine density on dissolved CO_2

0: brine density varies with dissolved CO_2 concentration, according to García's (2001) correlation for temperature dependence of molar volume of dissolved CO_2.

1: brine density is independent of CO_2 concentration.

IE(14) allows choice of treatment of thermophysical properties as a function of salinity

0: full dependence.

1: no salinity dependence of thermophysical properties (except for brine enthalpy; salt solubility constraints are maintained).

IE(15) allows choice of correlation for brine enthalpy at saturated vapor pressure

0: after Lorenz et al. (2000).

1: after Michaelides (1981).

2: after Miller (1978).

IE(16) allows choice of mutual solubility model and effect of water on CO_2-rich phase

0: mutual solubilities from Spycher and Pruess (2005, 2010); see Sections 3.4-3.6 for effect of water on thermophysical properties of the CO_2-rich phase.

1: exactly the same mutual solubility model for low temperature as implemented in ECO2N V1.0, ignoring the effects of water on the thermophysical properties of the CO_2-rich phase (not recommended for systems involving high temperature).

2: density and specific enthalpy of the CO_2-rich phase calculated using the approach based on the cubic EOS (Spycher and Pruess, 2011).

<u>Record SELEC.2</u> introduces parameters for functional dependence of permeability on solid saturation

Format(8E10.4)
FE(9), FE(10)

FE(9) parameter γ (for IE(11)=1); parameter ϕ_r (for IE(11) = 2, 3)
FE(10) parameter Γ (for IE(11) = 2, 3)

The ECO2N V2.0 module includes a customized version of a subroutine FGTAB that can write data files FOFT, COFT, and GOFT with time series of conditions at user-selected grid blocks and connections for plotting. The parameters written out in comma-delimited format at each time step are as follows.

FOFT:	(gas) pressure, dissolved CO_2 mass fraction in liquid, gas saturation, dissolved salt mass fraction and solid saturation (fraction of void space taken up by solid precipitate);
COFT:	flow rates of gas, liquid, and total CO_2 (as free phase and dissolved in aqueous phase);
GOFT:	well flow rate, flowing enthalpy, flowing CO_2 mass fraction, gas mass fraction of well flow, flowing wellbore pressure (production wells only).

5. Sample Problems

This section presents a number of sample problems for TOUGH2/ECO2N V2.0. The problems were chosen to demonstrate the preparation of input data, to illustrate code capabilities, and to provide benchmarks for proper code installation. Three of the problems were taken from a recent code intercomparison study, in which ten groups from six countries exercised different simulation codes to generate results for a suite of test problems (Pruess et al., 2002, 2004). These problems include a basic injection problem (Section 5.2), a basic fault leakage problem (Section 5.3), and a CO_2 storage problem with 2-D geometry loosely patterned after the Sleipner Vest CO_2 injection project (Kongsjorden et al., 1997; Lindeberg et al., 2002) in the Norwegian sector of the North Sea (Section 5.4).

5.1 Problem No. 1 (*rtab*) - Demonstration of Initialization Options

The input file as given in Fig. 5.1.1 performs just a single infinitesimal time step ($\Delta t = 10^{-9}$ s) and includes neither flow connections between grid blocks nor sinks or sources. Therefore, there is no flow and no changes in the initially specified thermodynamic conditions. The purpose of this problem is simply to demonstrate different options for initializing thermodynamic conditions.

Standard initialization with internally used primary variables (Table 2.1) is made for a number of grid blocks in single-phase liquid conditions (*a 1*, *a 3*, *a 5*), single-phase gas (*a 10*), and two-phase fluid (*A 14*, *A 15*, *A 19*,*A 22*). Several grid blocks are initialized with single-phase type primary variables, but with a CO_2 mass fraction (primary variable #3) that is larger than can be dissolved in the aqueous phase, and smaller than required for single-phase gas conditions (*a 2*, *a 6*, *a 9*, *A 18*). The CO_2 mass fractions for these blocks correspond to two-phase (liquid-gas) fluid conditions (see Fig. 2.1.2 and Section 4.1) and are internally converted to the appropriate gas saturation in the initialization phase. Primary variable #3 is then re-set to $S_g + 10$, as can be seen from the list of internally used primary variables that is generated by this problem (Fig. 5.1.2). Grid block *A 16* is initialized with primary variable #3 corresponding to internal ECO2N V1.0 usage, but primary variable #2 is larger than saturated salt mass fraction in the binary system water-salt. This specification corresponds to presence of solid salt, and is internally converted to $S_s + 10$. In some grid blocks both primary variables #2 and #3 are specified with conventions applicable for single-phase liquid conditions, but with salt mass fraction exceeding the solubility limit, and CO_2 mass fraction being in the intermediate range between the liquid and gas phase limits (*a 4*, *a 7*, *a 8*, *a 11*, *A 17*). Salt as well as CO_2 mass fractions for these blocks are converted to the appropriate internally used saturation variables. Finally, there are grid blocks (*A 20*, *A 21*,*A 23*,*A 24*) in which primary variable #2 is specified as salt molality (counted by convention as undissociated) in the binary water-salt system, which is internally converted to salt mass fraction. The internally used primary variables generated from the INCON data given in Fig. 5.1.1 are shown in Fig. 5.1.2. Fig. 5.1.3 shows part of the printed output for this problem. The last three grid blocks (*A 22*,*A 23*,*A 24*) have higher temperature.

```
*rtab* ... initialization test for ECO2N
ROCKS----1----*----2----*----3----*----4----*----5----*----6----*----7----*----8
SANDS    2  2600.e00       .35  100.e-15  100.e-15  100.e-15      2.51      920.
   4.5e-10
    7           .457       .30        1.       .05
    7           .457       .00    5.1e-5      1.e7      .999

MULTI----1----*----2----*----3----*----4----*----5----*----6----*----7----*----8
    3    4    3    6
START----1----*----2----*----3----*----4----*----5----*----6----*----7----*----8
----*----1 MOP: 123456789*123456789*1234 ---*----5----*----6----*----7----*----8
PARAM----1----*----2----*----3----*----4----*----5----*----6----*----7----*----8
   1   1       110 0900000000  4    3
                           -1.
     1.e-9
     1.E-5     1.E00
               60.e5                 0.0                0.01                20.0
SELEC....2....3....4....5....6....7....8....9...10...11...12...13...14...15...16
    1                                            0    0    0    0    0    0    0
        .8        .8
ELEME----1----*----2----*----3----*----4----*----5----*----6----*----7----*----8
a   1   10    1SANDS        1.
A  14   10    1SANDS        1.

CONNE----1----*----2----*----3----*----4----*----5----*----6----*----7----*----8
```

Figure 5.1.1. TOUGH2/ECO2N V2.0 input file (first part) for sample problem 1 – demonstration of initialization options.

```
INCON----1----*----2----*----3----*----4----*----5----*----6----*----7----*----8
a   1
              40.0e5                 0.0              3.9e-2                 30.
a   2
              40.0e5                 0.0              3.9e-1                 30.
a   3
             340.0e5                 0.0              6.6e-2                 30.
a   4
             340.0e5                 0.3              6.6e-1                 30.
a   5
             140.0e5             0.10466              3.6e-2                 30.
a   6
             140.0e5             0.10466              3.6e-1                 30.
a   7
             140.0e5                0.50              3.6e-2                 30.
a   8
             140.0e5                0.50              3.6e-1                 30.
a   9
             140.0e5               10.50                0.99                 30.
a  10
             140.0e5               10.50               0.999                 30.
a  11
             140.0e5                0.50                0.99                 30.
A  14
            216.18e5                0.05               10.50                45.0
A  15
            216.18e5               10.05               10.50                45.0
A  16
            216.18e5             0.50000               10.50                45.0
A  17
            216.18e5             0.50000                0.50                45.0
A  18
            216.18e5                10.2                0.50                45.0
A  19
            216.18e5                10.2               10.50                45.0
A  20
            216.18e5                -2.0               10.50                45.0
A  21
            216.18e5                -6.0               10.50                45.0
A  22
            216.18e5                10.2               10.50               145.0
A  23
            216.18e5                -2.0               10.50               145.0
A  24
            216.18e5                -6.0               10.50               145.0

GENER----1----*----2----*----3----*----4----*----5----*----6----*----7----*----8

ENDCY----1----*----2----*----3----*----4----*----5----*----6----*----7----*----8
```

Figure 5.1.1. TOUGH2/ECO2N V2.0 input file (first part) for sample problem 1 – demonstration of initialization options (continued).

We emphasize that the preferred and recommended option is to initialize flow problems by means of the internally used primary variables (Table 2.1). The options of allowing salt and CO_2 mass fractions that are out of range were created as a convenience to users, to avoid "erroneous initialization" errors when running TOUGH2/ECO2N V2.0.

```
    PRIMARY VARIABLES

     AT ELEMENT *a   1* ---   0.400000E+07  0.000000E+00  0.390000E-01  0.300000E+02
     AT ELEMENT *a   2* ---   0.400000E+07  0.000000E+00  0.108652E+02  0.300000E+02
     AT ELEMENT *a   3* ---   0.340000E+08  0.000000E+00  0.660000E-01  0.300000E+02
     AT ELEMENT *a   4* ---   0.340000E+08  0.100080E+02  0.106981E+02  0.300000E+02
     AT ELEMENT *a   5* ---   0.140000E+08  0.104660E+00  0.360000E-01  0.300000E+02
     AT ELEMENT *a   6* ---   0.140000E+08  0.104660E+00  0.103950E+02  0.300000E+02
     AT ELEMENT *a   7* ---   0.140000E+08  0.101997E+02  0.100235E+02  0.300000E+02
     AT ELEMENT *a   8* ---   0.140000E+08  0.101266E+02  0.103810E+02  0.300000E+02
     AT ELEMENT *a   9* ---   0.140000E+08  0.105000E+02  0.104969E+02  0.300000E+02
     AT ELEMENT *a  10* ---   0.140000E+08  0.105000E+02  0.999000E+00  0.300000E+02
     AT ELEMENT *a  11* ---   0.140000E+08  0.100016E+02  0.109923E+02  0.300000E+02
     AT ELEMENT *A  14* ---   0.216180E+08  0.500000E-01  0.105000E+02  0.450000E+02
     AT ELEMENT *A  15* ---   0.216180E+08  0.100500E+02  0.105000E+02  0.450000E+02
     AT ELEMENT *A  16* ---   0.216180E+08  0.101016E+02  0.105000E+02  0.450000E+02
     AT ELEMENT *A  17* ---   0.216180E+08  0.100958E+02  0.105286E+02  0.450000E+02
     AT ELEMENT *A  18* ---   0.216180E+08  0.102000E+02  0.104676E+02  0.450000E+02
     AT ELEMENT *A  19* ---   0.216180E+08  0.102000E+02  0.105000E+02  0.450000E+02
     AT ELEMENT *A  20* ---   0.216180E+08  0.104661E+00  0.105000E+02  0.450000E+02
     AT ELEMENT *A  21* ---   0.216180E+08  0.259637E+00  0.105000E+02  0.450000E+02
     AT ELEMENT *A  22* ---   0.216180E+08  0.102000E+02  0.105000E+02  0.145000E+03
     AT ELEMENT *A  23* ---   0.216180E+08  0.104661E+00  0.105000E+02  0.145000E+03
     AT ELEMENT *A  24* ---   0.216180E+08  0.259637E+00  0.105000E+02  0.145000E+03
```

Figure 5.1.2. Primary variables internally used in ECO2N V2.0 for the INCON data given in Fig. 5.1.1.

```
     *rtab* ... initialization test for ECO2N

          OUTPUT DATA AFTER (   1,  1)-2-TIME STEPS                          THE TIME IS 0.115741E-13 DAYS

@@@@@@@@@@@@@@@@@@@@@@@@@@@@@@@@@@@@@@@@@@@@@@@@@@@@@@@@@@@@@@@@@@

       TOTAL TIME     KCYC   ITER  ITERC   KON       DX1M        DX2M        DX3M         MAX. RES.      NER    KER       DELTEX

       0.100000E-08     1      1      1     2      0.00000E+00  0.00000E+00  0.00000E+00    0.00000E+00      1     1      0.10000E-08

@@@@@@@@@@@@@@@@@@@@@@@@@@@@@@@@@@@@@@@@@@@@@@@@@@@@@@@@@@@@@@@@@@

       ELEM. INDEX   P        T      SG        SS       XNACL      YH2OG      XCO2aq      PCAP     k-red.     DG       DL

                    (Pa)    (deg-C)                                                       (Pa)              (kg/m3)    (kg/m3)

       a   1   1 0.40000E+07  30.00 0.00000E+00 0.00000E+00 0.00000E+00 0.00000E+00 0.39000E-01 0.00000E+00 0.10000E+01    0.00   1004.90

       a   2   2 0.40000E+07  30.00 0.86520E+00 0.00000E+00 0.00000E+00 0.63109E-03 0.39454E-01 -.21040E+06 0.10000E+01   90.07   1004.99

       a   3   3 0.34000E+08  30.00 0.00000E+00 0.00000E+00 0.00000E+00 0.00000E+00 0.66000E-01 0.00000E+00 0.10000E+01    0.00   1020.79

       a   4   4 0.34000E+08  30.00 0.69810E+00 0.80125E-02 0.26055E+00 0.15528E-02 0.17890E-01 -.79901E+05 0.10000E+01  966.03   1209.48

       a   5   5 0.14000E+08  30.00 0.00000E+00 0.00000E+00 0.10089E+00 0.00000E+00 0.36000E-01 0.00000E+00 0.10000E+01    0.00   1077.59

       a   6   6 0.14000E+08  30.00 0.39503E+00 0.00000E+00 0.10085E+00 0.15214E-02 0.36419E-01 -.28543E+05 0.10000E+01  836.42   1077.66

       a   7   7 0.14000E+08  30.00 0.23480E-01 0.19966E+00 0.26112E+00 0.13455E-02 0.15733E-01 -.44443E+04 0.10000E+01  836.36   1200.64

       a   8   8 0.14000E+08  30.00 0.38104E+00 0.12655E+00 0.26112E+00 0.13455E-02 0.15733E-01 -.32229E+05 0.10000E+01  836.36   1200.64

       a   9   9 0.14000E+08  30.00 0.49693E+00 0.50000E+00 0.26112E+00 0.13455E-02 0.15733E-01 -.83013E+07 0.10000E+01  836.36   1200.64

       a  10  10 0.14000E+08  30.00 0.50000E+00 0.50000E+00 0.00000E+00 0.10000E-02 0.15733E-01 -.10000E+08 0.10000E+01  836.22   1000.76

       a  11  11 0.14000E+08  30.00 0.99228E+00 0.15781E-02 0.26112E+00 0.13455E-02 0.15733E-01 -.83013E+07 0.10000E+01  836.36   1200.64

       A  14  12 0.21618E+08  45.00 0.50000E+00 0.00000E+00 0.47736E-01 0.25023E-02 0.45289E-01 -.38997E+05 0.10000E+01  829.91   1040.26

       A  15  13 0.21618E+08  45.00 0.50000E+00 0.50000E-01 0.26328E+00 0.21334E-02 0.16025E-01 -.42289E+05 0.10000E+01  829.76   1200.88

       A  16  14 0.21618E+08  45.00 0.50000E+00 0.10155E+00 0.26328E+00 0.21334E-02 0.16025E-01 -.46536E+05 0.10000E+01  829.76   1200.88

       A  17  15 0.21618E+08  45.00 0.52855E+00 0.95754E-01 0.26328E+00 0.21334E-02 0.16025E-01 -.51022E+05 0.10000E+01  829.76   1200.88

       A  18  16 0.21618E+08  45.00 0.46762E+00 0.20000E+00 0.26328E+00 0.21334E-02 0.16025E-01 -.51022E+05 0.10000E+01  829.76   1200.88

       A  19  17 0.21618E+08  45.00 0.50000E+00 0.20000E+00 0.26328E+00 0.21334E-02 0.16025E-01 -.58702E+05 0.10000E+01  829.76   1200.88

       A  20  18 0.21618E+08  45.00 0.50000E+00 0.00000E+00 0.10097E+00 0.24195E-02 0.35269E-01 -.38997E+05 0.10000E+01  829.87   1075.80

       A  21  19 0.21618E+08  45.00 0.50000E+00 0.00000E+00 0.25531E+00 0.21487E-02 0.16655E-01 -.38997E+05 0.10000E+01  829.77   1194.06

       A  22  20 0.21618E+08 145.00 0.50000E+00 0.20000E+00 0.29062E+00 0.17166E-01 0.14534E-01 -.58702E+05 0.10000E+01  367.28   1157.97

       A  23  21 0.21618E+08 145.00 0.50000E+00 0.00000E+00 0.10139E+00 0.20282E-01 0.31256E-01 -.38997E+05 0.10000E+01  370.38   1010.73

       A  24  22 0.21618E+08 145.00 0.50000E+00 0.00000E+00 0.25542E+00 0.17791E-01 0.16227E-01 -.38997E+05 0.10000E+01  367.88   1128.87
```

Figure 5.1.3. Output data for sample problem 1.

5.2 Problem No. 2 (*rcc3*) - Radial Flow from a CO_2 Injection Well

This is the basic problem of CO_2 injection into a saline aquifer, examining two-phase flow with CO_2 displacing (saline) water under conditions that may be encountered in brine aquifers at a depth of approximately 1.2 km. A CO_2 injection well fully penetrates a homogeneous, isotropic, infinite-acting aquifer of 100 m thickness (Fig. 5.2.1), at conditions of 120 bar pressure, 45 ˚C temperature, and a salinity of 15 % by weight. CO_2 is injected uniformly at a constant rate of 100 kg/s. This problem had been included as test problem #3 in a code intercomparison project (Pruess et al., 2002, 2004); full specifications are given in Appendix A.

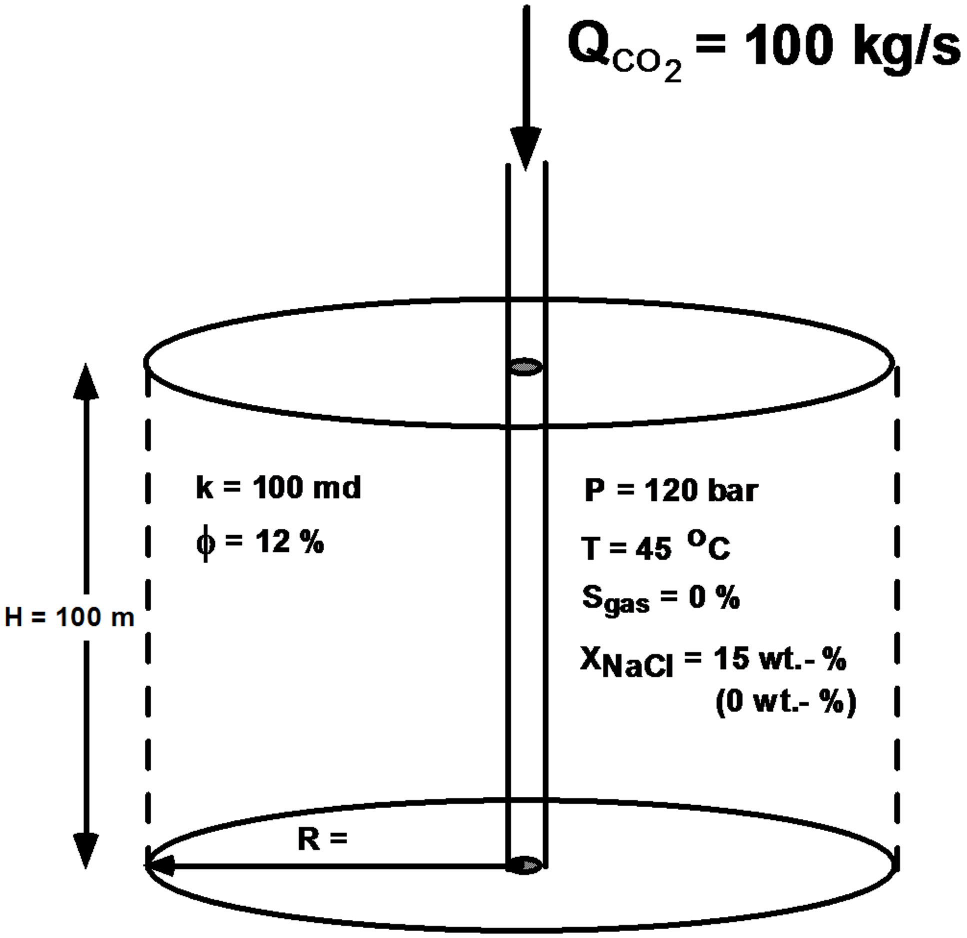

Figure 5.2.1. Schematic of sample problem 2.

The TOUGH2 input file used for grid generation is shown in Fig. 5.2.2. The well is modeled as a circular grid element of R = 0.3 m (≈ 12"). The numerical grid is extended to a large distance of 100 km, so that the system would be infinite-acting for the time period simulated (10,000 days, 27.38 years). Prior to the flow simulation, a minor amount of editing is performed on the MESH file. The well block is assigned to a domain #2, with a view on facilitating running of a non-isothermal variation of the problem. Further, the nodal distance corresponding to the well block was changed to an infinitesimal value. A fragment of the modified MESH file is shown in Fig. 5.2.3, and the TOUGH2 input file used for the simulation is shown in Fig. 5.2.4. The simulation is performed in isothermal mode (NEQ = 3 in data block MULTI). A separate ROCKS domain 'well ' with "infinite" rock grain density was included in the input file to enable running of a non-isothermal variation simply by setting NEQ = 4; the well block "A1 1" is assigned to domain 'well ' with "infinite" rock grain density, so that CO_2 injection would effectively occur at initial temperature of 45 ˚C, obviating the need for specifying an injection enthalpy. Part of the output generated from this problem is shown in Fig. 5.2.5. As can be seen, salt is precipitating around the injection well, but associated permeability reduction is turned off (IE(11) = 0).

```
*rcc3* ... Code Intercomparison problem3: Radial flow from a
MESHMAKER1----*----2----*----3----*----4----*----5----*----6-
RZ2D
RADII
    1
        0.
EQUID
    1             .3
LOGAR
  200           1.E3
LOGAR
  100           3.E3
LOGAR
  100           1.E4
LOGAR
   34           1.E5
LAYER----1----*----2----*----3----*----4----*----5----*----6-
    1
      100.

ENDFI----1----*----2----*----3----*----4----*----5----*----6-
```

Figure 5.2.2. TOUGH2 input file for grid generation for radial injection problem.

```
ELEME ---   435    1    1  434    .00000100000.000
A1  1              2 .2827E+02 .5655E+00                   .3000E+00
A1  2              1 .8728E+02 .1746E+01                   .4532E+00
A1  3              1 .1501E+03 .3002E+01                   .7630E+00
A1  4              1 .2169E+03 .4339E+01                   .1079E+01
...
...

CONNE
A1  1A1  2                   1 .1500E-05 .1532E+00 .1885E+03
A1  2A1  3                   1 .1532E+00 .1565E+00 .3811E+03
A1  3A1  4                   1 .1565E+00 .1599E+00 .5778E+03
...
```

Figure 5.2.3. Modified MESH file for radial injection problem.

```
*rcc3* ... Code Intercomparison problem3: Radial flow from a
ROCKS----1----*----2----*----3----*----4----*----5----*----6-
SAND     2  2600.e00       .12  100.e-15  100.e-15  100.e-15
   4.5e-10
    7           .457       .30        1.       .05
    7           .457       .00    5.1e-5      1.e7      .999
well     2  2600.e40       .12  100.e-15  100.e-15  100.e-15
   4.5e-10
    7           .457       .30        1.       .05
    7           .457       .00    5.1e-5      1.e7      .999

MULTI----1----*----2----*----3----*----4----*----5----*----6-
    3    3    3    6
SELEC....2....3....4....5....6....7....8....9...10...11...12.
    1                                       0    0    0    0
        .8   .8
SOLVR----1----*----2----*----3----*----4----*----5----*----6-
5  Z1   O0    8.0e-1    1.0e-7
START----1----*----2----*----3----*----4----*----5----*----6-
----*----1 MOP: 123456789*123456789*1234 ---*----5----*----6-
PARAM----1----*----2----*----3----*----4----*----5----*----6-
   1 999     9991000300000000  4    3
              8.64e8       -1.
        1.
     1.E-5     1.E00
              120.e5                 .15                 0.0
FOFT ----1----*----2----*----3----*----4----*----5----*----6-
A1 49              1 .1745E+04 .2685E+03                   .2570E+02
A12 2              1 .3080E+08 .4738E+07                   .1080E+04

GENER----1----*----2----*----3----*----4----*----5----*----6-
A1  1inj 1                         COM3       100.

INCON----1----*----2----*----3----*----4----*----5----*----6-

TIMES----1----*----2----*----3----*----4----*----5----*----6-
    4
 2.592E+06  8.64E+06  8.64E+07  8.64E+08
ENDCY----1----*----2----*----3----*----4----*----5----*----6-
```

Figure 5.2.4. TOUGH2 input file for radial injection problem.

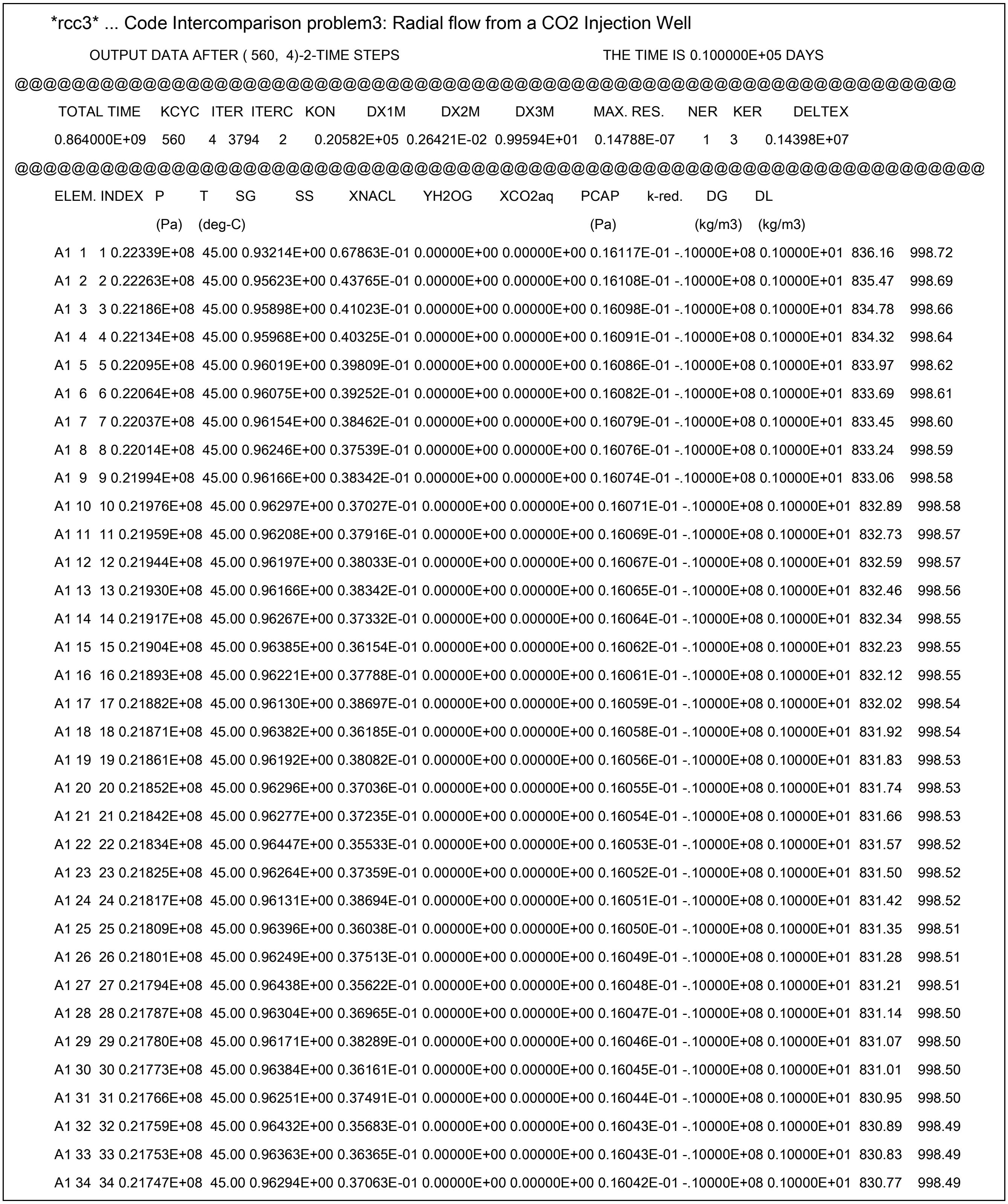

```
     *rcc3* ... Code Intercomparison problem3: Radial flow from a CO2 Injection Well
          OUTPUT DATA AFTER ( 560,  4)-2-TIME STEPS                               THE TIME IS 0.100000E+05 DAYS
@@@@@@@@@@@@@@@@@@@@@@@@@@@@@@@@@@@@@@@@@@@@@@@@@@@@@@@@@@@@@@@@@@@@@@@@@@@@@@@@@@@@@@@@
     TOTAL TIME   KCYC  ITER  ITERC   KON      DX1M       DX2M       DX3M       MAX. RES.    NER   KER       DELTEX
    0.864000E+09   560     4  3794     2      0.20582E+05  0.26421E-02  0.99594E+01   0.14788E-07     1     3      0.14398E+07
@@@@@@@@@@@@@@@@@@@@@@@@@@@@@@@@@@@@@@@@@@@@@@@@@@@@@@@@@@@@@@@@@@@@@@@@@@@@@@@@@@@@@@@@@@@@
    ELEM. INDEX  P       T     SG        SS       XNACL      YH2OG      XCO2aq      PCAP      k-red.     DG       DL
                (Pa)    (deg-C)                                                     (Pa)                (kg/m3)   (kg/m3)
    A1  1   1 0.22339E+08  45.00 0.93214E+00 0.67863E-01 0.00000E+00 0.00000E+00 0.16117E-01 -.10000E+08 0.10000E+01  836.16    998.72
    A1  2   2 0.22263E+08  45.00 0.95623E+00 0.43765E-01 0.00000E+00 0.00000E+00 0.16108E-01 -.10000E+08 0.10000E+01  835.47    998.69
    A1  3   3 0.22186E+08  45.00 0.95898E+00 0.41023E-01 0.00000E+00 0.00000E+00 0.16098E-01 -.10000E+08 0.10000E+01  834.78    998.66
    A1  4   4 0.22134E+08  45.00 0.95968E+00 0.40325E-01 0.00000E+00 0.00000E+00 0.16091E-01 -.10000E+08 0.10000E+01  834.32    998.64
    A1  5   5 0.22095E+08  45.00 0.96019E+00 0.39809E-01 0.00000E+00 0.00000E+00 0.16086E-01 -.10000E+08 0.10000E+01  833.97    998.62
    A1  6   6 0.22064E+08  45.00 0.96075E+00 0.39252E-01 0.00000E+00 0.00000E+00 0.16082E-01 -.10000E+08 0.10000E+01  833.69    998.61
    A1  7   7 0.22037E+08  45.00 0.96154E+00 0.38462E-01 0.00000E+00 0.00000E+00 0.16079E-01 -.10000E+08 0.10000E+01  833.45    998.60
    A1  8   8 0.22014E+08  45.00 0.96246E+00 0.37539E-01 0.00000E+00 0.00000E+00 0.16076E-01 -.10000E+08 0.10000E+01  833.24    998.59
    A1  9   9 0.21994E+08  45.00 0.96166E+00 0.38342E-01 0.00000E+00 0.00000E+00 0.16074E-01 -.10000E+08 0.10000E+01  833.06    998.58
    A1 10  10 0.21976E+08  45.00 0.96297E+00 0.37027E-01 0.00000E+00 0.00000E+00 0.16071E-01 -.10000E+08 0.10000E+01  832.89    998.58
    A1 11  11 0.21959E+08  45.00 0.96208E+00 0.37916E-01 0.00000E+00 0.00000E+00 0.16069E-01 -.10000E+08 0.10000E+01  832.73    998.57
    A1 12  12 0.21944E+08  45.00 0.96197E+00 0.38033E-01 0.00000E+00 0.00000E+00 0.16067E-01 -.10000E+08 0.10000E+01  832.59    998.57
    A1 13  13 0.21930E+08  45.00 0.96166E+00 0.38342E-01 0.00000E+00 0.00000E+00 0.16065E-01 -.10000E+08 0.10000E+01  832.46    998.56
    A1 14  14 0.21917E+08  45.00 0.96267E+00 0.37332E-01 0.00000E+00 0.00000E+00 0.16064E-01 -.10000E+08 0.10000E+01  832.34    998.55
    A1 15  15 0.21904E+08  45.00 0.96385E+00 0.36154E-01 0.00000E+00 0.00000E+00 0.16062E-01 -.10000E+08 0.10000E+01  832.23    998.55
    A1 16  16 0.21893E+08  45.00 0.96221E+00 0.37788E-01 0.00000E+00 0.00000E+00 0.16061E-01 -.10000E+08 0.10000E+01  832.12    998.55
    A1 17  17 0.21882E+08  45.00 0.96130E+00 0.38697E-01 0.00000E+00 0.00000E+00 0.16059E-01 -.10000E+08 0.10000E+01  832.02    998.54
    A1 18  18 0.21871E+08  45.00 0.96382E+00 0.36185E-01 0.00000E+00 0.00000E+00 0.16058E-01 -.10000E+08 0.10000E+01  831.92    998.54
    A1 19  19 0.21861E+08  45.00 0.96192E+00 0.38082E-01 0.00000E+00 0.00000E+00 0.16056E-01 -.10000E+08 0.10000E+01  831.83    998.53
    A1 20  20 0.21852E+08  45.00 0.96296E+00 0.37036E-01 0.00000E+00 0.00000E+00 0.16055E-01 -.10000E+08 0.10000E+01  831.74    998.53
    A1 21  21 0.21842E+08  45.00 0.96277E+00 0.37235E-01 0.00000E+00 0.00000E+00 0.16054E-01 -.10000E+08 0.10000E+01  831.66    998.53
    A1 22  22 0.21834E+08  45.00 0.96447E+00 0.35533E-01 0.00000E+00 0.00000E+00 0.16053E-01 -.10000E+08 0.10000E+01  831.57    998.52
    A1 23  23 0.21825E+08  45.00 0.96264E+00 0.37359E-01 0.00000E+00 0.00000E+00 0.16052E-01 -.10000E+08 0.10000E+01  831.50    998.52
    A1 24  24 0.21817E+08  45.00 0.96131E+00 0.38694E-01 0.00000E+00 0.00000E+00 0.16051E-01 -.10000E+08 0.10000E+01  831.42    998.52
    A1 25  25 0.21809E+08  45.00 0.96396E+00 0.36038E-01 0.00000E+00 0.00000E+00 0.16050E-01 -.10000E+08 0.10000E+01  831.35    998.51
    A1 26  26 0.21801E+08  45.00 0.96249E+00 0.37513E-01 0.00000E+00 0.00000E+00 0.16049E-01 -.10000E+08 0.10000E+01  831.28    998.51
    A1 27  27 0.21794E+08  45.00 0.96438E+00 0.35622E-01 0.00000E+00 0.00000E+00 0.16048E-01 -.10000E+08 0.10000E+01  831.21    998.51
    A1 28  28 0.21787E+08  45.00 0.96304E+00 0.36965E-01 0.00000E+00 0.00000E+00 0.16047E-01 -.10000E+08 0.10000E+01  831.14    998.50
    A1 29  29 0.21780E+08  45.00 0.96171E+00 0.38289E-01 0.00000E+00 0.00000E+00 0.16046E-01 -.10000E+08 0.10000E+01  831.07    998.50
    A1 30  30 0.21773E+08  45.00 0.96384E+00 0.36161E-01 0.00000E+00 0.00000E+00 0.16045E-01 -.10000E+08 0.10000E+01  831.01    998.50
    A1 31  31 0.21766E+08  45.00 0.96251E+00 0.37491E-01 0.00000E+00 0.00000E+00 0.16044E-01 -.10000E+08 0.10000E+01  830.95    998.50
    A1 32  32 0.21759E+08  45.00 0.96432E+00 0.35683E-01 0.00000E+00 0.00000E+00 0.16043E-01 -.10000E+08 0.10000E+01  830.89    998.49
    A1 33  33 0.21753E+08  45.00 0.96363E+00 0.36365E-01 0.00000E+00 0.00000E+00 0.16043E-01 -.10000E+08 0.10000E+01  830.83    998.49
    A1 34  34 0.21747E+08  45.00 0.96294E+00 0.37063E-01 0.00000E+00 0.00000E+00 0.16042E-01 -.10000E+08 0.10000E+01  830.77    998.49
```

Figure 5.2.5. Part of printed output for radial flow problem.

An important advantage of the radial flow problem considered here is that it admits a similarity solution. Specifically, the solution depends on radial distance R and time t only through the similarity variable $\xi = R^2/t$, even when taking into account all the non-linearities due to PVT properties and two-phase flow (O'Sullivan, 1981; Doughty and Pruess, 1992). The space and time discretization employed for finite difference simulation will violate the rigorous R^2/t invariance, so that the similarity property will be maintained only approximately. The accuracy of the numerical simulation can be checked by plotting the results as a function of the similarity variable R^2/t. Fig. 5.2.6 shows the results for pressure as a function of the similarity variable. Data were plotted from the time series data for grid block A1 49, at a radial distance of R = 25.25 m, which were generated by means of FOFT specifications in the input file (Fig. 5.2.4). The agreement between ECO2N V2.0 and ECO2N V1.0 is excellent. The slightly different solubility calculation does not have significant impact on the simulated pressure response. The impact of the water in the gas phase on the thermophysical properties (which is ignored in V1.0) is not significant either, because the amount of water in the CO_2-rich phase is very small under these pressure and temperature conditions. Fig. 5.2.7 presents simulated results for gas saturation as a function of the similarity variable, showing three distinct regions emerging from the CO_2 injection process. The first region with $R^2/t \leq 1.3\text{x}10^{-5}$ m^2/s corresponds to a zone where complete dry-out of aqueous phase has occurred. Gas saturation in this region is slightly less than 1, however, due to the presence of solid precipitate (Fig. 5.2.8). The dry-out zone is followed by an intermediate zone extending to $R^2/t \approx 10^{-2}$ m^2/s where liquid and gas phases coexist. Finally, there is an outer region with $R^2/t > 10^{-2}$ m^2/s in which single-phase liquid conditions prevail.

As shown in Fig. 5.2.8, ECO2N V2.0 predicts slightly higher solid salt saturation than ECO2N V1.0 in the dry-out zone. This is related to its different water-CO_2 solubility model as discussed in Section 2.1, which predicts lower dissolved CO_2 mass fraction in liquid phase (Figure 5.2.9). ECO2N V2.0 offers users an option to use the exact same water-CO_2 solubility model (for low temperature) as ECO2N V1.0 by setting IE(16)=1 in the input file, if 100% consistency with ECO2N V1.0 in the low temperature range is preferable.

The peculiar behavior of NaCl mass fraction in liquid seen in Fig. 5.2.10 is due to dissolution of CO_2. At large $R^2/t > 10^{-2}$ m^2/s, NaCl mass fraction is unchanged from the initial value of 0.15. The modest reduction of NaCl mass fraction to approximately 0.146 in the two-phase zone ($1.3\text{x}10^{-5}$ $m^2/s < R^2/t < 10^{-2}$ m^2/s) is due to the volume increase of the aqueous phase upon CO_2 dissolution. The sharp peak in NaCl concentration at the inner boundary of the two-phase zone ($R^2/t \approx 1.3\text{x}10^{-5}$ m^2/s) occurs because conditions are approaching dry-out there.

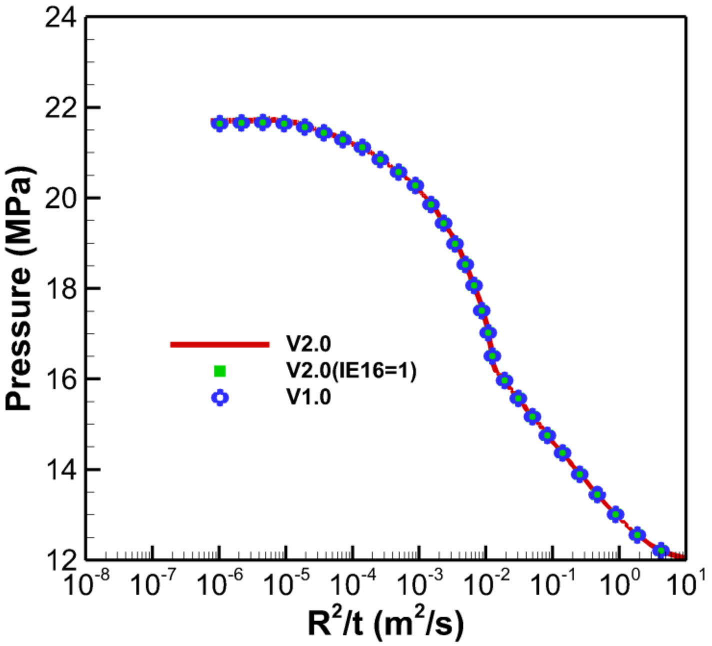

Figure 5.2.6. Simulated pressures as a function of the similarity variable. The thick solid red line represents the result simulated by new code (ECO2N V2.0) while the blue symbols represent the result simulated by ECO2N V1.0. The green symbols represent the result simulated by ECO2N V2.0 with IE(16)=1 to enforce using the exact same routines for calculation of mutual solubility in low T and gas phase properties as ECO2N V1.0. All results are time series of data for a grid block at a radial distance of R = 25.25 m.

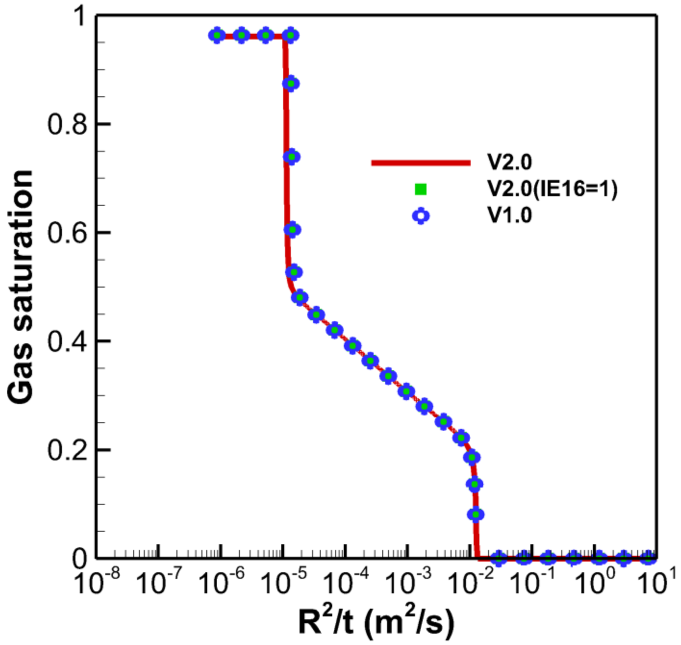

Figure 5.2.7. Simulated gas saturations.

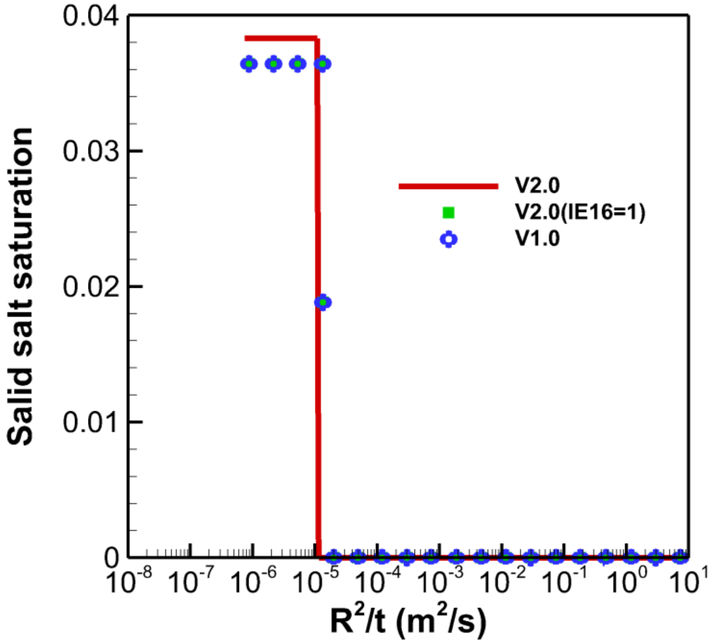

Figure 5.2.8. Simulated solid saturations.

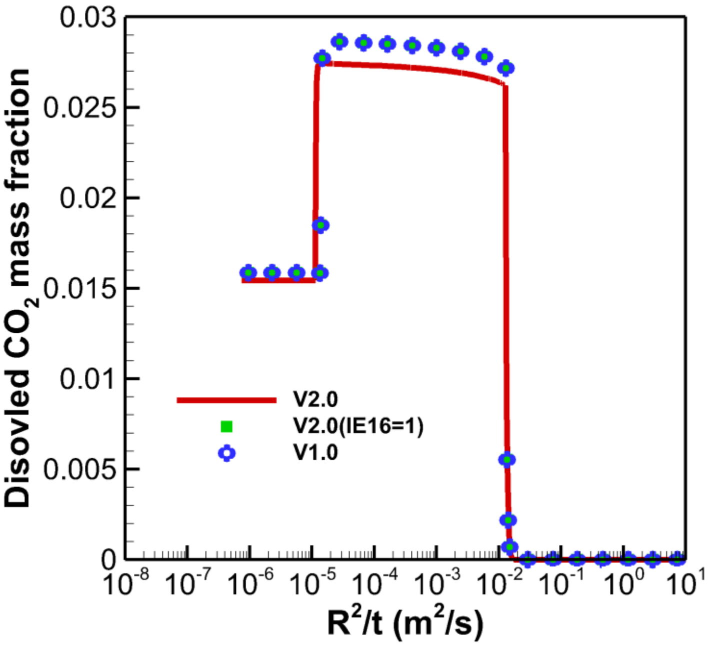

Figure 5.2.9. Simulated CO_2 mass fraction in aqueous phase.

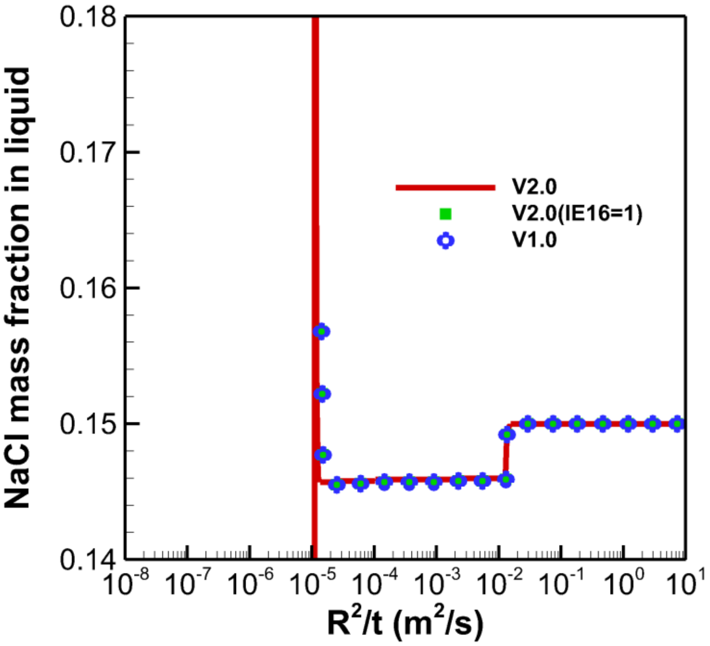

Figure 5.2.10. Simulated NaCl mass fraction in aqueous phase.

5.3 Problem No. 3 (*r1dv*) - CO_2 Discharge Along a Fault Zone

The amounts of CO_2 that would need to be disposed of at fossil-fueled power plants are very large. A coal-fired plant with a capacity of 1,000 MWe generates approximately 30,000 tonnes of CO_2 per day (Hitchon 1996). When disposed of into brine formations, CO_2 injection plumes would over time extend to large distances of the order of ten kilometers or more, making it likely that geologic discontinuities such as faults and fractures will be encountered, with an associated potential for CO_2 losses from the primary disposal aquifer. CO_2 leaks through caprock discontinuities have a potential for self-enhancement, because pressures can actually decrease and/or flow rates increase as escaping CO_2 creates a pathway towards shallower strata. It is not known whether or not it may be possible for a runaway process to develop where an initially “small” leak could accelerate and grow over time to the point of an eruptive release.

Migration of CO_2 along a water-saturated fault zone would be subject to gravitational and viscous instabilities, and would likely involve complex two- and three-dimensional flow effects. As a first approximation to this kind of problem, we consider here a highly simplified situation in which a potential CO_2 leakage path is modeled as a 500-m long 1-D column (Fig. B.1). This problem was also included as #4 in the code intercomparison project (Pruess et al., 2002, 2004); specifications are given in Appendix B.

The problem is run in two segments. A first run segment obtains gravity equilibrium relative to a pressure of 100 bar prescribed at the top boundary. The gravity-equilibrated conditions are then used as initial conditions in a second run segment, where conditions of $P = 240$ bar and a mass fraction $X_{CO2} = 1$ are maintained at the lower boundary, while upper boundary conditions are unchanged. Note that the CO_2 discharge conditions correspond to a large overpressure, exceeding initial hydrostatic pressure by approximately 60%. It is unlikely that overpressures this large would be used in practical CO_2 storage systems. All runs are performed for pure water (no salinity) in isothermal mode at $T = 45^\circ C$. Capillary pressure parameters were chosen so that maximum P_{cap} is 10^7 Pa, and P_{cap} vanishes for small gas saturations of $S_g \leq 0.001$. These and other simulation parameters can be seen from the TOUGH2 input file shown in Fig. 5.3.1. For this simple 1-D problem, the calculational mesh is generated simply by directly specifying "repeat" elements and connections in the TOUGH2 input file. The 500 m vertical extent of the fault zone is evenly divided into 100 grid blocks of 5 m height. Additional blocks *top 0* and *bot 0* are used to represent boundary conditions. For the 1 m length of the 25 m wide fault zone modeled, interface areas are 25 m^2. Input data also include COFT and FOFT blocks for generating output data for plotting. For reference we list representative fluid properties used in the simulation in Table 5.3.1.

```
*r1dv* ... 1-D vertical column; CO2 migration up a fault zone
ROCKS----1----*----2----*----3----*----4----*----5----*----6-
fault    2  2600.e00       .35  100.e-15  100.e-15  100.e-15
   4.5e-10
    7           .457       .30        1.       .05
    7           .457       .00    5.1e-5      1.e7      .999
CO2in    2  2600.e00       .35  100.e-15  100.e-15  100.e-15
   4.5e-10
    7           .457       .30        1.       .05
    8

MULTI----1----*----2----*----3----*----4----*----5----*----6-
    3    3    3    6
SELEC....2....3....4....5....6....7....8....9...10...11...12.
    1                                            0    0    0
        .8   .8
SOLVR----1----*----2----*----3----*----4----*----5----*----6-
5  Z1   O0    8.0e-1    1.0e-7
START----1----*----2----*----3----*----4----*----5----*----6-
----*----1 MOP: 123456789*123456789*1234 ---*----5----*----6-
START----1----*----2----*----3----*----4----*----5----*----6-
PARAM----1----*----2----*----3----*----4----*----5----*----6-
   11000    9999 000 00000000  4    3
                           -1.                          9.81
        1.        9.      9.e1      9.e2
     1.E-5     1.E00
              100.e5                 .00                 0.0
INDOM----1----*----2----*----3----*----4----*----5----*----6-
CO2in
              240.e5                 .00                 1.0

ELEME----1----*----2----*----3----*----4----*----5----*----6-
flt 0    99    1fault      125.
ina
top 0
bot 0          CO2in

CONNE----1----*----2----*----3----*----4----*----5----*----6-
bot 0flt 0                   3     1.e-3       2.5       25.
flt 0flt 1   98    1    1    3       2.5       2.5       25.
flt99top 0                   3       2.5     1.e-3       25.

COFT ----1----*----2----*----3----*----4----*----5----*----6-
bot 0flt 0                   3     1.e-3       2.5       25.
flt99top 0                   3       2.5     1.e-3       25.

FOFT ----1----*----2----*----3----*----4----*----5----*----6-
flt74
flt75

GENER----1----*----2----*----3----*----4----*----5----*----6-

TIMES----1----*----2----*----3----*----4----*----5----*----6-
    8
      1.E5      1.e6      1.e7      2.e7      1.e8      1.e9
ENDCY----1----*----2----*----3----*----4----*----5----*----6-
```

Figure 5.3.1. TOUGH2 input file for fault zone problem.

Table 5.3.1. PVT properties at a temperature of 45˚C at selected pressures, as used in the TOUGH2/ECO2N simulation.

Pressure (bar) fluid phase	120	160	200	240
pure water				
density (kg/m^3)	994.768	996.292	997.821	999.354
viscosity (Pa s)	5.97778e-4	5.98341e-4	5.98929e-4	5.99540e-4
water with CO_2				
density (kg/m^3)	1005.79	1008.00	1009.94	1011.74
viscosity (Pa s)	5.97778e-4	5.98341e-4	5.98929e-4	5.99540e-4
CO_2 mass fraction	5.20592e-2	5.55092e-2	5.76593e-2	5.91875e-2
gas				
density (kg/m^3)	659.261	760.931	813.504	850.176
viscosity (Pa s)	5.17641e-5	6.56503e-5	7.45231e-5	8.15904e-5
water mass fraction	2.14658e-3	2.41648e-3	2.54446e-3	2.62678e-3

5.3.1 Gravity Equilibration

Gravity-equilibrated initial conditions are obtained from a simulation in which the element *bot 0* is removed from the input file. Large time steps (Δt_1 = 1.e3, Δt_2 = 9.e3 s) are used, along with a tight convergence tolerance of RE1 = 1.e-10. Pore compressibility is set to 0 in this part of the simulation, so that porosity remains a constant 35% throughout as fluid pressures change. After 26 time steps and a simulation time of t = 4.08x10^9 seconds, an accurate hydrostatic equilibrium is obtained, with maximum pore velocities of 6.7x10^{-19} m/s. Pressure in the lowest grid block, 2.5 m above the lower boundary, is computed as 148.56 bar. ECO2N V1.0 is used to calculate the gravity equilibrium profile and the resulteding SAVE file will be used as INCON for simulations of CO_2 displacement by all codes in the next step.

5.3.2 CO_2 Displacement

Migration of CO_2 up the fault zone is simulated with the input file as given in Fig. 5.3.1, and using the SAVE file from the gravity equilibration as INCON. The main process in this problem is immiscible displacement of water by CO_2. In response to the applied step change in pressure at the bottom of the fault, CO_2 enters the system at the lower boundary and migrates up the fault, displacing some of the water and also partially dissolving in residual water, while some water also dissolves in the CO_2. The problem is also run using ECO2N V1.0 for comparison.

```
   *r1dv* ... 1-D vertical column; CO2 migration up a fault zone

        OUTPUT DATA AFTER (  12,  3)-2-TIME STEPS                          THE TIME IS 0.115741E+01 DAYS

@@@@@@@@@@@@@@@@@@@@@@@@@@@@@@@@@@@@@@@@@@@@@@@@@@@@@@@@@@@@@@@@@

     TOTAL TIME    KCYC   ITER  ITERC   KON      DX1M       DX2M       DX3M       MAX. RES.    NER   KER      DELTEX

    0.100000E+06    12     3    50    2     0.24500E+06  0.00000E+00  0.20341E-01   0.38201E-05     2    3     0.12600E+05

@@@@@@@@@@@@@@@@@@@@@@@@@@@@@@@@@@@@@@@@@@@@@@@@@@@@@@@@@@@@@@@@@

    ELEM. INDEX   P        T     SG        SS       XNACL      YH2OG      XCO2aq      PCAP      k-red.     DG       DL

                 (Pa)    (deg-C)                                                     (Pa)                (kg/m3)   (kg/m3)

    flt 0   1 0.23971E+08  45.00 0.20262E+00 0.00000E+00 0.00000E+00 0.26273E-02 0.57357E-01 -.15358E+05 0.10000E+01  850.24   1011.35

    flt 1   2 0.23419E+08  45.00 0.77164E-01 0.00000E+00 0.00000E+00 0.26153E-02 0.57124E-01 -.79464E+04 0.10000E+01  845.75   1011.10

    flt 2   3 0.22875E+08  45.00 0.00000E+00 0.00000E+00 0.00000E+00 0.10000E+01 0.10226E-01 0.00000E+00 0.10000E+01    0.00   1001.04

    flt 3   4 0.22714E+08  45.00 0.00000E+00 0.00000E+00 0.00000E+00 0.10000E+01 0.12666E-02 0.00000E+00 0.10000E+01    0.00    999.12

    flt 4   5 0.22553E+08  45.00 0.00000E+00 0.00000E+00 0.00000E+00 0.10000E+01 0.13427E-03 0.00000E+00 0.10000E+01    0.00    998.83

    flt 5   6 0.22392E+08  45.00 0.00000E+00 0.00000E+00 0.00000E+00 0.10000E+01 0.12938E-04 0.00000E+00 0.10000E+01    0.00    998.74

    flt 6   7 0.22232E+08  45.00 0.00000E+00 0.00000E+00 0.00000E+00 0.10000E+01 0.11673E-05 0.00000E+00 0.10000E+01    0.00    998.68
```

Figure 5.3.2. Part of printed output for fault leakage problem.

Part of the printed output is shown in Fig. 5.3.2. Simulation results are plotted in Figs. 5.3.3 – 5.3.7, with thick red solid lines representing the results of ECO2N V2.0, and thick blue dashed lines representing the results of ECO2N V1.0.

The simulated evolution of the system proceeds through four stages (Figs. 5.3.3, 5.3.4). In Stage 1, CO_2 enters the first grid block above the lower boundary, evolving a gas phase there and causing rapid pressurization that migrates up the fault. Stage 1 ends at approximately 10^4 seconds when the pressure pulse reaches the top of the fault, causing outflow of water to commence. During the subsequent Stage 2, the CO_2 displacement front migrates up the fault until, after about $3x10^7$ seconds, the front reaches the top.

At this time CO_2 discharge from the fault begins, while water discharge is reduced because of relative permeability effects, and also because capillary effects reduce the effective pressure gradient for the aqueous phase at the top of the fault. This is Stage 3, which lasts from approximately $3x10^7$ to $3x10^9$ seconds, is characterized by two-phase outflow of liquid and gas from the fault. Water continues to be removed from the fault not only by advection, but also by dissolution into the flowing gas phase, causing gas relative permeabilities and flow rates to increase. As gas saturations increase, capillary pressures get stronger, and at $3.1x10^9$ seconds the effective pressure gradient for the aqueous phase at the top of the fault reverses, leading to downflow of water from the top boundary. The water dissolves into the flowing CO_2 stream and is carried right back out at the top. Eventually the entire flow system dries out, and in Stage 4 we have a steady single-phase gas flow up the fault. TOUGH2 recognizes a steady state, and the simulation terminates after 368 time steps and a simulation time of $7.2x10^{11}$ seconds. The simulations terminated with ECO2N V1.0 after 449 time steps and a simulation time of $3.1x10^{11}$, mainly due to smaller time steps during the period of transition to Stage 4. Other than that, the two codes produced identical flux responses.

Simulation progress and time stepping reflect non-linearities of the flow processes. Many relatively small time steps are required toward the end of Stage 2 as the two-phase front approaches the upper boundary (Fig. 5.3.3). Smaller time steps again occur towards the end of Stage 3 when the dryout front approaches the top boundary.

Gas saturations are shown at times of 10^7 and 10^9 seconds in Fig. 5.3.5. The pressure profile at 10^7 seconds has a change in slope at an elevation of 215 m, due to the transition from two-phase conditions below to single-phase conditions above (Fig. 5.3.6). The pressure gradient in the two-phase zone is larger than in the single-phase region, indicating that mobility loss from relative permeability effects dominates over mobility gain from the lower viscosity of CO_2 as compared to water. At late time, pressure gradients are smaller in the single-phase dry-out region, due to increased fluid mobility there, while gradients are larger in the overlying two-phase zone. Upward movement of the dry-out zone results in increasing pressure gradients at the top of the fault, giving rise to a local maximum in water outflow rate at about $3x10^9$ s (Fig. 5.3.4). Simulated phase partitioning after 10^7 seconds is shown in Fig. 5.3.7. For the reasons discussed previously, ECO2N V2.0 predicts slightly lower CO_2 mass fraction in the aqueous phase. The user can use the option of IE(16)=1 to duplicate the results of ECO2N V1.0. As shown in these figures, this slightly different phase partition model does not result in any notable differences in all other variables of interest.

Results for the simulated CO_2 inventory of the system at t = 10^7 and $2x10^7$ seconds are given in Table 5.3.2. The slightly different phase partition model in ECO2N V2.0 results in a few percentages less

CO_2 inventory in the aqueous phase than ECO2N V1.0 but the total inventory in the system is very close (<1%).

Table 5.3.2. CO_2 inventory (unit: tonnes).

	ECO2N V2.0		ECO2N V1.0		ECO2N V2.0/ECO2N V1.0	
time (seconds)	10^7	2x10^7	10^7	2x10^7	10^7	2x10^7
gas phase	402.516	694.112	401.455	692.311	1.00264	1.00260
aqueous phase	82.643	142.460	85.322	147.252	0.96860	0.96746
total	485.160	836.572	486.777	839.563	0.99668	0.99644

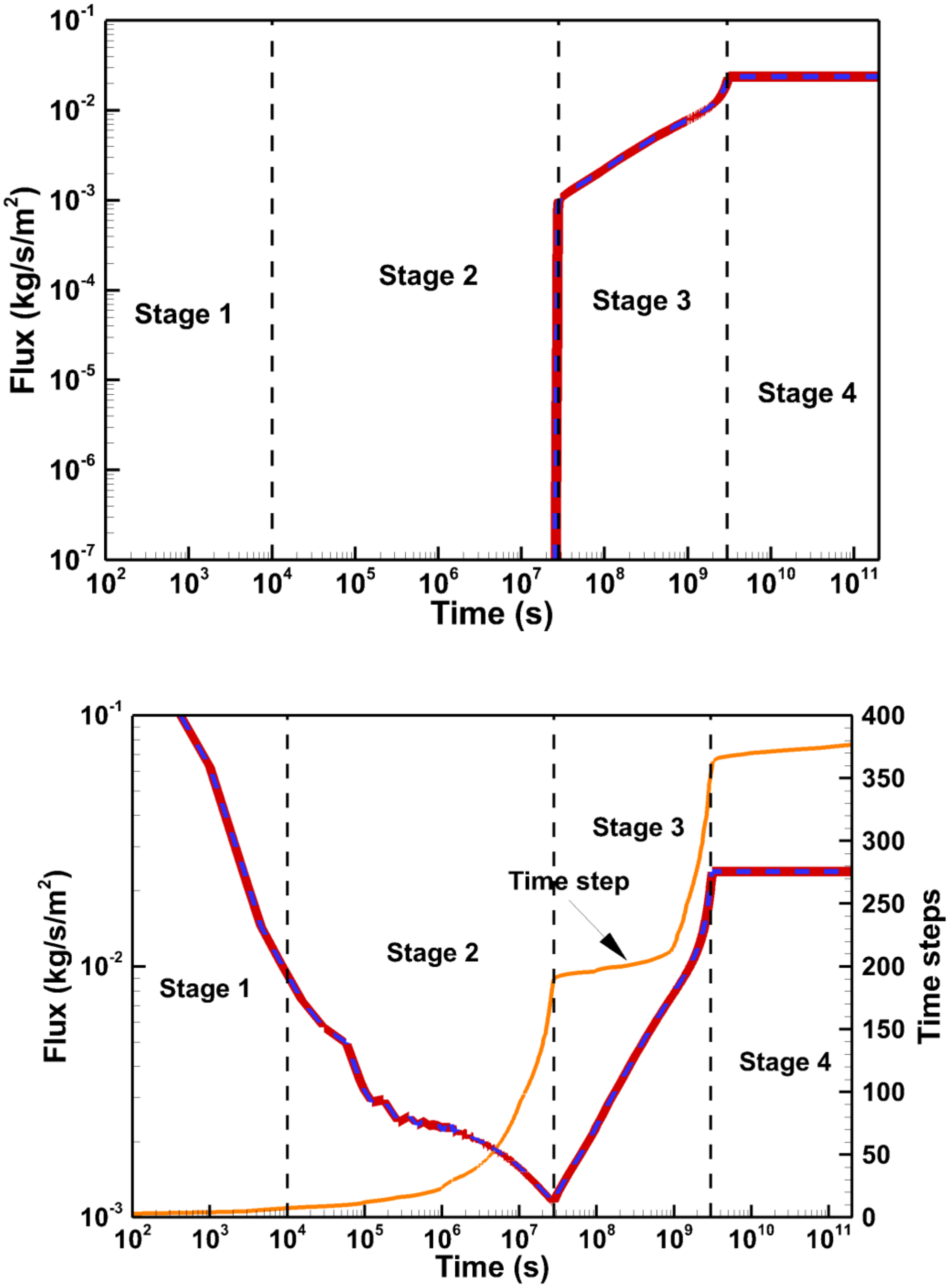

Figure 5.3.3. Simulated CO_2 fluxes at bottom (lower frame) and top (upper frame) of fault zone. Thick red lines are for ECO2N V2.0, while blue dashed lines are for ECO2N V1.0. Two curves are essentially identical. The dashed vertical lines mark the different stages in the evolution of the system.

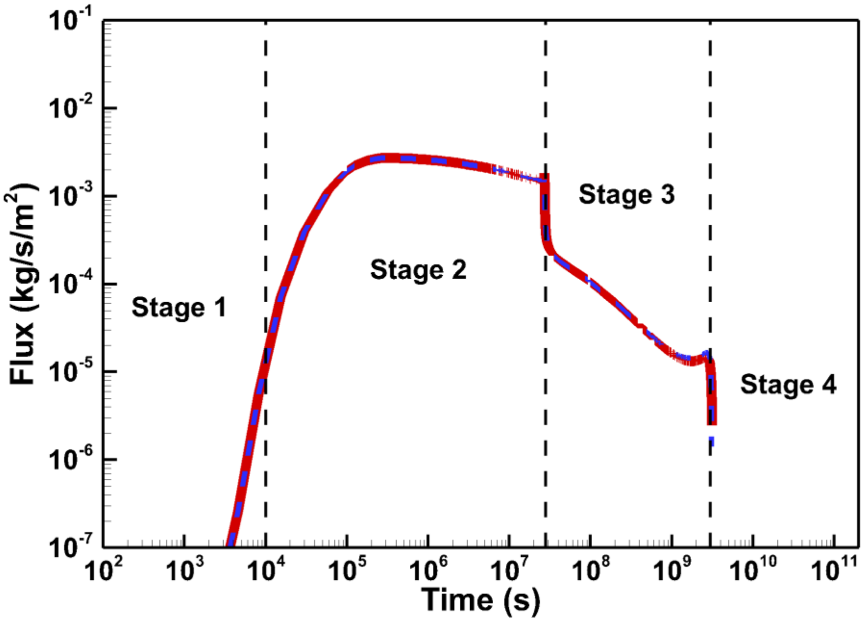

Figure 5.3.4. Simulated water flux at top of fault zone. Thick line is for ECO2N V2.0, and thin dash line is for ECO2N V1.0.

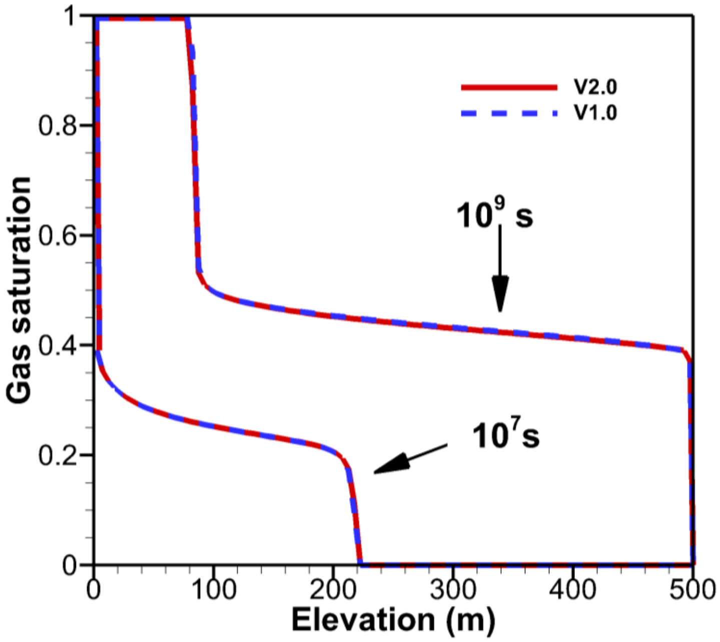

Figure 5.3.5. Gas saturation profiles at times of 10^7 and 10^9 seconds. Thick line is for ECO2N V2.0, and dashed line for ECO2N V1.0.

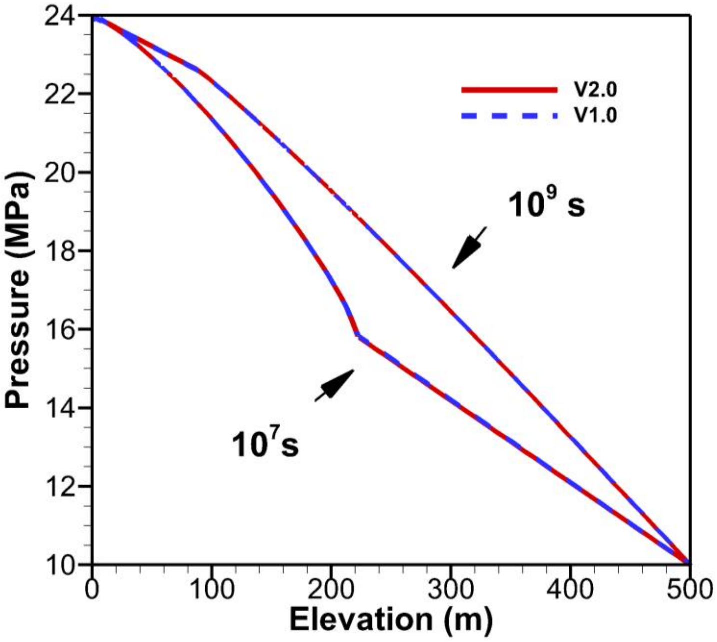

Figure 5.3.6. Pressure profiles at times of 10^7 and 10^9 seconds. Solid lines are for ECO2N V2.0, dashed lines for ECO2N V1.0.

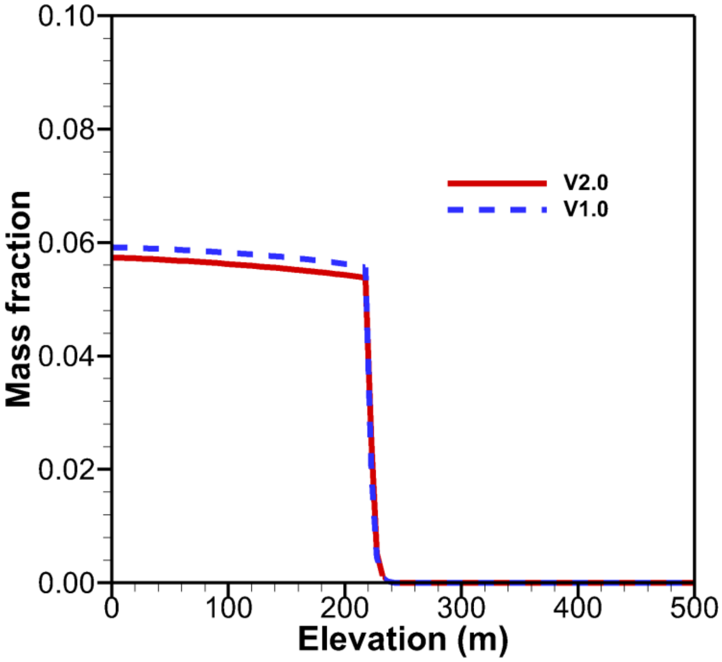

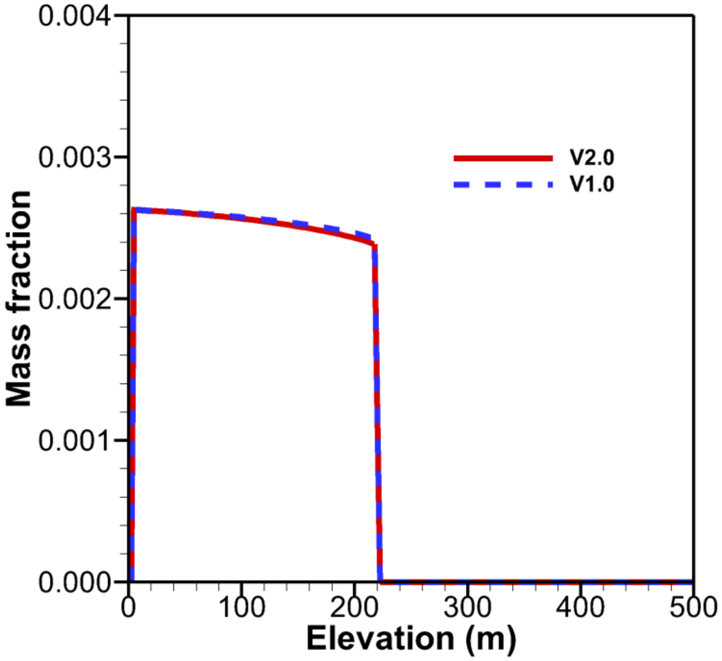

Figure 5.3.7. Dissolved CO_2 mass fraction in aqueous phase (top) and dissolved water mass fraction in gas phase (bottom) after 10^7 s. Thick lines are for ECO2N V2.0, and dashed lines for ECO2N V1.0.

5.4 Problem No. 4 (*rtp7*) - CO_2 Injection into a 2-D Layered Brine Formation

The first industrial-scale CO_2 disposal project to become operational is at the Sleipner Vest field in the Norwegian sector of the North Sea, where approximately 10^6 tonnes of CO_2 per year have been injected since 1996 through a horizontal well into sands of the Utsira formation. Time-lapse seismic surveys have shown that CO_2 migration at Sleipner is dominated by buoyancy effects and is strongly affected by shale interbeds of low permeability (Lindeberg et al., 2002). The present test problem was patterned after conditions at Sleipner and was designed to investigate CO_2 migration in a heterogeneous sand-shale sequence. It had been included as #7 in the code intercomparison project (Pruess et al., 2002, 2004). A 2-D vertical section was modeled (Fig. C.1, Appendix C), with problem specifications given in Appendix C. The problem was run in several segments to first obtain the initial and boundary conditions, and then inject CO_2 according to specifications. All runs were performed in isothermal mode at a temperature of 37 ˚C and a salinity of 3.2 wt.-% NaCl.

The grid should be designed in such a way as to obtain “adequate” spatial resolution in regions where significant gradients occur, i.e., near the injection well, and near the shale layers (Fig. C.1). The grid is generated with the MESHMAKER facility of TOUGH2 as a horizontal (x-y) grid and is then rotated by 90 degrees around the x-axis to obtain a vertical section. Subroutine GXYZ was modified to automatically assign “sand” and “shale” domain identifiers to grid blocks at the appropriate elevations (Fig. 5.4.1). Gridding in the x-direction starts with 1 m increments at the well, and becomes coarser at increasing distance (Table 5.4.1). 28 grid blocks are used to get out to a distance of 6,000 m, followed by a small grid increment of 10^{-3} m to serve as boundary blocks to maintain a hydrostatic pressure profile. Gridding in the y-direction also uses a 1 m increment at the well, with coarser gridding below and above. The shale layers are represented as single grid layers of 3 m height, with 3 m gridding also in the sands above and below. The thickness of the grid is 1 m. Overall the gridding is considered rather coarse, meeting minimum requirements for spatial resolution at the well and at the shale layers.

```
      DO1 J=1,NY
      JM=MOD(J-1,35)+1
      NOVJ=(J-1)/35
      IF(J.GT.1) YJ=YJ+DY(J)/2.+DY(J-1)/2.
c
c.....10-12-01: add domain identifiers
      dom='sand '
      yj52=yj-52.
      if(yj52.ge.0..and.mod(yj52,33.).le.3.) dom='shale'
```

Figure 5.4.1. Code fragment of subroutine GXYZ (module meshm.f), showing modifications for assigning domain identifiers to the heterogeneous sand-shale medium.

Table 5.4.1. MESHMAKER input data for grid generation.

```
MESHMAKER1----*----2----*----3----*----4----*----5----*----6----*----7----*----8
XYZ
       90.
NX      29
        1.        1.        2.        4.        4.        8.       15.       20.
       30.       40.       50.       50.      100.      150.       50.      150.
      300.       50.      475.      500.      500.      500.      500.      500.
      500.      500.      500.      500.     1.e-3
NY      34
        7.        6.        6.       2.5        1.       2.5        6.       12.
        6.        3.        3.        3.        6.       12.        6.        3.
        3.        3.        6.       12.        6.        3.        3.        3.
        6.       12.        6.        3.        3.        3.        6.       12.
        6.        3.
NZ       1       1.0


ENDFI----1----*----2----*----3----*----4----*----5----*----6----*----7----*----8
```

5.4.1 Gravity Equilibration

Initial conditions are generated in stages. A first simulation run uses a slightly modified version of the input file shown in Fig. 5.4.2 and involves just the column of boundary grid blocks beyond x = 6,000 m. Thermodynamic properties are specified as P = 110 bars, T = 37 ˚C, salinity X_S = 0.032, CO_2 mass fraction X_{CO2} = 4.54104x10^{-4}. The latter value was obtained by trial and error, executing a few single-grid block initializations to obtain the desired P_{CO2} = 0.5 bar. Pressure is held constant at P = 110 bar at the elevation of the injection node (22 m) and the system is run to gravity equilibrium. To facilitate reaching an accurate equilibrium state, the shale layers are given the same absolute permeability as the sand layers for this simulation. Gravity equilibrium using a tight convergence tolerance of 10^{-8} is attained in seven time steps, corresponding to a simulation time of 3.25x10^{9} s. Maximum pore velocities in the equilibrium state are below 10^{-17} m/s. A second run with the full two-dimensional grid is then performed, using the same initialization as for the 1-D gravity equilibration just described, and maintaining the 1-D gravity equilibrium as boundary conditions at the right hand side. For this calculation we again specify the same absolute permeability for shale as for sand. Gravity equilibration in the 2-D grid takes 12 time steps and a simulation time of 2.93x10^9 s. Both gravity equilibration simulations were conducted by ECO2N V1.0.

5.4.2 Response to CO_2 Injection

CO_2 injection at a constant prescribed rate of 0.1585 kg/s is simulated with the input file as shown in Fig. 5.4.2. This input file specifies a total simulation time of 63.1152x10^6 s (2 years), with additional printout generated at times of 30 days (2.592x10^6 s) and one year (31.5576x10^6 s). A portion of the printed output is shown in Fig. 5.4.3, and results are given in Figs. 5.4.4-5.4.12

Startup of CO_2 injection causes pressures to rise initially, most strongly and rapidly in the well block, and less strongly and with some time delay at more distant locations (Fig. 5.4.4). The system quickly establishes quasi-steady flow conditions at the well block (Fig. 5.4.5), and the sum of the absolute values of the flow rates quickly approaches the total injection rate of 0.1585 kg/s. As gas saturations increase near the injection point, injection pressures actually decline slowly. The plot of time steps vs. time shows decreasing slope over time (Fig. 5.4.4), reflecting an overall trend towards increasing time step sizes as the simulation progresses.

Gas saturations at and near the well block (A15 1) show interesting non-monotonic behavior (Fig. 5.4.6), due to an interplay of gas-liquid counterflow, relative permeability effects and precipitation of solid salt. After approximately 4.5x10^6 s, gas saturation at the well block reaches a maximum value of 75.1 % and then declines slowly. This decline is caused by increasing salt precipitation (Fig. 5.4.7). Liquid saturation declines rapidly initially, but later almost stabilizes near 20 % (note the logarithmic time scale on Fig. 5.4.7), due to capillary-driven inflow of liquid from neighboring grid blocks. At early time liquid flow is away from the well block, but at approximately 5x10^5 s liquid flow reverses and subsequently is towards the well block, as capillary pressures there become stronger due to increasing gas saturation (Fig. 5.4.8). As time goes on, gas saturations in the blocks adjacent to the well block continue a slow increase (Fig. 5.4.6). This reduces relative permeability to liquid, but liquid flow rates into the well block remain essentially constant for a while, because increasing strength of capillary pressure in the well block compensates for the reduction in relative permeability. After approximately 10^7 s, capillary pressure in the well block reaches the cutoff value of 10^7 Pa specified in the input file (Fig. 5.4.2). Subsequently the flow of aqueous phase towards the well block brings in less water than is carried out by the gas phase, leading to accelerated precipitation and rapid dry-out. This explains the very rapid increase in gas saturation in the well block at approximately 1.1x10^7 s. Fig. 5.4.6 shows similar patterns of gas saturation behavior in grid blocks neighboring the well block that dry out at later times. The evolution of solid saturations in selected blocks is shown in Fig. 5.4.9.

```
*rtp7* ... test problem # 7: CO2 in layered formation
ROCKS----1----*----2----*----3----*----4----*----5----*----6----*----7----*----8
sand     2  2600.e00       .35    3.e-12    3.e-12    3.e-12      2.51      920.
   0.0e-10
    7           0.40      0.20        1.      0.05
    7           0.40      0.20   2.79e-4      1.e7      .999
shale    2  2600.e00     .1025   10.e-15   10.e-15   10.e-15      2.51      920.
   0.0e-10
    7           0.40      0.20        1.      0.05
    7           0.40      0.20   1.61e-5      1.e7      .999
MULTI----1----*----2----*----3----*----4----*----5----*----6----*----7----*----8
    3    3    3    6
SELEC....2....3....4....5....6....7....8....9...10...11...12...13...14...15...16
    1                                            0    0    0    0    0    0    0
        .8   .8
START----1----*----2----*----3----*----4----*----5----*----6----*----7----*----8
----*----1 MOP: 123456789*123456789*1234 ---*----5----*----6----*----7----*----8
PARAM----1----*----2----*----3----*----4----*----5----*----6----*----7----*----8
   1 600    99991000 00000000  4    3
           63.1152e6       -1.                             -9.81
      1.e2
     1.E-5     1.E00
              110.e5              3.2e-2         .454104e-03                 37.
SOLVR----1----*----2----*----3----*----4----*----5----*----6----*----7----*----8
5  Z1   O0    8.0e-1    1.0e-7
GENER----1----*----2----*----3----*----4----*----5----*----6----*----7----*----8
A15 1inj 1                   1     COM3      .1585
TIMES----1----*----2----*----3----*----4----*----5----*----6----*----7----*----8
    3
   2.592e6 31.5576e6 63.1152e6
FOFT ----1----*----2----*----3----*----4----*----5----*----6----*----7----*----8
A14 1          sand  .2500E+01 .5000E+01           .5000E+00 .2025E+02-.5000E+00
A15 1          sand  .1000E+01 .2000E+01           .5000E+00 .2200E+02-.5000E+00
A16 1          sand  .2500E+01 .5000E+01           .5000E+00 .2375E+02-.5000E+00
A1G 1          sand  .3000E+01 .6000E+01           .5000E+00 .8350E+02-.5000E+00
A15 2          sand  .1000E+01 .2000E+01           .1500E+01 .2200E+02-.5000E+00
COFT ----1----*----2----*----3----*----4----*----5----*----6----*----7----*----8
A14 1A15 1                   2 .1250E+01 .5000E+00 .1000E+01 .1000E+01
A15 1A15 2                   1 .5000E+00 .5000E+00 .1000E+01
A15 1A16 1                   2 .5000E+00 .1250E+01 .1000E+01 .1000E+01

ENDCY----1----*----2----*----3----*----4----*----5----*----6----*----7----*----8
```

Figure 5.4.2. TOUGH2 input file for CO_2 injection into a 2-D layered brine formation.

```
     *rtp7* ... test problem # 7: CO2 in layered formation

          OUTPUT DATA AFTER ( 118,  4)-2-TIME STEPS                               THE TIME IS 0.300000E+02 DAYS

@@@@@@@@@@@@@@@@@@@@@@@@@@@@@@@@@@@@@@@@@@@@@@@@@@@@@@@@@@@@@@@@@@

        TOTAL TIME    KCYC   ITER  ITERC   KON       DX1M        DX2M        DX3M         MAX. RES.     NER    KER       DELTEX

       0.259200E+07      118        4      784       2         0.15333E+05   0.40602E-02   0.20421E-01      0.20599E-06       351       3         0.48300E+05

@@@@@@@@@@@@@@@@@@@@@@@@@@@@@@@@@@@@@@@@@@@@@@@@@@@@@@@@@@@@@@@@@@

       ELEM. INDEX  P        T      SG         SS        XNACL       YH2OG       XCO2aq       PCAP       k-red.      DG       DL

                  (Pa)    (deg-C)                                                              (Pa)                 (kg/m3)    (kg/m3)


       A11 1   1 0.13065E+08  37.00 0.21797E+00 0.00000E+00 0.30477E-01 0.18344E-02 0.47519E-01 -.40146E+04 0.10000E+01  771.59   1028.40

       A12 1   2 0.13017E+08  37.00 0.35422E+00 0.00000E+00 0.30479E-01 0.18322E-02 0.47496E-01 -.73381E+04 0.10000E+01  770.68   1028.38

       A13 1   3 0.12975E+08  37.00 0.41386E+00 0.00000E+00 0.30484E-01 0.18303E-02 0.47475E-01 -.95923E+04 0.10000E+01  769.88   1028.36

       A14 1   4 0.12948E+08  37.00 0.55908E+00 0.00000E+00 0.31471E-01 0.18280E-02 0.47235E-01 -.20992E+05 0.10000E+01  769.36   1028.98

       A15 1   5 0.12937E+08  37.00 0.73114E+00 0.00000E+00 0.23639E+00 0.15813E-02 0.16267E-01 -.14148E+06 0.10000E+01  769.03   1176.84

       A16 1   6 0.12921E+08  37.00 0.53256E+00 0.00000E+00 0.31424E-01 0.18268E-02 0.47233E-01 -.17779E+05 0.10000E+01  768.86   1028.93
```

Figure 5.4.3. Part of printed output for problem of CO_2 injection into a layered brine formation.

The simulation of this problem previously submitted by LBNL for the code intercomparison project did not generate any solid precipitate (Pruess et al., 2002, 2004). The different behavior seen in the present simulation is due to the much more vigorous evaporation of water into the flowing gas stream, as compared to the evaporation model for water partitioning into the gas phase that had been used in the earlier calculation. The mechanisms contributing to solid precipitation and formation dry-out near the injection well are believed to be represented realistically in the present simulation, but the space discretization near the injection well is rather coarse, and considerably finer gridding would be needed to achieve accurate results.

Figs. 5.4.10-5.4.12 show contour maps of pressure, gas saturation, and dissolved CO_2 mass fraction after two years of simulation time. These results are all very similar to our earlier calculations using an evaporation model for water in the CO_2 rich phase. Highest gas saturations of approximately 60 % occur beneath the shale layers at elevations of 52, 85, and 118 m. Gas is just beginning to reach the top shale layer at an elevation of 151 m. CO_2 mass fraction dissolved in the aqueous phase after two years is in the range of 4.0 - 4.8 % throughout most of the two-phase zone, with smaller but significant CO_2 concentrations occurring beyond the two-phase region.

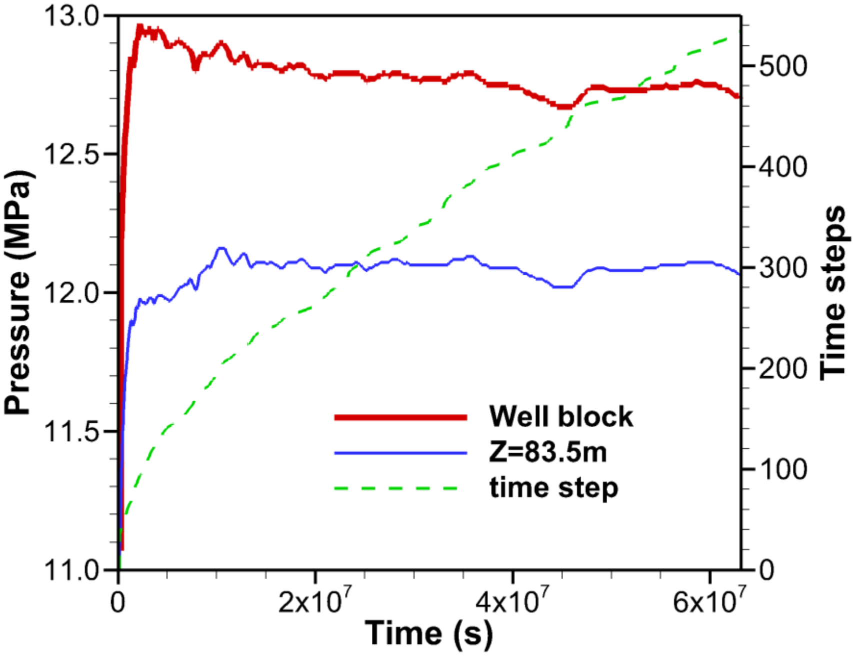

Figure 5.4.4. Time evolution of pressures in two grid blocks, well block (A15 1) and block at Z = 83.5 m (A1G 1) and time stepping for CO2 injection into a layered brine formation.

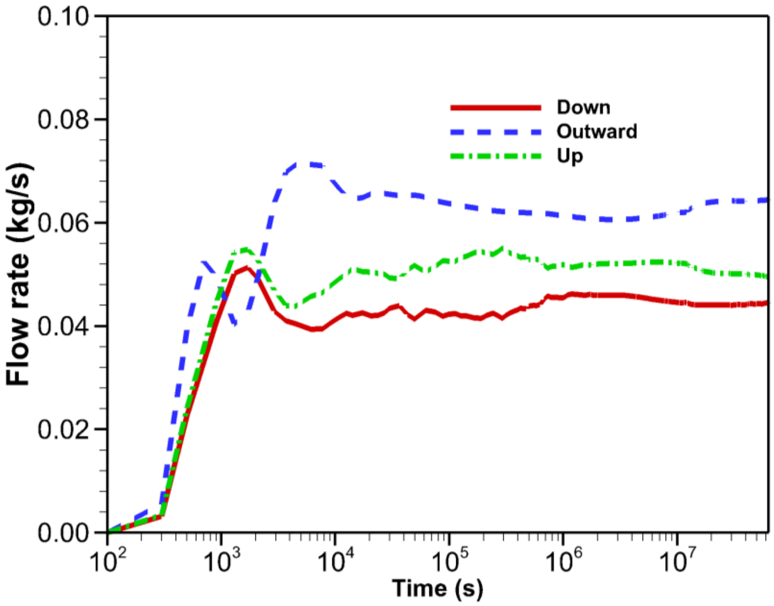

Figure 5.4.5. Gas flow rates away from the well block.

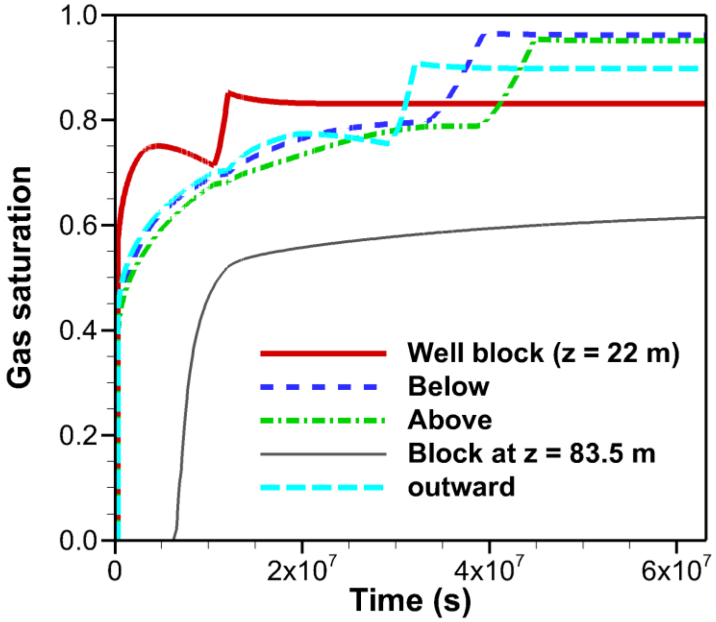

Figure 5.4.6. Gas saturations at the well block and its neighbors (above - A16 1; outward - A15 2; below - A14 1). Gas saturations at block A1G 1 at an elevation of 83.5 m (61.5 m above well block) are also shown.

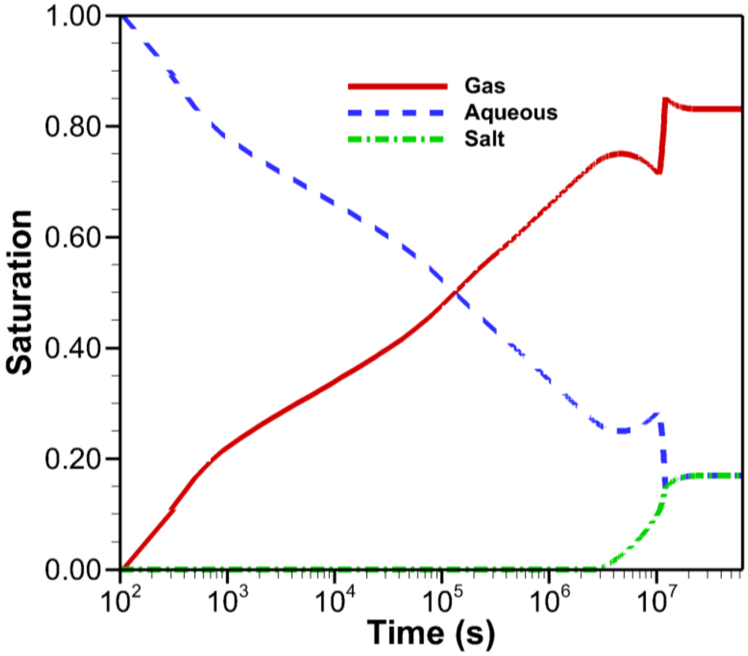

Figure 5.4.7. Phase saturations at the well block (A15 1).

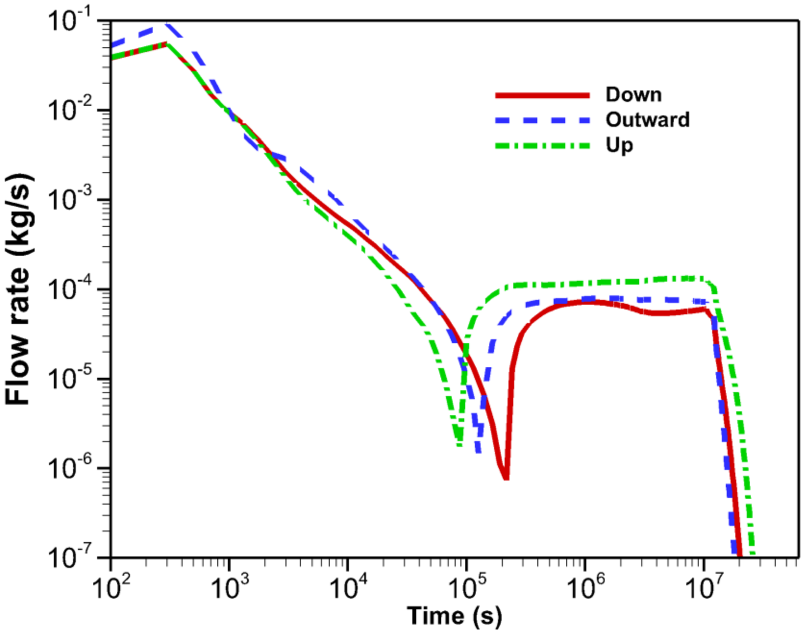

Figure 5.4.8. Absolute values of aqueous phase flow rates between the well block and neighboring grid blocks. Up to approximately 10^5 s flow is away from the well block, then reverses.

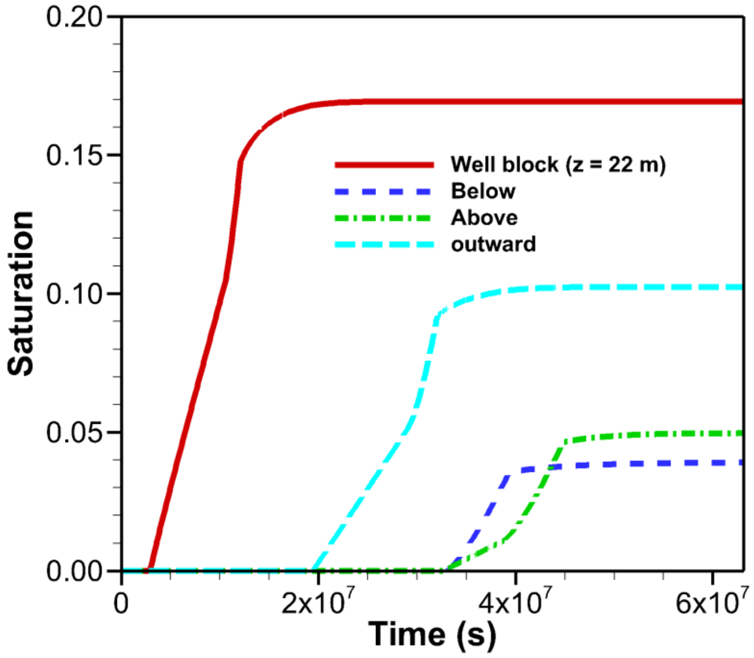

Figure 5.4.9. Solid saturations (fraction of void space taken up by solid precipitate) in the well block and its neighbors.

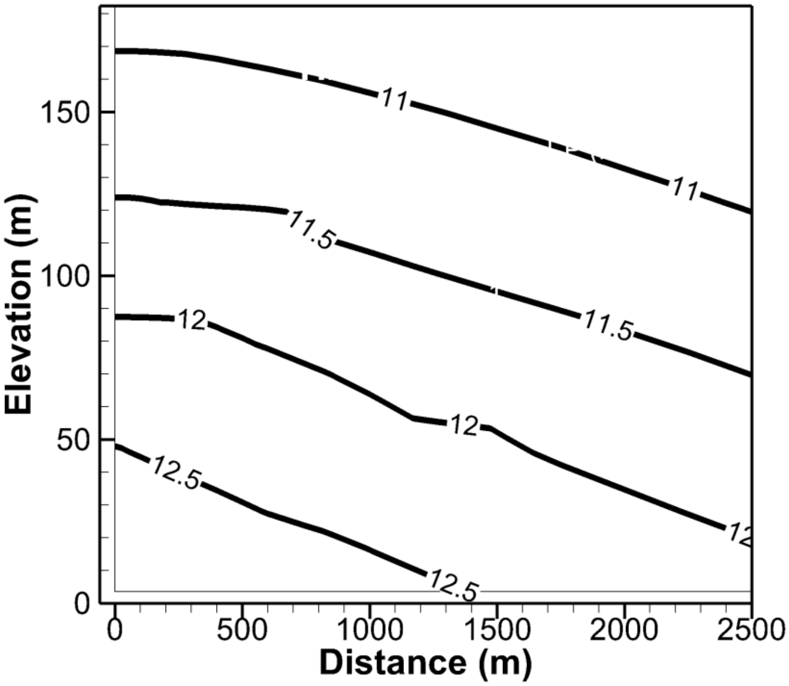

Figure 5.4.10. Contour map of fluid pressures (MPa) after 2 years of CO_2 injection.

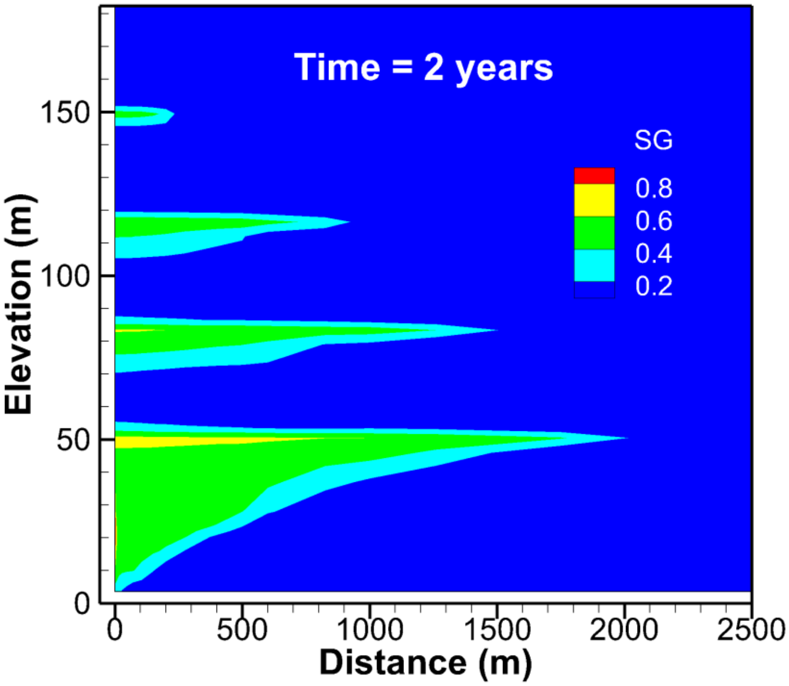

Figure 5.4.11. Contour map of gas saturations after 2 years of CO_2 injection.

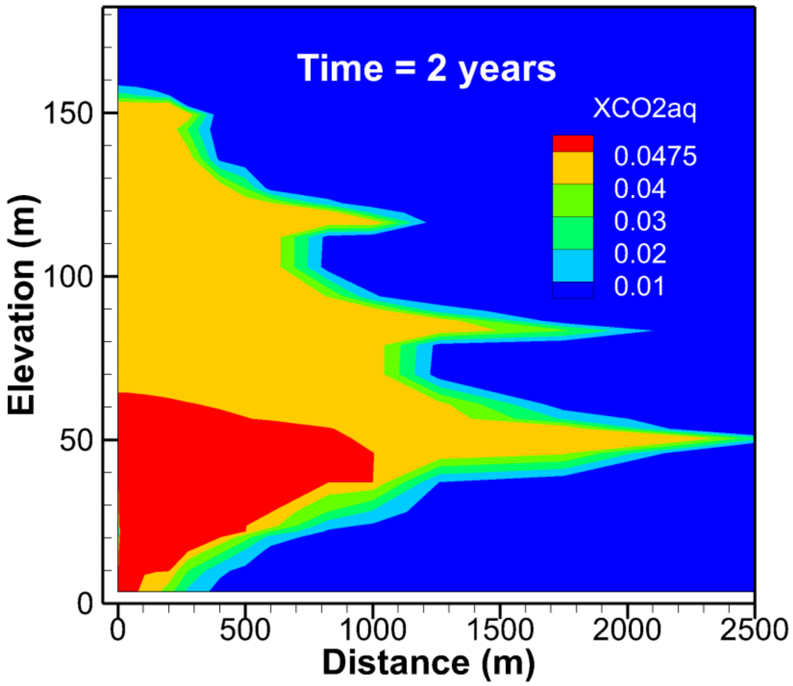

Figure 5.4.12. Contour map of dissolved CO_2 mass fractions after 2 years of CO_2 injection.

Table 5.4.2. CO_2 inventory (in units of 10^6 kg) for injection into a saline 2-D layered system.

	t = 0	30 days	1 year	2 years
total CO_2	0.17869	0.58935	5.17779	10.1768
CO_2 injected	0	0.41083	5.0019	10
CO_2 (aq.)	0.17869	0.26890	1.10278	2.0071
CO_2 (gas)	0	0.32045	4.07501	8.1697
fraction of CO_2 in aq. Phase	1	0.4563	0.2130	0.1972

5.5 Problem No. 5 (*rcc3_35C*) – Nonisothermal Radial Flow from a CO_2 Injection Well

This is a variation of the problem described in Section 5.2 except that the flow process is nonisothermal here, i.e., a problem of colder CO_2 (35 °C) injection into a warmer saline aquifer (45°C). The description of the problem and the model set-up can be found in Section 5.2 and will not be duplicated here. The only modifications to the input files are (1) NEQ=4 (nonisothermal) and (2) initial conditions specified for the injection cell “A1 1” with a temperature of 35°C (Figure 5.5.1).

```
*rcc3_35C* ... nonisothermal Radial flow from a CO2 Injection Well
ROCKS----1----*----2----*----3----*----4----*----5----*----6----*----7----*----8
SAND     2  2600.e00       .12  100.e-15  100.e-15  100.e-15      2.51      920.
   4.5e-10
    7          .457       .30        1.       .05
    7          .457       .00    5.1e-5      1.e7      .999
well     2  2600.e40       .12  100.e-15  100.e-15  100.e-15      2.51      920.
   4.5e-10
    7          .457       .30        1.       .05
    7          .457       .00    5.1e-5      1.e7      .999
MULTI----1----*----2----*----3----*----4----*----5----*----6----*----7----*----8
    3    4    3    6
SELEC....2....3....4....5....6....7....8....9...10...11...12...13...14...15...16
    1                                       0    0    0    0    0    0    0    0
        .8        .8
SOLVR----1----*----2----*----3----*----4----*----5----*----6----*----7----*----8
5  Z1   O0    8.0e-1    1.0e-7
START----1----*----2----*----3----*----4----*----5----*----6----*----7----*----8
----*----1 MOP: 123456789*123456789*1234 ---*----5----*----6----*----7----*----8
PARAM----1----*----2----*----3----*----4----*----5----*----6----*----7----*----8
   1 999     9991000300000000   4    3
              8.64e8       -1.
        1.
     1.E-5     1.E00
              120.e5                 .15                 0.0                 45.
FOFT ----1----*----2----*----3----*----4----*----5----*----6----*----7----*----8
A1 49              1 .1745E+04 .2685E+03           .2570E+02          -.6500E+01
A12 2              1 .3080E+08 .4738E+07           .1080E+04          -.6500E+01
GENER----1----*----2----*----3----*----4----*----5----*----6----*----7----*----8
A1  1inj 1                         COM3       100.
INCON----1----*----2----*----3----*----4----*----5----*----6----*----7----*----8
A1  1
 0.2500000000000E+08 0.0000000000000E+02 0.1000000000000E+01 0.3500000000000E+02
TIMES----1----*----2----*----3----*----4----*----5----*----6----*----7----*----8
    4
 2.592E+06  8.64E+06  8.64E+07  8.64E+08
```

Figure 5.5.1. Part of TOUGH input file for nonisothermal radial flow from a CO_2 injection well into a saline aquifer. Note the differences from the input file in Figure 5.2.4: NEQ=4 under MULTI section and T=35°C at the cell “A1 1” under INCON section.

Fig. 5.5.2-5.5.6 shows model results as a function of the similarity variable plotted from the time series data for grid block “A1 49”, at a radial distance of R = 25.25 m, which were generated by means of FOFT specifications in the input file (Fig. 5.5.1).

Similar to the isothermal problem presented in Section 5.2, three distinct regions of gas saturation (Fig. 5.5.3), solid salt saturation (Fig. 5.5.4), CO_2 mass fraction in liquid (Fig. 5.5.5), and NaCl mass fraction in liquid (Fig. 5.5.6), can be found in this nonisothermal CO_2 injection process. The difference is that two sub-regions occur within the two phase region in the nonisothermal case (Fig. 5.5.5 and Fig. 5.5.6) that do not exist in the isothermal case (Fig. 5.2.9 and Fig. 5.2.10). In the sub-region near the dry end, CO_2 mass fraction is higher than that in the sub-region near the wet end. The dividing point corresponds to the temperature front formed during injection of colder CO_2 into a warm aquifer (Fig. 5.5.8). Behind the front, the temperature is low and more CO_2 can be dissolved in water, while higher temperature and less dissolved CO_2 exist ahead of the front. Interestingly, the temperature in the dry sub-region is slightly lower than the injection temperature, implying that the cooling effect due to water evaporation into the flowing CO_2 is dominating behind the temperature front, whereas the temperature in the wet sub-region is slightly lower than the ambient aquifer temperature, implying that the heating effect due to dissolution of CO_2 into water is dominating ahead of the temperature front. Such feedback of temperature change on CO_2-water solubility also causes a slightly higher gradient of gas saturation near the temperature front (Fig. 5.5.3) than in the case of isothermal simulation (Fig.5.2.7). Note from the temperature profile (Fig. 5.5.7) that when accounting for the effects of water in the CO_2-rich phase on the enthalpy calculation, the water-evaporation induced temperature drop predicted by ECO2N V2.0 is smaller than that obtained by the cases using pure CO_2 properties for the gas phase (V1.0 or V2.0 with IE(16)=1).

The agreement between ECO2N V2.0 and ECO2N V1.0 is excellent in terms of pressure (Fig. 5.5.2), gas saturation (Fig. 5.5.3), and temperature (Fig. 5.5.7), except for the differences noted above, based on more complete physics. Similar to the isothermal case, ECO2N V2.0 predicts slightly higher solid salt saturation than ECO2N V1.0 in the dry-out zone (Fig. 5.5.4). This is related to its different water-CO_2 solubility model as discussed in Section 2.1, which predicts lower dissolved CO_2 mass fraction in liquid phase (Figure 5.5.5). ECO2N V2.0 offers users an option to use the exact same water-CO_2 solubility model (at low temperature) as ECO2N V1.0 by setting IE(16)=1 in the input file, if 100% consistency with ECO2N V1.0 in the low temperature range is preferable.

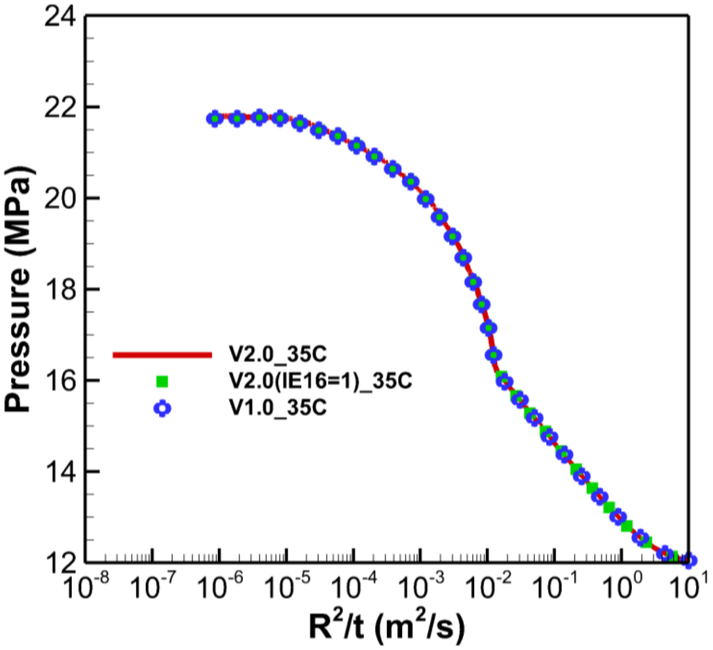

Figure 5.5.2. Simulated pressures as a function of the similarity variable (nonisothermal radial flow). The thick solid red line represents the result simulated by new code (ECO2N V2.0) while the blue symbols represent the result simulated by ECO2N V1.0. The green symbols represent the result simulated by ECO2N V2.0 with IE(16)=1 to enforce using the exact same routine for calculation of mutual solubility as ECO2N V1.0. All results are time series of data for a grid block at a radial distance of R = 25.25 m.

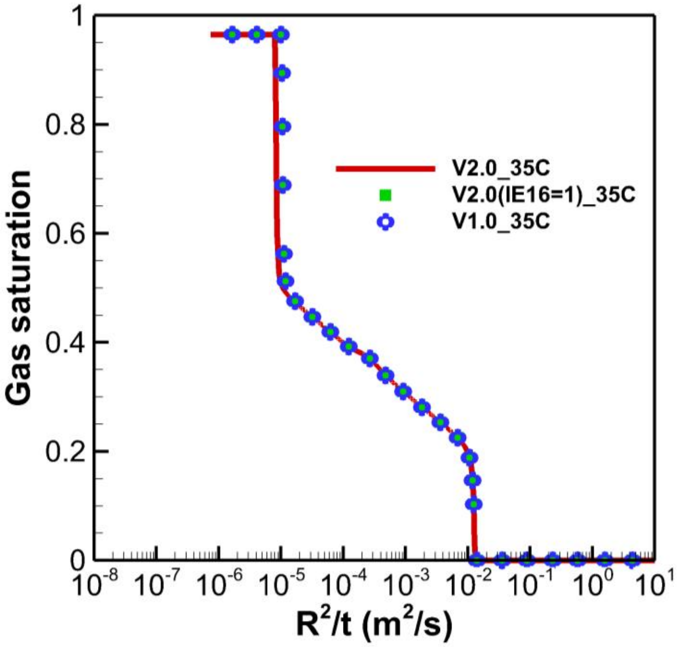

Figure 5.5.3. Simulated gas saturations.

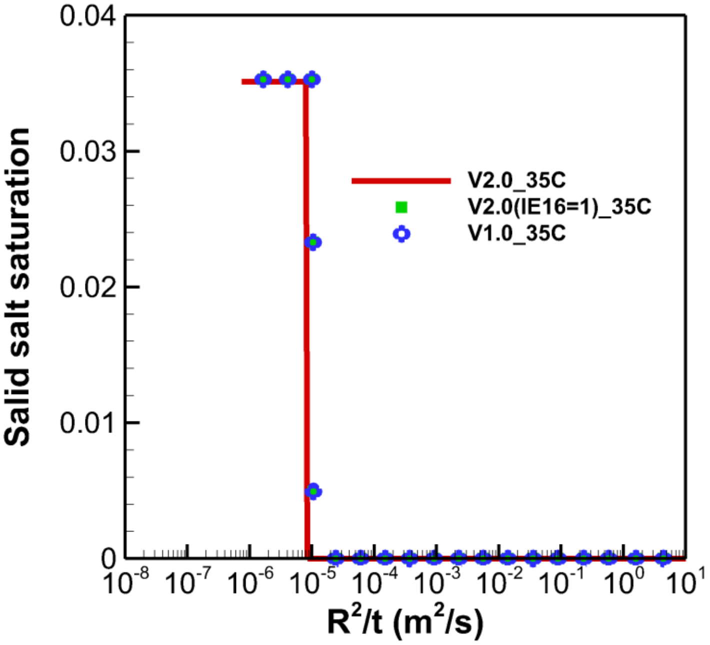

Figure 5.5.4. Simulated solid saturations.

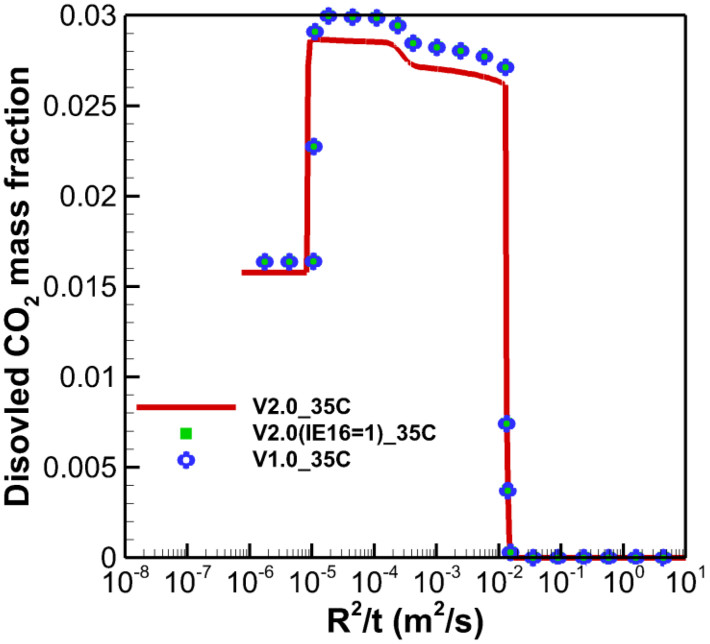

Figure 5.5.5. Simulated CO_2 mass fraction in aqueous phase.

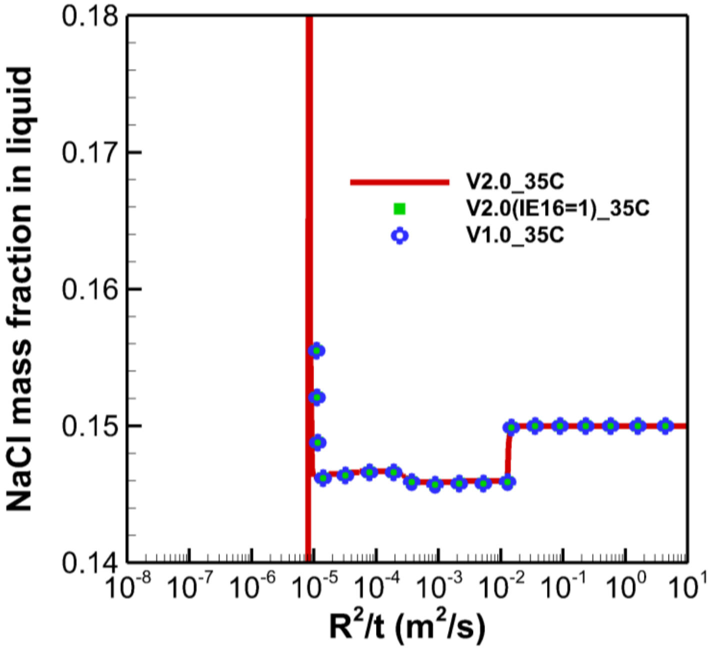

Figure 5.5.6. Simulated NaCl mass fraction in aqueous phase.

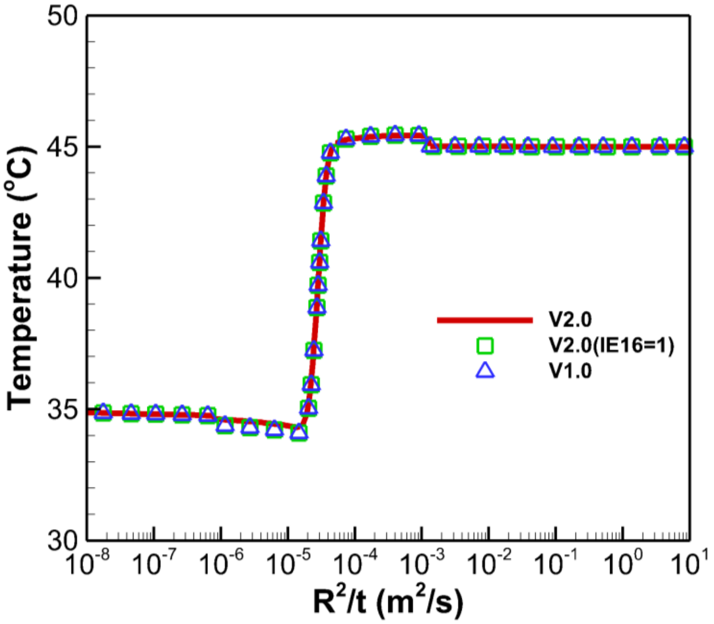

Figure 5.5.7. Simulated temperature as a function of the similarity variable (nonisothermal radial flow). The thick solid red line represents the result simulated by new code (ECO2N V2.0) while the blue symbols represent the result simulated by ECO2N V1.0. The green symbols represent the result simulated by ECO2N V2.0 with IE(16)=1 to enforce using the exact same routine for calculation of mutual solubility as ECO2N V1.0. All results are spatial data at time = 8.64E7 seconds (1000 days).

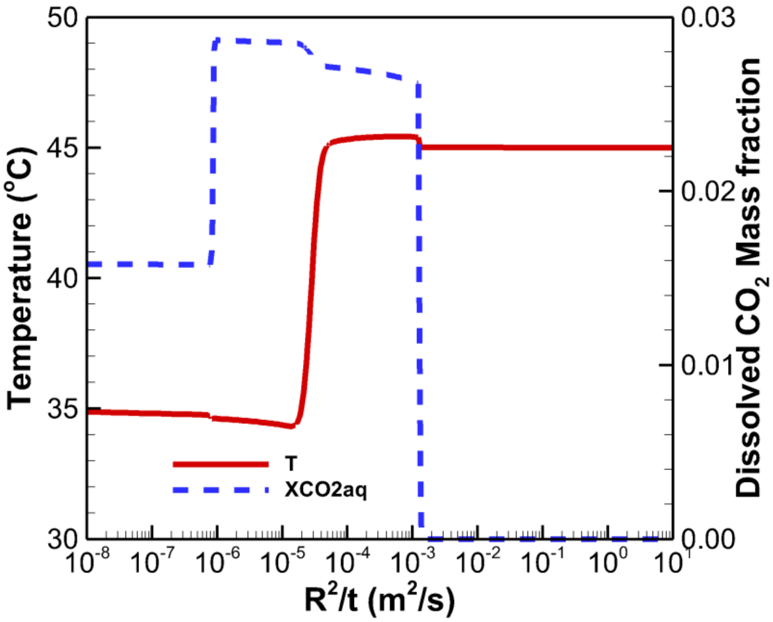

Figure 5.5.8. Simulated temperature and dissolved CO_2 mass fraction as a function of the similarity variable (nonisothermal radial flow). The thick solid red line represents temperature simulated by new code (ECO2N V2.0) while the blue symbols represent the mass fraction of the dissolved CO_2 in aqueous phase. All results are spatial data at time = 8.64E7 seconds (1000 days).

5.6 Problem No.6 (*Case6_50kg_DP*) – GCS/GHE with a double-porosity reservoir

In this problem, we consider one injection-well/production-well pair (known as a doublet) of the five-spot pattern (Figure 5.6.1) that makes up a geothermal heat extraction (GHE) system combined with geological carbon sequestration (GCS). The geothermal reservoir we consider here is an idealized 100 m thick, double porosity reservoir whose parameters are shown in Table 5.6.1 and Table 5.6.2. In the double porosity model, one continuum represents the mobile (higher permeability) regions and the other represents the immobile (lower permeability) regions. The reservoir is assumed to be initially filled with pure CO_2 in the mobile continuum and pure water in the immobile continuum, under the same hydraulic static pressure (29.15 MPa) and temperature (152.2°C). Because the mobile continuum makes up 20% of the reservoir, this initial condition is equivalent to an initial bulk gas saturation of 20%.

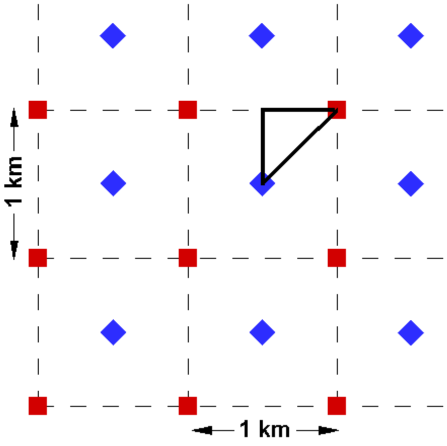

Figure 5.6.1. Diagram of five-spot pattern of geothermal wells (blue-injector; red-producer).

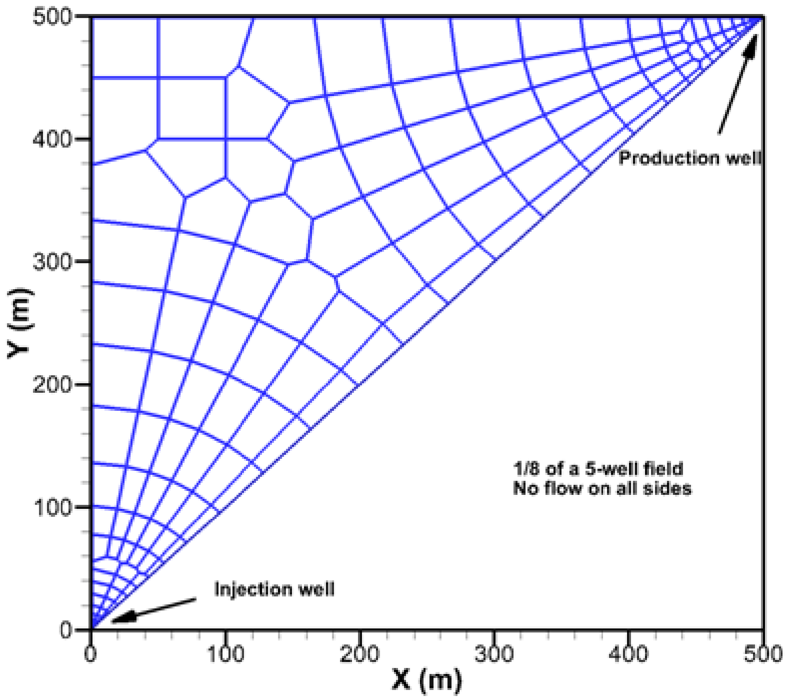

Figure 5.6.2. Map view of the numerical grid used in the simulation. Finer grid resolution is used near the two wells.

A two-dimensional, irregular, dual-continuum grid was created to represent the reservoir, in which each continuum is represented by a 2D mesh having the same geometry (Figure 5.6.2) except that the immobile continuum mesh does not have lateral connections. Two overlapping meshes are connected locally by the mobile/immobile interface defined in Table 5.6.1. In other words, fluid can flow from the injection well to the production well through the mobile continuum only, whereas the immobile continuum plays a passive role through mass and heat exchange with the mobile continuum. Grid resolution varies from 0.1 m near the wells to 50 m at far field to capture the important details of the flow field. Both the injection and the production wells are fully perforated in the reservoir (connected to the mobile continuum only). The parameters for the double porosity model used in this study are shown in Table 5.6.1.

Table 5.6.1 Parameters of the Double Porosity Model

Parameter	Value
Percentage of the mobile pores (%)	20
Permeability of the mobile continuum (m^2)	2E-14
Permeability of the immobile continuum (m^2)	2E-17
Percentage of the immobile pores (%)	80
Mobile/immobile interface area per unit volume (m^2/m^3)	0.2
Characteristic mobile/immobile distance (m)	5.0

With the exception of capillary strength, the parameters for relative permeability and capillary functions are the same for both continua, as shown in Table 5.6.2.

Table 5.6.2 Other Properties of the Reservoir (Both Continua).

Parameter	Value	Note
Porosity	0.254	Uniform
Thermal conductivity	2.51 W m^{-1} K^{-1}	
Pore compressibility	10^{-10} Pa^{-1}	
Parameters for relative permeability:		Liquid relative permeability using van Genuchten-Mualem model (van Genuchten, 1980) and gas relative permeability using Corey model (Corey, 1954)
Residual gas saturation	0.01	
m_{VG}	0.65	
Residual liquid saturation	0.05	
Saturated liquid saturation	1.0	
Parameters for capillary pressure:		Capillary pressure using van Genuchten model
Residual liquid saturation	0.03	
m_{VG}	0.4118	
α	6.08E-5 Pa^{-1} (mobile continuum) 1.216E-6 Pa^{-1} (immobile continuum)	
Maximum capillary pressure	$6.4x10^{7}$ Pa	
Saturated liquid saturation	1.0	

No-flow boundaries are assigned on all sides except for heat flow through the reservoir/basement rock interface, which is calculated using the semianalytical solution implemented in TOUGH2. Injection of CO_2 is simulated as a source term at the well cell ('*1a 1') with a strength of 6.25 kg/s (1/8 of 50 kg/s for the full well). The same flow rate is assigned for the mass produced at the production well cell ('*1b 1'). Large heat capacity was assigned to the injection cell ('*1a 1'), which keeps the temperature at that cell unchanged throughout the 30 years. As a result, the temperature of the injected CO_2 is constant at $75^{o}C$ (specified in INCON). Figure 5.6.3 shows part of the input file.

```
*Generic CO2 geothermal 5Wells (1km spacing) configuration* ... 100m reservoir
ROCKS----1----*----2----*----3----*----4----*----5----*----6----*----7----*----8
wellb    2     2600.       1.0    1.e-12    1.e-12    1.e-6       2.51     1000.
    0.e-10                          1.00
    7           0.20       .00        1.      0.01
    8
wells    2     2600.      0.99    1.e-12    1.e-12    1.e-6       2.51     2.e50
    0.e-10                          1.00
    7           0.20       .00        1.      0.01
    8
RocF1    2  2600.000      .254  20.0E-15  20.0E-15 20.00E-18     2.510   920.000
  .100E-09
   07      .6500     .050      1.000     0.01      .0000     .0000     .0000
   07      .4118     .030      6.080E-05 6.400E+05 1.000     .0000     .0000
RocM1    2  2600.000      .254  20.0E-18  20.0E-18 20.00E-18     2.510   920.000
  .100E-09
   07      .6500     .050      1.000     0.01      .0000     .0000     .0000
   07      .4118     .030      1.216E-06 6.400E+09 1.000     .0000     .0000
CAPRK    0  2600.000      .283 225.7e-15 225.7e-15 2.229E-15     2.510   920.000

MULTI----1----*----2----*----3----*----4----*----5----*----6----*----7----*----8
    3    4    3    6
START----1----*----2----*----3----*----4----*----5----*----6----*----7----*----8
----*----1 MOP: 123456789*123456789*1234 ---*----5----*----6----*----7----*----8
PARAM----1----*----2----*----3----*----4----*----5----*----6----*----7----*----8
   35000    200010 030001020001400015
          9.46702E+8     2.e+0   1.00e8              9.8066
   1.00e-6                                         1.e-8
 0.2914791867980E+08 0.0000000000000E+00 1.0000000000000E+00 0.1521650000000E+03
SOLVR----1----*----2----*----3----*----4----*----5----*----6----*----7----*----8
3  Z1   O0    4.0e-3    1.0e-7
TIMES----1----*----2----*----3----*----4----*----5----*----6----*----7----*----8
    5
   8.640e5   8.640e63.15576E7 3.15576E8 6.31152E8
SELEC....2....3....4....5....6....7....8....9...10...11...12...13...14...15...16
    1                                       9
      1.e0        .1       1.0      1.53       8.0  0.15e-5
GENER----1----*----2----*----3----*----4----*----5----*----6----*----7----*----8
*1a 1inj 1                         COM3   6.2500
*1b 1pro 1                         MASS  -6.2500
```

Figure 5.6.3. Part of the input file for Problem 6

Figure 5.6.4 shows six snapshots of pressure drop (from the initial pressure) in the mobile continuum during the production. The reservoir pressure drops quickly at early time and then slowly recovers to some degree. As a result, the pressure drop after 1 year is the biggest among the six snapshots. This implies that the reservoir pressure loss is mainly caused by the volume imbalance due to production of hot CO_2 and injection of cold CO_2. Such volume loss is gradually compensated by the expansion of the injected “cold” CO_2 with time. Such reservoir pressure evolution trend is also reflected in the well bottom pressure (Figure 5.6.5).

Figure 5.6.6 shows the temperature distribution in both continua at various times. The cold front advances with time from the injection well to the production well. There is a time-delay in the immobile continuum in such propagation, especially at early time.

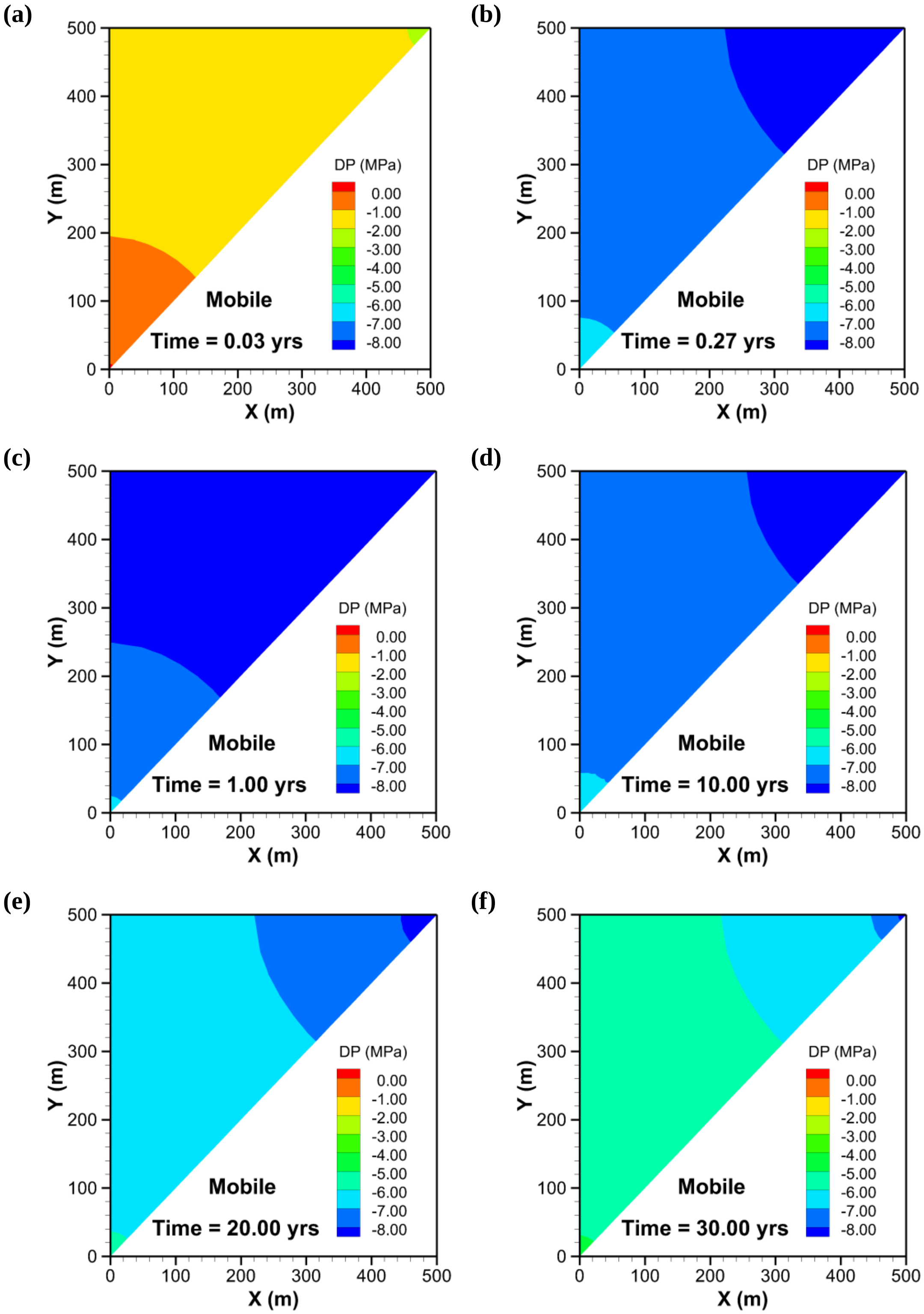

Figure 5.6.4. Simulated pressure drop (from the initial reservoir pressure) in the reservoir (a) 10 days, (b) 100 days, (c) 1 yrs, (d) 10 yrs, (e) 20 yrs and (f) 30yrs.

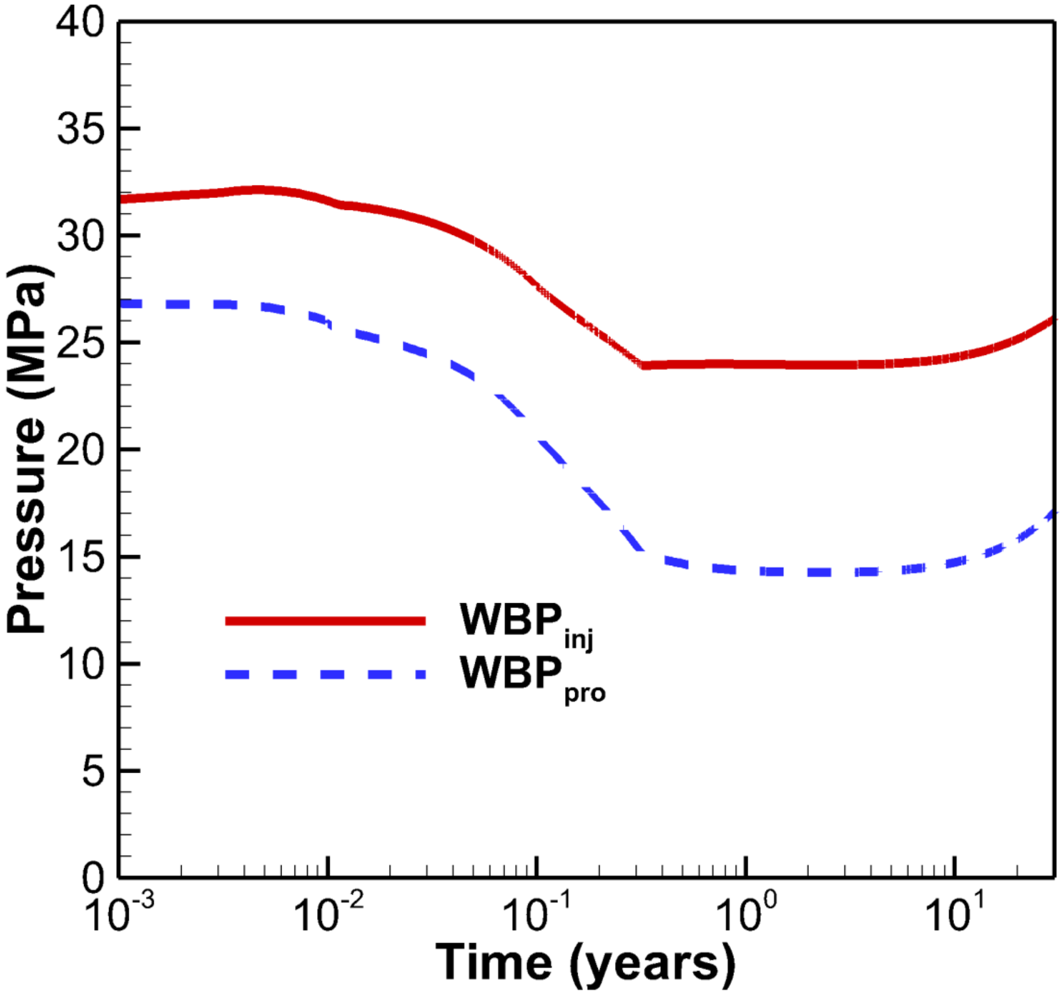

Figure 5.6.5. Evolution of well bottom pressures at injection and production wells.

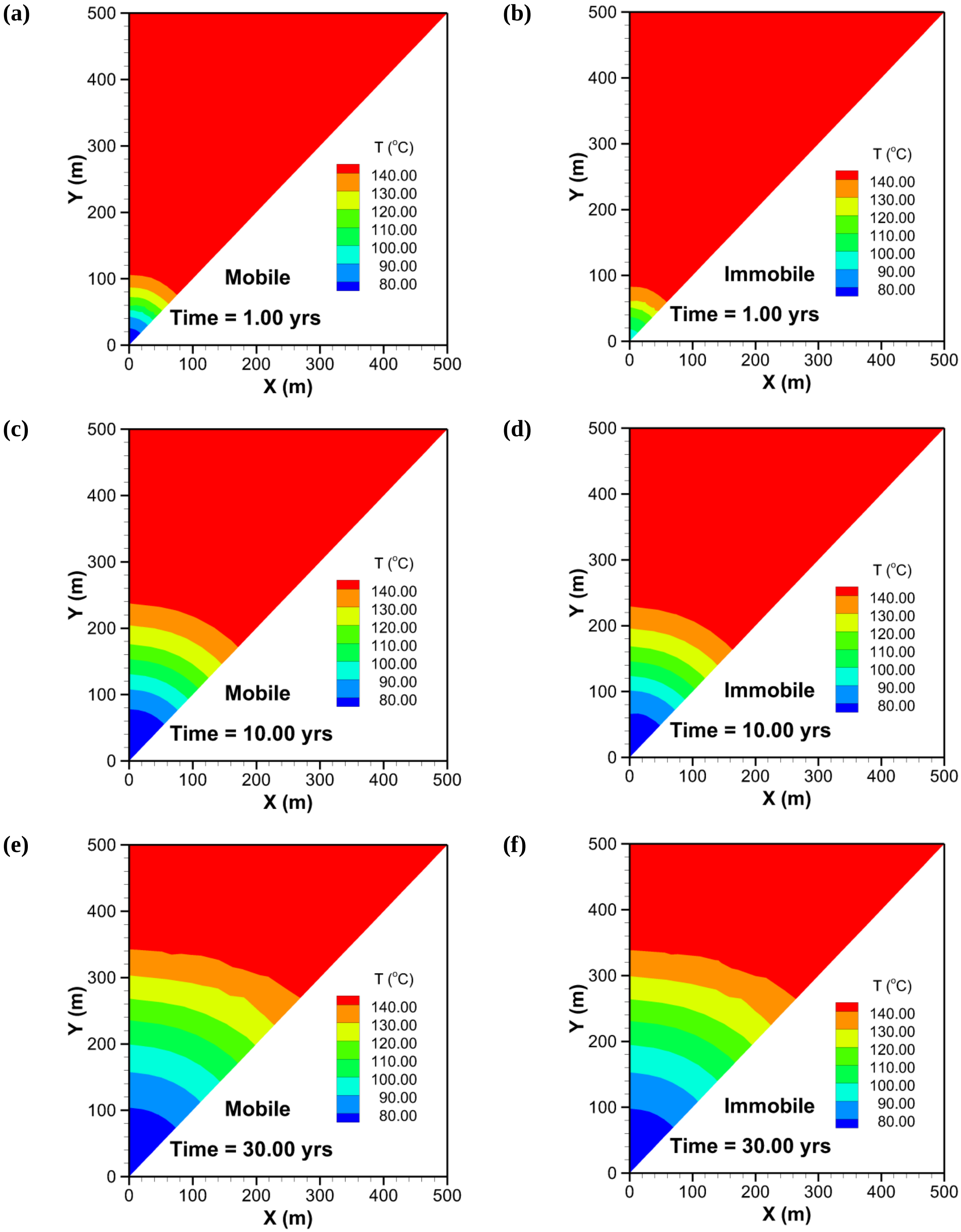

Figure 5.6.6. Simulated temperature in the reservoir after 1 year ((a) and (b)), 10 years ((c) and (d)), and 30 years ((e) and (f)) in the two continua.

Figure 5.6.7 shows three snapshots of gas saturation in each continuum during production. The gas saturation in the immobile continuum slowly increases with time as CO_2 enters from the mobile continuum. The gas saturation in the mobile continuum first drops over the entire domain and then increases near the injection well as injection continues, forming a significant gradient from the injection well to the production well. Water accumulates in the region close to the production well (Figure 5.6.7e). However, the liquid phase production rate is small for most times (Figure 5.6.8), and the CO_2 component in the total production is larger than 97% (Figure 5.6.9).

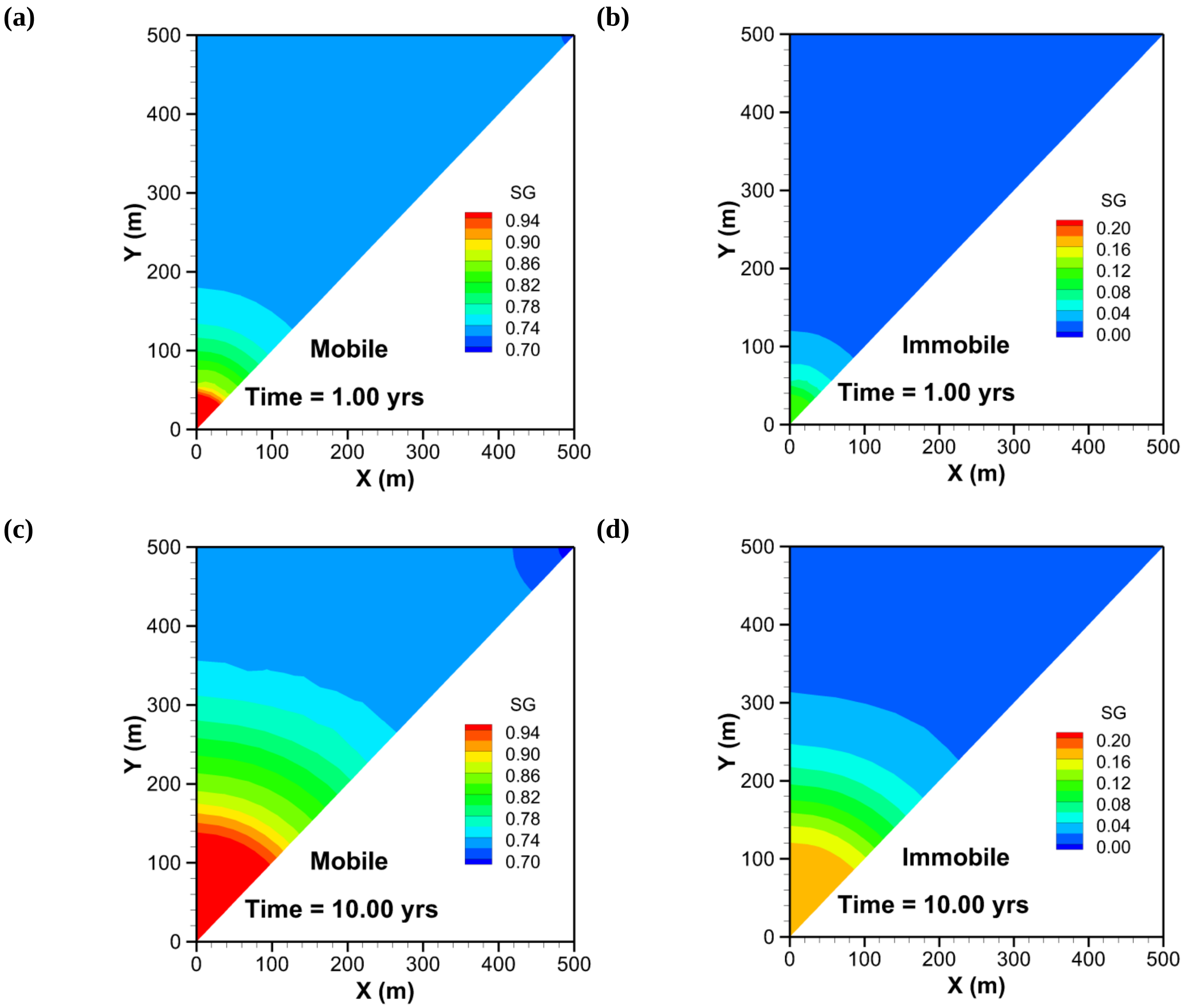

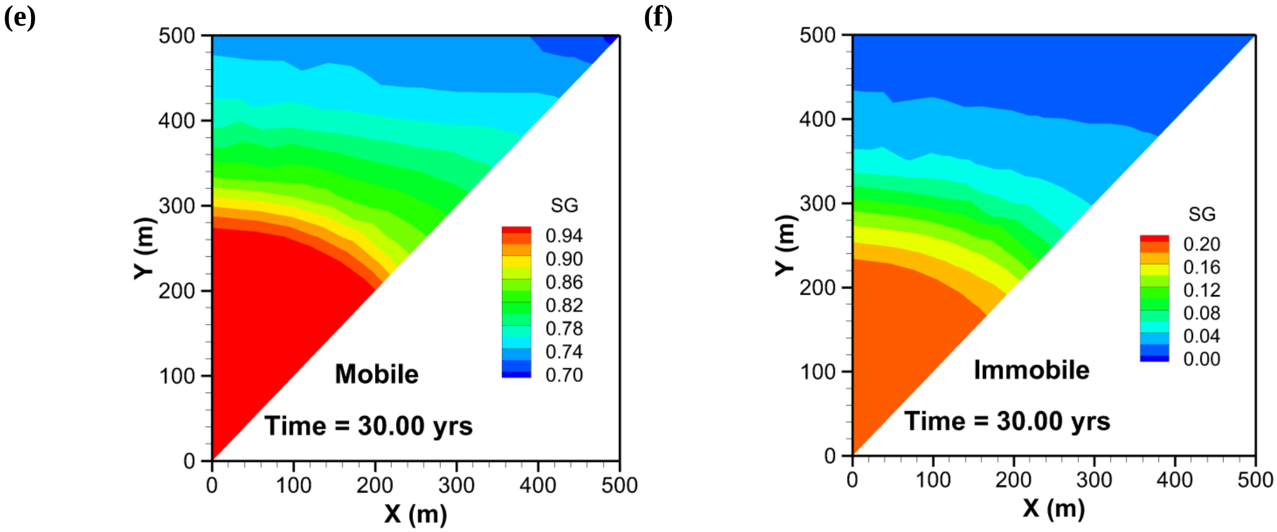

Figure 5.6.7. Simulated gas saturation in the reservoir after 1 year ((a) and (b)), 10 years ((c) and (d)), and 30 years ((e) and (f)) in the two continua. Different color scales are used for each continuum.

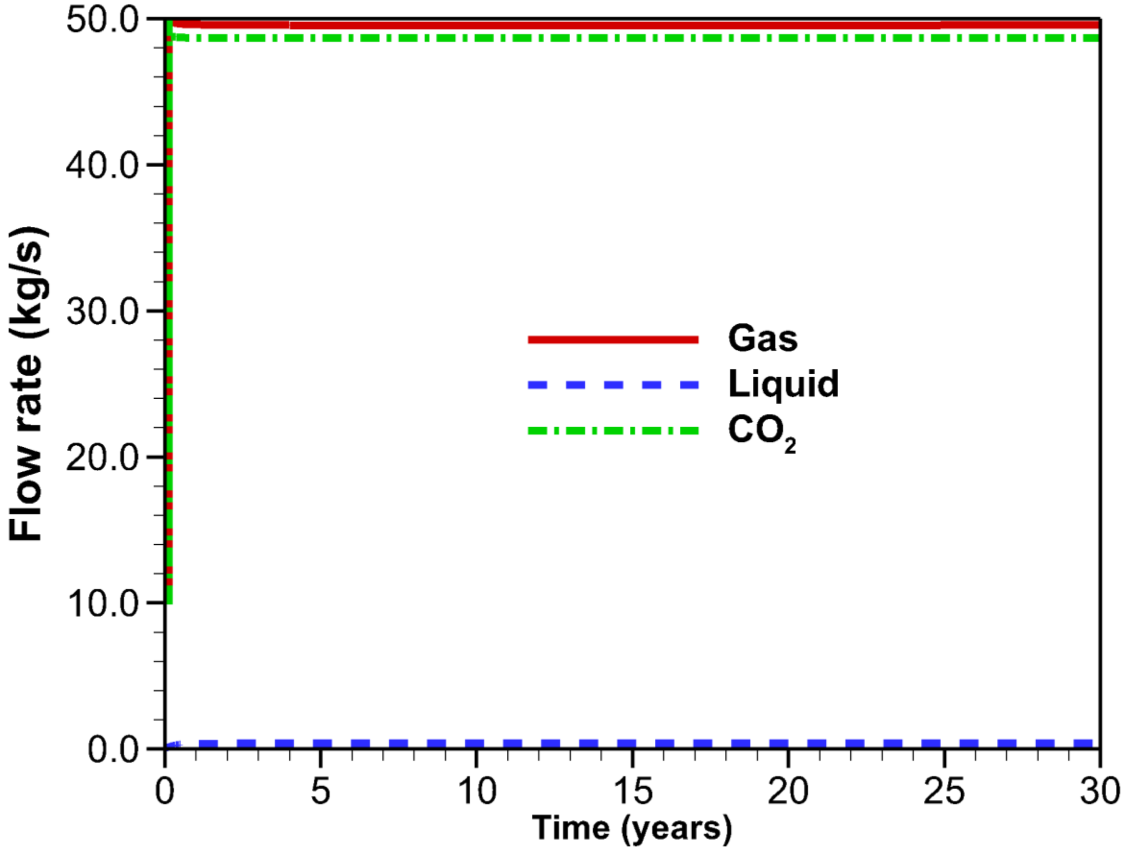

Figure 5.6.8. Simulated gas and liquid phase flow rates as well as CO_2 component flow rate.

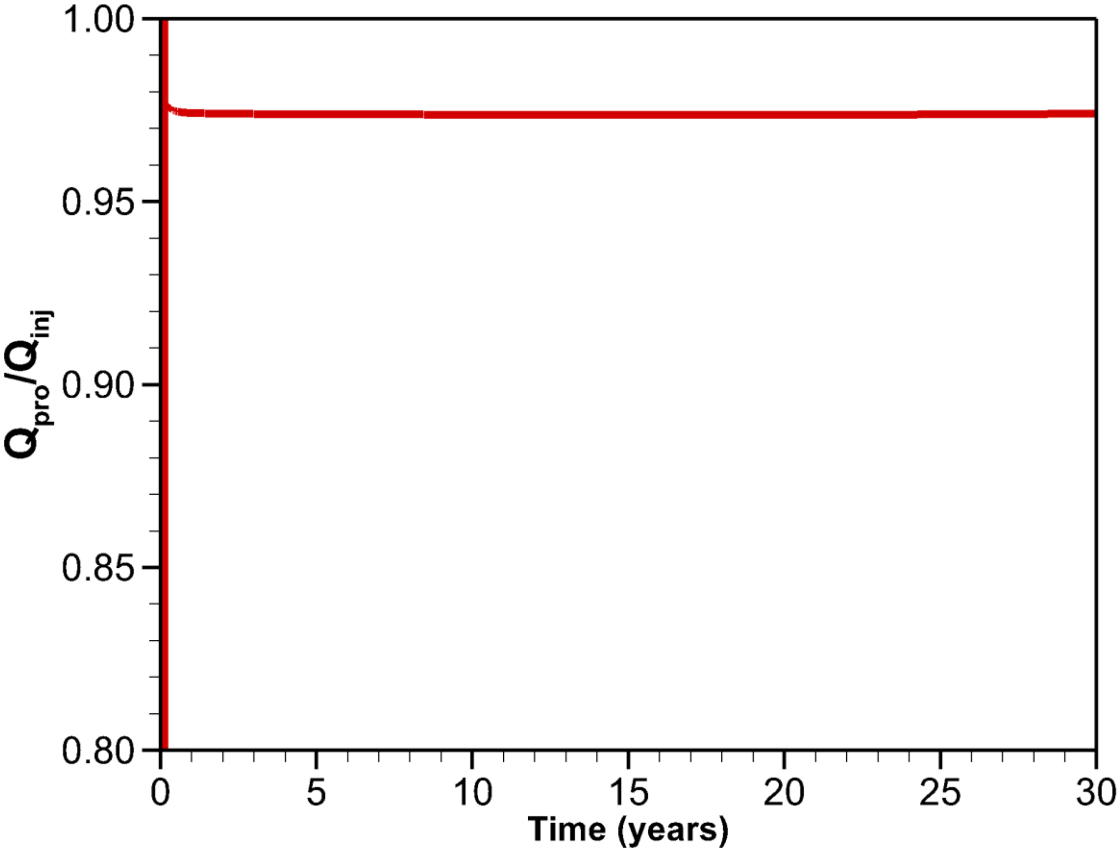

Figure 5.6.9. Ratio of CO_2 injection rate and production rate. Because the total injection (pure CO_2) rate and the total production (mixture) rate are equal, this ratio is also a measure of how much CO_2 enters the production stream.

6. Concluding Remarks

ECO2N V2.0 is an extension and upgrade of ECO2N V1.0, a fluid property module for the multiphase, multicomponent simulator TOUGH2, Version 2.1. It provides capabilities for modeling advective and diffusive flow and transport in multidimensional heterogeneous systems containing H_2O - NaCl - CO_2 mixtures. Process capabilities include coupling between fluid and heat flow, partitioning of H_2O and CO_2 among different phases, and precipitation/dissolution of solid salt. The code represents thermophysical properties of brine-CO_2 mixtures generally within experimental accuracy for the range of conditions of interest in geologic disposal of CO_2 and CO_2 enhanced geothermal reservoirs. A fluid property table provided with ECO2N V2.0 covers temperatures from ambient to 307˚C and pressures from ambient to 600 bars. Super- as well as sub-critical conditions may be modeled, but the code currently has no provisions to treat separate liquid and gas CO_2 phases, or transitions between them.

Acknowledgement

We thank Stefan Finsterle for his constructive comment as the internal reviewer. This work was partly supported by the TOUGH Royalty Fund, the Director, Office of Science, Office of Basic Energy Sciences of the U.S. Department of Energy, and by the Zero Emission Research and Technology project (ZERT) under Contract No. DE-AC03-76SF00098, and the Assistant Secretary for Energy Efficiency and Renewable Energy, Geothermal Technologies Program of the U.S. Department of Energy under Contract No. DE-AC02-05CH11231.

References

Altunin, V.V. *Thermophysical Properties of Carbon Dioxide,* Publishing House of Standards, 551 pp., Moscow, 1975 (in Russian).

Andersen, G., A. Probst, L. Murray and S. Butler. An Accurate PVT Model for Geothermal Fluids as Represented by H_2O-NaCl-CO_2 Mixtures, *Proceedings 17th Workshop on Geothermal Reservoir Engineering,* pp. 239 - 248, Stanford, CA, 1992.

Battistelli, A., C. Calore and K. Pruess. The Simulator TOUGH2/EWASG for Modeling Geothermal Reservoirs with Brines and Non-Condensible Gas, *Geothermics,* Vol. 26, No. 4, pp. 437 - 464, 1997.

Bottini, S. B., and Saville, G. (1985), "Excess enthalpies for (water + itrogen)(g) and (water + carbon dioxide)(g) at 520 to 620 K and up to 4.5 MPa," J. Chem. Thermodynamics, 17, 83–97.

Chou, I.M. Phase Relations in the System NaCl–KCl–H_2O: III: Solubilities of Halite in Vapor-Saturated Liquids Above 445 ˚C and Redetermination of Phase Equilibrium Properties in the System NaCl–H_2O, *Geochim. Cosmochim. Acta,* Vol. 51, pp. 1965–1975, 1987.

Davidson, T. A., A Simple and Accurate Method for calculating Viscosity of Gaseous Mixtures. Bureau of Mines, US Department of The Interior, Report of Investigations 9456, 1993.

Doughty, C. and K. Pruess. A Similarity Solution for Two-Phase Water, Air and Heat Flow Near a Linear Heat Source in a Porous Medium, *J. of Geophys. Res.*, Vol. 97 (B2), pp. 1821 - 1838, 1992.

Evans, R.D. *The Atomic Nucleus,* Reprint Edition, Robert E. Krieger Publ. Co., Malabar, FL, 1982.

Fenghour, A., and Wakeham, W. A. (1996), Densities of (water + carbon dioxide) in the temperature range 415 K to 700 K and pressures up to 35 MPa. J. Chem. Thermodynamics, 28,

433–446.

García, J.E. Density of Aqueous Solutions of CO2, Lawrence Berkeley National Laboratory Report LBNL-49023, Berkeley, CA, 2001.

García, J.E. *Fluid Dynamics of Carbon Dioxide Disposal into Saline Aquifers,* PhD Thesis, University of California at Berkeley, December 2003.

Haas, J.L. Jr. Physical Properties of the Coexisting Phases and Thermochemical Properties of the H2O Component in Boiling NaCl solutions, USGS Bulletin 1421-A, Washington, DC, 73 pp., 1976.

Himmelblau, D.M. Partial Molal Heats and Entropies of Solution for Gases Dissolved in Water from the Freezing to the Near Critical Point, *J. of Phys. Chem.,* Vol. 63, pp. 1803–1808, 1959.

Hitchon, B. (ed.). *Aquifer Disposal of Carbon Dioxide,* Geoscience Publishing, Ltd., Sherwood Park, Alberta, Canada, 1996.

International Formulation Committee. *A Formulation of the Thermodynamic Properties of Ordinary Water Substance,* IFC Secretariat, Düsseldorf, Germany, 1967.

Kongsjorden, H., O. Karstad and T.A. Torp. Saline Aquifer Storage of Carbon Dioxide in the Sleipner Project, *Waste Management*, Vol. 17, No. 5/6, pp. 303 - 308, 1997.

Lindeberg, E., P. Bergmo and A. Moen. The Long-Term Fate of CO2 Injected into an Aquifer, paper G1-4, presented at Sixth International Conference on Greenhouse Gas Technologies (GHGT-6), Kyoto, Japan, October 1-4, 2002.

Lorenz, S., D. Maric and C. Rirschl. Eine analytische Funktion zur Bestimmung der Enthalpie wässriger NaCl Lösungen, draft report, Institut für Sicherheitstechnologie, Köln, Germany, April 2000.

Michaelides, E.E. Thermodynamic Properties of Geothermal Fluids, Geothermal Resources Council Transactions, Vol. 5, pp. 361 - 364, 1981.

Miller, A.B. A Brine-Steam Properties Computer Program for Geothermal Energy Calculations, Lawrence Livermore National Laboratory Report UCRL-52495, Livermore, CA, June 1978.

NIST Standard Reference Data, 2011. (http://webbook.nist.gov/chemistry/fluid/)

O’Sullivan, M.J. A Similarity Method for Geothermal Well Test Analysis, *Water Resour. Res.*, Vol. 17, No. 2, pp. 390 – 398, 1981.

Patel, M.R. and Eubank, P.T., Experimental densities and derived thermodynamic properties for carbon dioxide-water mixtures. Journal of Chemical and Engineering Data, 33 (2), 185–193, 1988.

Patel, M. R., Holste, J. C., Hall, K. R., and Eubank, P.T., Thermophysical properties of gaseous carbon dioxide-water mixtures. Fluid Phase Equilibria, 36, 279–299, 1987. Phillips, S.L., A. Igbene, J.A. Fair, H. Ozbek and M. Tavana. A Technical Databook for Geothermal Energy Utilization, Lawrence Berkeley National Laboratory Report LBL-12810, Berkeley, CA, 46 pp., 1981.

Prausnitz, J. M., R. N. Lichtenthaler, and E. G. de Azevedo. *Molecular Thermodynamics of Fluid-Phase Equilibria,* Prentice-Hall Inc., Englewood Cliffs, N. J., 1986.

Pruess, K. The TOUGH Codes—A Family of Simulation Tools for Multiphase Flow and Transport Processes in Permeable Media, *Vadose Zone J.,* Vol. 3, pp. 738 - 746, 2004.Pruess, K. ECO2N: A TOUGH2 Fluid Property Module for Mixtures of Water, NaCl, and CO_2, Lawrence Berkeley National Laboratory Report LBNL-57952, Berkeley, CA, August 2005.

Pruess, K., C. Oldenburg and G. Moridis. TOUGH2 User's Guide, Version 2, Lawrence Berkeley National Laboratory Report LBNL-43134, Berkeley, CA, November 1999, revised 2012.

Pruess, K. and J. García. Multiphase Flow Dynamics During CO2 Injection into Saline Aquifers, *Environmental Geology,* Vol. 42, pp. 282 - 295, 2002.

Pruess, K., J. García, T. Kovscek, C. Oldenburg, J. Rutqvist, C. Steefel and T. Xu. Intercomparison of Numerical Simulation Codes for Geologic Disposal of CO2, Lawrence Berkeley National Laboratory Report LBNL-51813, Berkeley, CA 94720, December 2002.

Pruess, K., J. García, T. Kovscek, C. Oldenburg, J. Rutqvist, C. Steefel and T. Xu. Code Intercomparison Builds Confidence in Numerical Simulation Models for Geologic Disposal of CO2, *Energy*, Vol. 29, Issues 9-10, pp. 1431-1444, doi:10.1016/j.energy.2004.03.077, July-August 2004.

Span, R. and W. Wagner. A New Equation of State for Carbon Dioxide Covering the Fluid Region from the Triple-Point Temperature to 1100 K at Pressures up to 800 MPa, *J. Phys. Chem. Ref. Data,* Vol. 25, No. 6, pp. 1509 - 1596, 1996.

Spycher, N., K. Pruess and J. Ennis-King. CO_2-H_2O Mixtures in the Geological Sequestration of CO_2. I. Assessment and Calculation of Mutual Solubilities from 12 to 100 °C and up to 600 bar, *Geochim. Cosmochim. Acta*, Vol. 67, No. 16, pp. 3015 - 3031, doi:10.1016/S0016-7037(03)00273-4, 2003.

Spycher, N. and K. Pruess. CO_2-H_2O Mixtures in the Geological Sequestration of CO_2. II. Partitioning in Chloride Brines at 12–100 ˚C and up to 600 bar, *Geochim. Cosmochim. Acta,* Vol. 69, No. 13, pp. 3309–3320, doi:10.1016/j.gca.2005.01.015, 2005.

Spycher, N. and K. Pruess. A Phase Partitioning Model for CO_2-Brine Mixtures at Elevated Temperatures and Pressures: Application to CO_2-Enhanced Geothermal Systems. Transp. Porous Med. 82:173-196. DOI 10.1007/s11242-009-9425-y. 2010.

Spycher, N. and K. Pruess. A Model for Thermophysical Properties of CO_2-Brine Mixtures at Elevated Temperatures and Pressures. PROCEEDINGS, Thirty-Sixth Workshop on Geothermal Reservoir Engineering, Stanford University, Stanford, California, January 31-February 2, 2011.

Takenouchi, S., Kennedy, G.C.: The binary system H2O–CO2 at high temperatures and pressures. Am. J. Sci. 262, 1055–1074, 1964.

Vargaftik, N.B. *Tables on the Thermophysical Properties of Liquids and Gases*, 2nd Ed., John Wiley & Sons, New York, NY, 1975.

Verma, A. and K. Pruess. Thermohydrologic Conditions and Silica Redistribution Near High-Level Nuclear Wastes Emplaced in Saturated Geological Formations, *Journal of Geophysical Res.*, Vol. 93 (B2), pp. 1159-1173, 1988.

Wendland M., Hasse H., and Maurer G. Experimental pressure temperature data on three- and four-phase equilibria of fluid, hydrate, and ice phases in the system carbon dioxide-water. J. Chem. Eng. Data 44, 5, 901–906, 1999.

Wormald, C. J., Lancaster, N. M., Sellars, A. J., The excess molar enthalpies of {xH2O+(l -x)CO}(g) and {xH2O+(l - x)CO2}(g) at high temperatures and pressures. J. Chem. Thermodynamics, 18, 135–147, 1986.

Zawisza, A., and Maleslnska, B. Y., Solubility of carbon dioxide in liquid water and of water in gaseous carbon dioxide in the range 0.2-5 MPa and at temperatures up to 473 K. Journal of Chemical and Engineering Data, 20(4), 288–391, 1981.

Zakirov, I. V., The P-V-T relations in the H2O-CO2 system at 300 and 400 ^{o}C. Geochem. Intl. 21, 13-20, 1984.

Appendix A: Code Intercomparison Problem 3: Radial Flow from a CO2 Injection Well[&]

1. INTRODUCTION AND GENERAL DESCRIPTION

This problem addresses two-phase flow of CO_2 and water for simplified flow geometry and medium properties. The aquifer into which injection is made is assumed infinite-acting, homogenoeus, and isotropic. Gravity and inertial effects are neglected, injection is made at a constant mass rate, and flow is assumed 1-D radial (line source). Under the conditions stated the problem has a similarity solution where dependence on radial distance R and time t occurs only through the similarity variable $\xi = R^2/t$ (O'Sullivan 1981; Doughty and Pruess 1992).

2. LIST OF PROCESSES BEING STUDIED

Two-phase flow of CO_2 and water subject to relative permeability and capillary effects.

Change of fluid density, viscosity, and CO_2 solubility with pressure and salinity.

Formation dry-out with precipitation of salt.

3. DEFINITION OF THE PROBLEM AND INPUT DATA

Problem parameters are summarized in Tables A.1 and A.2.

4. PROBLEM VARIATIONS

Neglect salinity of the aqueous phase. Include non-isothermal effects. Include permeability changes due to precipitation. Inject gas that is 50 % CO_2, 50 % N2.

5. DEFINITION OF RESULTS TO BE CALCULATED

Data on CO_2 and brine density and viscosity, and CO_2 solubility, for the range of thermodynamic conditions encountered in the problem. Gas saturation, dissolved CO_2 mass fraction, fraction of void space containing precipitated salt, and fluid pressure as functions of the similarity variable $\xi = R^2/t$. (Use both profiles at constant time and time-series data at a specific location for plotting.)

6. COMPARISON CRITERIA

Results should match within +/- 5 %.

7. REFERENCES

[&] proposed by Karsten Pruess; e-mail: K_Pruess@lbl.gov

Corey, A.T. The Interrelation Between Gas and Oil Relative Permeabilities, *Producers Monthly*, pp. 38 - 41, November 1954.

Doughty, C. and K. Pruess. A Similarity Solution for Two-Phase Water, Air and Heat Flow Near a Linear Heat Source in a Porous Medium, *J. of Geophys. Res.*, 97 (B2), 1821-1838, 1992.

O'Sullivan, M.J. A Similarity Method for Geothermal Well Test Analysis, *Water Resour. Res.*, Vol. 17, No. 2, pp. 390 – 398, 1981.

van Genuchten, M.Th. A Closed-Form Equation for Predicting the Hydraulic Conductivity of Unsaturated Soils, *Soil Sci. Soc. Am. J.*, Vol. 44, pp. 892 - 898, 1980.

Table A.1 Hydrogeologic parameters.

Permeability	$k = 10^{-13}\ m^2$
Porosity	$\phi = 0.12$
Pore compressibility	$c = 4.5x10^{-10}\ Pa^{-1}$
Aquifer thickness	100 m
Relative permeability	
liquid: van Genuchten function (1980) $k_{rl} = \sqrt{S^*}\left\{1-\left(1-\left[S^*\right]^{1/\lambda}\right)^{\lambda}\right\}^2$	$S^* = (S_l - S_{lr})/(1 - S_{lr})$
irreducible water saturation	$S_{lr} = 0.30$
exponent	$\lambda = 0.457$
gas: Corey curve (1954) $k_{rg} = \left(1-\hat{S}\right)^2\left(1-\hat{S}^2\right)$	$\hat{S} = \dfrac{(S_l - S_{lr})}{(1 - S_{lr} - S_{gr})}$
irreducible gas saturation	$S_{gr} = 0.05$
Capillary pressure	
van Genuchten function (1980)	

$P_{cap} = -P_0 \left(\left[S^* \right]^{-1/\lambda} - 1 \right)^{1-\lambda}$	$S^* = (S_l - S_{lr})/(1 - S_{lr})$
irreducible water saturation	$S_{lr} = 0.0$
exponent	$\lambda = 0.457$
strength coefficient	$P_0 = 19.61$ kPa

Table A.2 Initial conditions and injection specifications

Pressure	120 bar
Temperature	45˚C
Salinity	15 wt.-% NaCl
CO_2 injection rate	100 kg/s

Appendix B: Code Intercomparison Problem 4: CO2 Discharge Along a Fault Zone[*]

1. INTRODUCTION AND GENERAL DESCRIPTION

This problem explores CO2 loss from storage through a leaky fault, using a highly simplified 1-D linear flow geometry. It is envisioned that an aquifer into which CO2 disposal is made is intersected by a vertical fault, which establishes a connection through an otherwise impermeable caprock to another aquifer 500 m above the storage aquifer (Fig. B.1a). This situation is idealized by assuming 1-D flow geometry and constant pressure boundary conditions as shown in Fig. B.1b (Pruess and García, 2000).

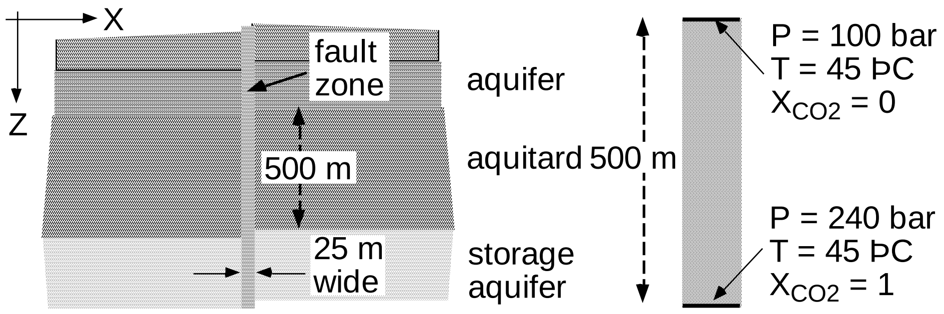

(a) (b)

Figure B.1 Schematic of the fault zone model (a) and applied boundary conditions (b).

2. LIST OF PROCESSES BEING STUDIED

Immiscible displacement of water by CO2 subject to pressure, gravity, and capillary pressure effects.

Change of fluid density, viscosity, and CO2 solubility with pressure.

Formation dry-out.

3. DEFINITION OF THE PROBLEM AND INPUT DATA

Hydrogeologic parameters are identical to those of problem 3 (Table A.1), except that porosity is increased to 35 %. The fault zone is assumed to be 25 m wide and 500 m tall, with boundary conditions as given in Fig. B.1b. The reservoir fluid is assumed to be pure water (no salinity). Initial conditions are pressures in hydrostatic equilibrium relative to P = 100 bar at the top; temperature is held constant at T = 45 ˚C throughout.

---

[*] proposed by Karsten Pruess; e-mail: K_Pruess@lbl.gov

4. PROBLEM VARIATIONS

Include salinity of the aqueous phase and permeability changes due to precipitation. Include non-isothermal effects. Assume gas composition is 50 % CO2, 50 % N2.

5. DEFINITION OF RESULTS TO BE CALCULATED

Data on CO2 and water density and viscosity, and CO2 solubility, for the range of thermodynamic conditions encountered in the problem. Vertical profiles of gas saturation, fluid pressure, and dissolved CO2 mass fraction at different times. CO2 inventory in gas and liquid phases after 10^7 seconds. Mass flow rates of CO2 at the bottom and of water at the top vs. time (normalized for a 1 m thick section).

6. COMPARISON CRITERIA

Results should match to with +/- 5 %.

7. REFERENCES

Pruess, K. and J. García. Multiphase Flow Dynamics During CO2 Injection into Saline Aquifers, *Environmental Geology,* Vol. 42, pp. 282 - 295, 2002.

APPENDIX C: Code Intercomparison Problem 7: CO_2 Injection into a 2-D Layered Brine Formation[#]

1. INTRODUCTION AND GENERAL DESCRIPTION

This test problem is patterned after the CO_2 injection project at the Sleipner Vest field in the Norwegian sector of the North Sea, and is intended to investigate the dominant physical processes associated with the injection of supercritical CO_2 into a layered medium. Significant simplifications have been made, the most important of which is the assumption of isothermal conditions (37 ˚C, the ambient temperature of the formation). CO_2 injection rates (1,000,000 tonnes per year), system geometry, and system permeabilities correspond approximately to those at Sleipner, although no attempt was made to represent details of the permeability structure within the host formation. Injection of the supercritical CO_2, which is less dense than the saline formation waters into which it is injected, causes it to rise through the formation. Its rate of ascent, however, is limited by the presence of four relatively low permeability shales. The top and bottom of the formation is assumed to be impermeable. The only reactive chemistry considered in this problem is the dissolution of CO_2 in the aqueous phase.

2. LIST OF PROCESSES BEING STUDIED

a) Gravity-driven advection in response to strong vertical and lateral density gradients induced by the injection of CO_2 into saline formation water.

b) Density, viscosity, and solubility formulations of water and CO_2 as a function of pressure and temperature (P and T).

3. DEFINITION OF THE PROBLEM AND INPUT DATA

System Geometry:

The system is idealized as a two dimensional symmetric domain perpendicular to the horizontal injection well which has a screen length of 100 meters (Figure C.1). A one meter thick section perpendicular to the horizontal well is considered. The thickness of the formation at the injection site is 184 meters. The injection point is 940 meters below the sea floor, while the ocean depth at the site is 80 meters. The formation is assumed to consist of four lower permeability shale units 3 meters thick which are distributed within the high permeability sand. Each shale unit is separated by 30 meters. The well is 30 meters below the lowest shale unit, while the bottom of the aquifer is another 22 meters below the well.

[#] proposed by Carl Steefel; e-mail: CISteefel@lbl.gov

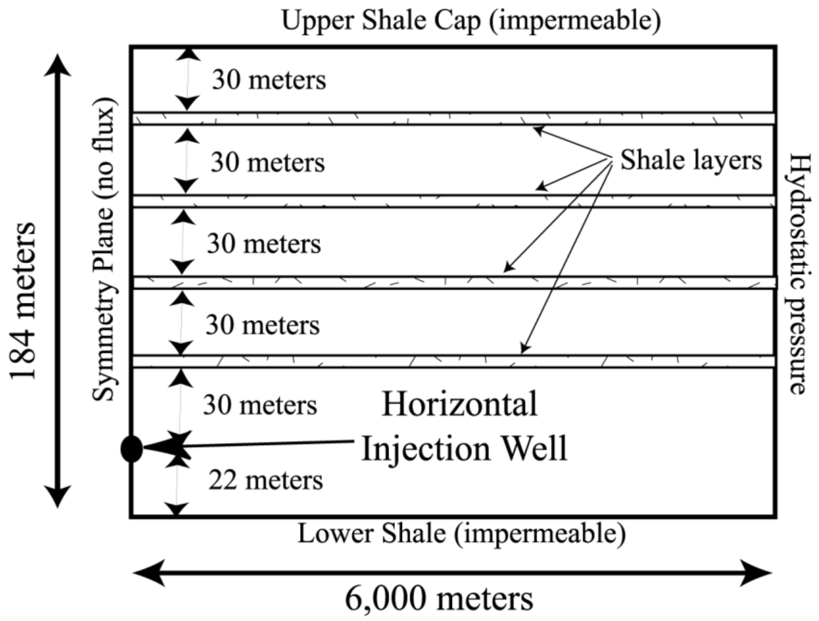

Figure C.1 Schematic representation of geometry for CO2 injection in Utsira Formation.

Boundary conditions:

No heat or mass flux is allowed across any of the boundaries except the vertical boundary 6,000 meters from the injection well. This boundary is fixed at hydrostatic pressure, thus allowing flow into and out of the domain so as to avoid overpressuring the formation. The 6,000 meter boundary is chosen, however, to be far enough from the injection well that the CO_2 does not reach this boundary after 2 years of injection.

Initial conditions (Table C.1):

a) T = 37˚C (isothermal throughout)

b) P = hydrostatic (approximately 110 bars at injection point, approximately 90 bars at top of formation).

c) CO_2 in the aqueous phase in equilibrium with a P_{CO2} of 0.5 bars, a typical value for sedimentary formation waters at the temperature we are considering.

Table C.1 Initial conditions and injection specifications

Pressure at well	110 bar
Temperature	37˚C
Salinity	3.2 wt.-% NaCl
CO2 injection rate	0.1585 kg/s in half space

Injection specifications (Table C.1):

a) Temperature = 37˚C

b) Injection rate: 31.7 kg/s over entire screen length (100 meters), corresponding to 0.317 kg/s for the 1 meter thick section considered. Because of symmetry, injection rate in half space is therefore 0.1585 kg/s.

c) Height of well cell: 1 meter.

d) Injection time scale: 2 years

Input data (Table C.2):

a) Capillary pressure and liquid relative permeability described with van Genuchten (1980) functions; gas relative permeability after Corey (1954). Porosity is 35% for sands, 10.25 % for shales.

b) Fully saturated permeability ($k = 3 \times 10^{-12}$ m^2 in sand layers, $10^{-14} m^2$ in shales)

c) Density, viscosity, and solubility in water of CO_2 as functions of P and T (Span and Wagner, 1996).

d) Vapor-liquid equilibrium properties of water.

4. PROBLEM VARIATIONS

Include non-isothermal effects by making the CO_2 injection temperature equal to 65 ˚C.

5. RESULTS TO BE CALCULATED

Liquid and gas saturations as a function of space and time. CO_2 concentration in the aqueous phase as a function of space. Gas and liquid fluxes.

6. COMPARISON CRITERIA

Results should match within +/- 5%.

IMPORTANT NOTICE

A first version of this test problem had specified that gas relative permeability was to be calculated from a van Genuchten function. In a workshop held in October 2001 in Berkeley, participants in the code intercomparison project agreed to change this specification to using a Corey (1954) curve instead, with parameters as given in Table C.2. In two subsequently issued laboratory reports with results of the code intercomparison project (Pruess and García, 2002; Pruess et al., 2002), the original van Genuchten specifications were inadvertently retained, even though all simulations had used the altered (Corey, 1954) specifications.

Table C.2 Hydrogeologic parameters

Permeability Porosity Aquifer thickness	Sands: 3x10^{-12} m^2; Shales: $10^{-14}$$m^2$ Sands: $\phi = 0.35$; Shales: $\phi = 0.1025$ 184 m
Relative permeability	
liquid: van Genuchten function (1980) $k_{rl} = \sqrt{S^*}\left\{1-\left(1-\left[S^*\right]^{1/\lambda}\right)^{\lambda}\right\}^2$ irreducible water saturation exponent	$S^* = (S_l - S_{lr})/(1 - S_{lr})$ $S_{lr} = 0.20$ $\lambda = 0.400$
gas: Corey (1954) $k_{rg} = \left(1-\hat{S}\right)^2\left(1-\hat{S}^2\right)$ irreducible water saturation irreducible gas saturation	$\hat{S} = (S_l - S_{lr})/(1 - S_{lr} - S_{gr})$ $S_{lr} = 0.20$ $S_{gr} = 0.05$
Capillary pressure	
van Genuchten function (1980) $P_{cap} = -P_0\left([S^*]^{-1/\lambda} - 1\right)^{1-\lambda}$ irreducible water saturation exponent strength coefficient	$S^* = (S_l - S_{lr})/(1 - S_{lr})$ $S_{lr} = 0.20$ $\lambda = 0.400$ Sand: $P_0 = 3.58$ kPa; Shale: $P_0 = 62.0$ kPa

7. REFERENCES

Corey, A.T. The Interrelation Between Gas and Oil Relative Permeabilities, *Producers Monthly*, 38-41, November 1954.

Pruess, K. and J. García. Solutions of Test Problems for Disposal of CO2 in Saline Aquifers, Lawrence Berkeley National Laboratory Report LBNL-51812, December 2002.

Pruess, K., J. García, T. Kovscek, C. Oldenburg, J. Rutqvist, C. Steefel and T. Xu. Intercomparison of Numerical Simulation Codes for Geologic Disposal of CO2, Lawrence Berkeley National Laboratory Report LBNL-51813, Berkeley, CA 94720, December 2002.

van Genuchten, M.Th. A Closed-Form Equation for Predicting the Hydraulic Conductivity of Unsaturated Soils, *Soil Sci. Soc. Am. J.*, Vol. 44, pp. 892 - 898, 1980.

Span, R. and W. Wagner. A New Equation of State for Carbon Dioxide Covering the Fluid Region from the Triple-Point Temperature to 100 K at Pressures up to 800 MPa, *J. Phys. Chem. Ref. Data*, Vol. 25, No. 6, pp. 1509 - 1596, 1996.

Appendix D: Effective thermal conductivity as a function of rock, brine, and CO$_2$ thermal conductivities

Standard TOUGH2 calculates the thermal conductivity of a grid block as a function of material type and liquid saturation. The parameters CWET and CDRY in the ROCKS block represent the thermal conductivity of a rock fully saturated with wetting phase or non-wetting phase, respectively. The parameter MOP(10) controls the dependence of grid-block thermal conductivity on liquid saturation, which varies with the square root (MOP(10) = 0) or linearly (MOP(10) = 1). For most fluid combinations available in TOUGH2 EOS modules, the wetting phase is a liquid and the non-wetting phase is a gas, with thermal conductivities of the rock and the liquid much larger than that of the gas. The square-root dependence on liquid saturation is the default, and it yields a slower decline in thermal conductivity as liquid saturation decreases, reflecting the notion that as liquid saturation decreases, the wetting phase remains preferentially in pore throats, providing a connected network of high-conductivity material for heat transfer.

For many fluids, including water, brine, steam, and air, assuming constant thermal conductivities for the wetting and non-wetting fluids is a good approximation. However for ECO2N, the thermal conductivity of CO$_2$ varies greatly, since CO$_2$ may exist as a gas, a liquid, or in a supercritical state. Therefore, a new thermal conductivity subroutine THCOND has been written to incorporate this variation in TOUGH2. In order to use it, the call to subroutine THCOND must be added to the subroutine MULTI where the thermal conductivity at an interface between two grid blocks is calculated, as shown below. Subroutine MULTI is found in the source file t2fm.f. Existing code is shown in normal type and the new code is shown in italics.

```
C
      IF(MOP(10).NE.0) GOTO 22
      S1X=MAX(S1,0.)
      S2X=MAX(S2,0.)
          CON1=CDRY(NMAT1)+SQRT(S1X)*(CWET(NMAT1)-CDRY(NMAT1))
          CON2=CDRY(NMAT2)+SQRT(S2X)*(CWET(NMAT2)-CDRY(NMAT2))
      GOTO23
C
   22 CONTINUE
          CON1=CDRY(NMAT1)+S1*(CWET(NMAT1)-CDRY(NMAT1))
          CON2=CDRY(NMAT2)+S2*(CWET(NMAT2)-CDRY(NMAT2))
   23 CONTINUE
ccd..thermal cond
      if(eosn(1).EQ.'ECO2N     ')
     X CALL THCOND(N1LM2,N2LM2,NMAT1,NMAT2,PHI1,PHI2,PRES1,PRES2,CON1,
     X CON2)
ccd..end
      DCONI=WT1*CON1+WT2*CON2
      CONI=0.
      IF(DCONI.NE.0.) CONI=CON1*CON2/DCONI
```

```
      IF(D1.EQ.0.) CONI=CON2
      IF(D2.EQ.0.) CONI=CON1
C
```

Then the file thcondsubs.f must be compiled and linked along with the rest of the TOUGH2 source code. Input parameters to subroutine THCOND identify the locations of grid-block parameters in the PAR array (N1LM2, N2LM2), materials (NMAT1, NMAT2), porosities (PHI1, PHI2), and pressures (PRES1, PRES2) for the two grid blocks making up the connection. Output parameters are the thermal conductivities of the two grid blocks, CON1 and CON2. Common blocks for the PAR array and ROCK block properties CWET and CDRY are also passed to the subroutine.

The SELEC block parameter IE(10) controls how the thermal conductivity calculation is done.

IE(10) = 0	Do nothing (code uses CON1 and CON2 calculated in MULTI using CWET and CDRY from ROCKS block, where CWET is thermal conductivity of rock saturated with brine, and CDRY is thermal conductivity of rock saturated with CO_2). This choice is equivalent to not calling Subroutine THCOND.
IE(10) = 1	Calculate CON1 and CON2 from rock, brine, and CO_2 conductivities using effective medium theory (read rock thermal conductivity in CWET and pore shape factor in CDRY; code calculates brine and CO_2 thermal conductivities internally – details below)
IE(10) = 2	Calculate CON1 and CON2 using CWET and CDRY from ROCKS block and FE(11+m-1) from SELEC block, where CWET is thermal conductivity of rock saturated with brine, CDRY is thermal conductivity of rock saturated with gaseous CO_2, and FE(11+m-1) is thermal conductivity of material m saturated with liquid CO_2. CO_2 thermal conductivity is then linearly scaled between CDRY and FE(11+m-1) according to CO_2 density of grid block (details below).

Using IE(10) = 1 may add noticeably to the CPU time required for a given TOUGH problem, as many calculations must be done to calculate effective thermal conductivity for each grid block. For some 1D test problems, using IE(10) = 1 required 30% more CPU time than using IE(10) = 0 or IE(10) = 2.

IE(10)=1 Calculate grid-block thermal conductivity from rock, brine, and CO_2 conductivities using the effective medium theory of Zimmerman (1989)

An algorithm developed by Zimmerman (1989) is used to calculate the effective thermal conductivity of rock saturated with a single phase fluid, given the thermal conductivities of the rock and the fluid, the porosity, and a shape factor α that describes the shape of the pores. This algorithm is used to calculate the effective thermal conductivity of brine-saturated rock and the effective thermal conductivity of CO_2-saturated rock. The rock thermal conductivity, K_s, is input via the CWET parameter in the ROCKS block. If solid salt is present, porosity is reduced accordingly, and the salt is assumed to have the same thermal conductivity as the rock. Table D.1 provides typical thermal conductivity values for various rocks, along with thermal conductivity values for a selection of fluids, for comparison. The α parameter is input via the CDRY parameter in the ROCKS block. It is dimensionless and formally lies in the range:

$0 < \alpha < 1$	pores are oblate spheroids (penny-shaped cracks as $\alpha \rightarrow 0$)
$\alpha = 1$	pores are spherical
$\alpha > 1$	pores are prolate spheroids (needle shaped cracks as $\alpha \rightarrow \infty$)

In practice, the range of α that has a significant effect on the effective thermal conductivity is $0.0001 < \alpha < 1$, with most of the variability occurring for $0.001 < \alpha < 0.5$. Do not specify α exactly equal to zero, because this will cause CWET to be used for α. Figure D.1 shows the effective thermal conductivity K_{eff} versus porosity ϕ for a CO_2-saturated rock with K_s = 6 W/(m K), and K_{CO2} = 0.1 W/(m K), for a range of α values. Also shown is the weighted geometric mean of K_s and K_{CO2}, which is given by

$$K_{eff} = K_s^{(1-\phi)} K_{CO2}^{\phi} , \quad (D.1)$$

and is invoked for IE(10)=1 by setting $\alpha < 0$. Zimmerman (1989) notes that of all the ways of combining K_s and K_{CO2}, the maximum K_{eff} is obtained from the weighted arithmetic mean and the minimum K_{eff} is obtained from the weighted harmonic mean – these are also shown in Figure D.1, along with more stringent limits derived by Hashin and Shtrikman (1962), which provide bounds for the K_{eff} values calculated using Zimmerman's algorithm.

Table D.1. Typical thermal conductivities of selected rocks and fluids.

Material	Thermal conductivity, W/(m K)	Reference
Rocks or Minerals (for IE(10) = 1)		
Quartz	7.6 8.4 6.2 - 10.4	Railsback, 2011 Zimmerman, 1989 Kappelmeyer and Haenel, 1974
Quartzite	3.5 – 6.0	Railsback, 2011
Halite/Salt	5.9 4.4 - 5.7 5.2 – 6.9	DeMarsily, 1986 Kappelmeyer and Haenel, 1974 Railsback, 2011
Granite	2.5 – 3.8 3.0 – 3.4 1.7 - 4	DeMarsily, 1986 Zimmerman, 1989 Engineering Toolbox, 2015
Illite and smectite	1.8	Railsback, 2011
Feldspars	1.9 – 2.4	Railsback, 2011
Calcite	3.2 - 3.7	Kappelmeyer and Haenel, 1974
Olivine	5.1	Kappelmeyer and Haenel, 1974
Basalt	1.3 – 2.8	Kappelmeyer and Haenel, 1974
Fluid-Saturated Rocks (for IE(10)=2)		
Dry sand (air + rock)	0.15 – 0.25 0.4 – 0.8	Engineering Toolbox, 2015 DeMarsily, 1986
Wet sand (water + rock)	2.5 – 3.5 2 – 4	DeMarsily, 1986 Engineering Toolbox, 2015

Dry clay (air + rock)	0.15 0.8 – 2.0	Engineering Toolbox, 2015 DeMarsily, 1986
Wet clay (water + rock)	1.2 – 1.7 0.6 – 2.5	DeMarsily, 1986 Engineering Toolbox, 2015
Dry welded tuff (air + rock)	1.2 – 1.4	Birkholzer and Mukhopadhyay, 2004
Wet welded tuff (water + rock)	1.7 – 2.1	Birkholzer and Mukhopadhyay, 2004
Dry soil	0.33	Engineering Toolbox, 2015
Wet soil	0.6 - 4	Engineering Toolbox, 2015
Fluids		
Liquid water	0.54 – 0.72	Powell, 1958
Steam	0.016 – 0.019	Engineering Toolbox, 2015
Air	0.026	Zimmerman, 1989
CO_2	0.018 – 0.14	Scalabrin et al., 2006
CH_4	0.030	Engineering Toolbox, 2015

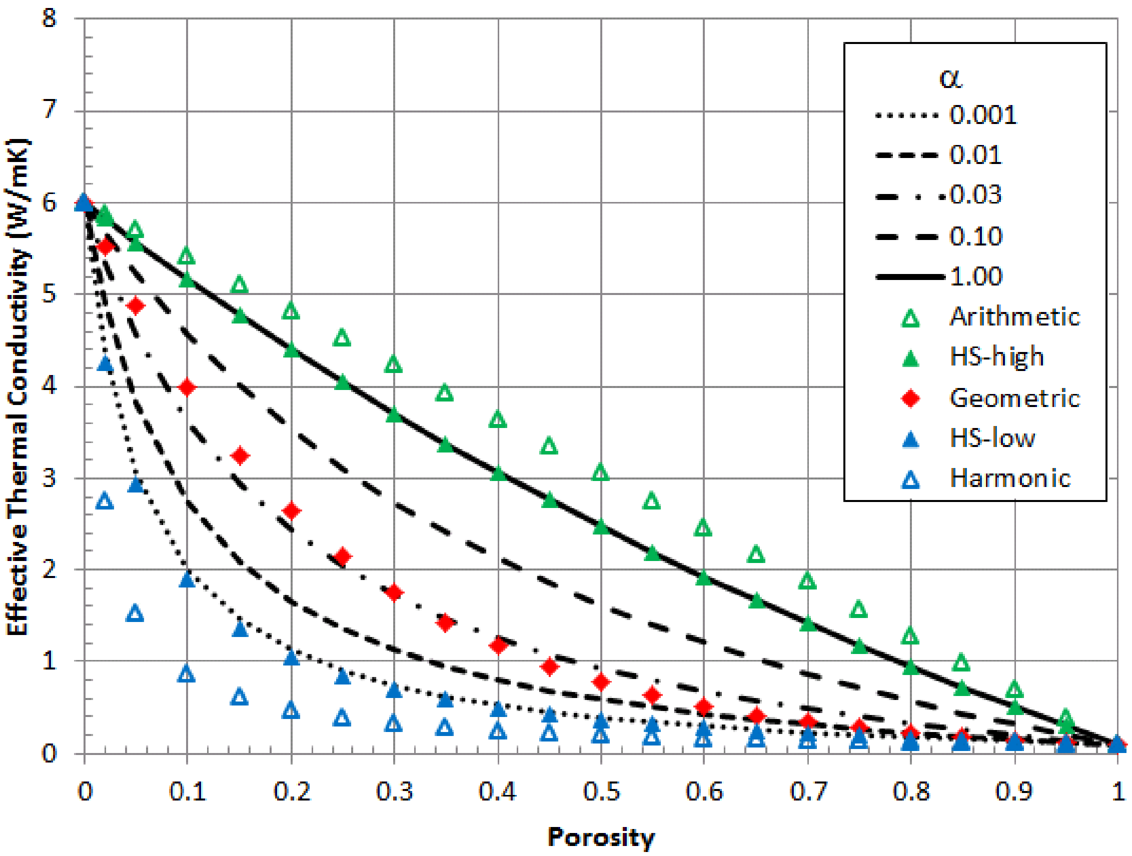

Figure D.1. Effective thermal conductivity of CO_2-saturated rock versus porosity, calculated from the algorithm of Zimmerman (1989), for a range of α values (lines), invoked by setting IE(10) = 1. Shown as symbols are various ways of calculating K_{eff} without explicitly describing the shape of the pores: arithmetic, harmonic, and geometric means, and the Hashin and Shtrikman (HS, 1962) low and high limits, which bound the values of K_{eff} calculated for various α values.

The code calculates brine thermal conductivity K_b as a function of temperature T, pressure P, and salt mass fraction X_s, fitting curves to a compilation of experimental data (Powell, 1958) for fresh water thermal conductivity K_{fw} for $0 \le T \le 370^oC$, $1 \le P \le 400$ atm, then applying a salinity correction (Sharqawy, 2013), derived for $0.05 \le X_s \le 0.2$. The biggest variation in K_b is due to temperature, and for baseline pressure P_0 (1 atm for $T \le 100^oC$; saturation pressure for $T > 100^oC$), the temperature dependence of Powell's fresh water data can be well fit for $10 \le T \le 300^oC$ with a quadratic form:

$$K_{fw}(T) = 0.568 + 1.69E\text{-}3\ T - 6.00E\text{-}6\ T^2, \quad (D.2)$$

where T is in degrees C. Then a pressure correction is applied for pressures in the range 100 – 400 atm. The pressure correction is constant for $T \le 150^oC$, but varies with T^2 for $T > 150^oC$:

$$K_{fw}(T,P) = (0.568 + 1.69E\text{-}3\ T - 6.00E\text{-}6\ T^2)\{\ 1 + 1.1E\text{-}9(\ P - P_0)$$
$$(1 + [\max(0,(T - 150))/103]^2)\ \}, \qquad (D.3)$$

where T is in degrees C and P is in Pa. K_{fw} obtained from this equation is compared to Powell's data in Figure D.2. The fit is good for $10 \leq T \leq 300^{o}C$.

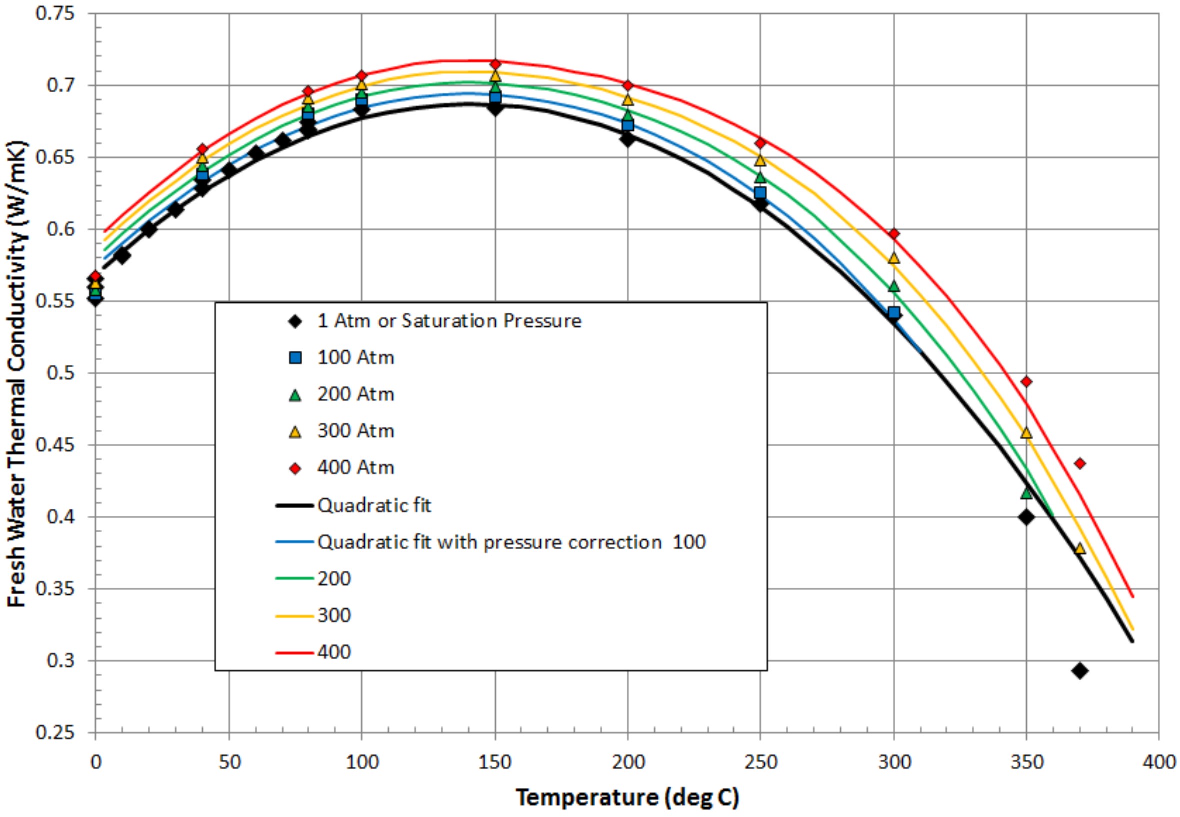

Figure D.2. Fresh water thermal conductivity versus temperature for a range of pressures; symbols are experimental data compiled by Powell (1958) and lines are fitting functions given by Equations (D.2) and (D.3). Used when IE(10) = 1.

Sharqawy's salinity correction is

$$K_b = K_{fw}\ (1 + 0.22{*}X_s) \qquad (D.4)$$

based on data in the range $0 < T < 90^{o}C$ and P = 1 atm. Figure D.3 shows K_b from Equation (D.4), using K_{fw} from Equation (D.2) with $P = P_0$. Although the salinity correction was derived for a limited (T,P) range, Equation (D.4) is applied throughout the (T,P) range of ECO2N V2.0. Because the dependence of K_b on X_s is small, this approximation is expected to be reasonable. Note that the effect of CO_2 dissolved in the aqueous phase on K_b is not considered, but it is also expected to be small.

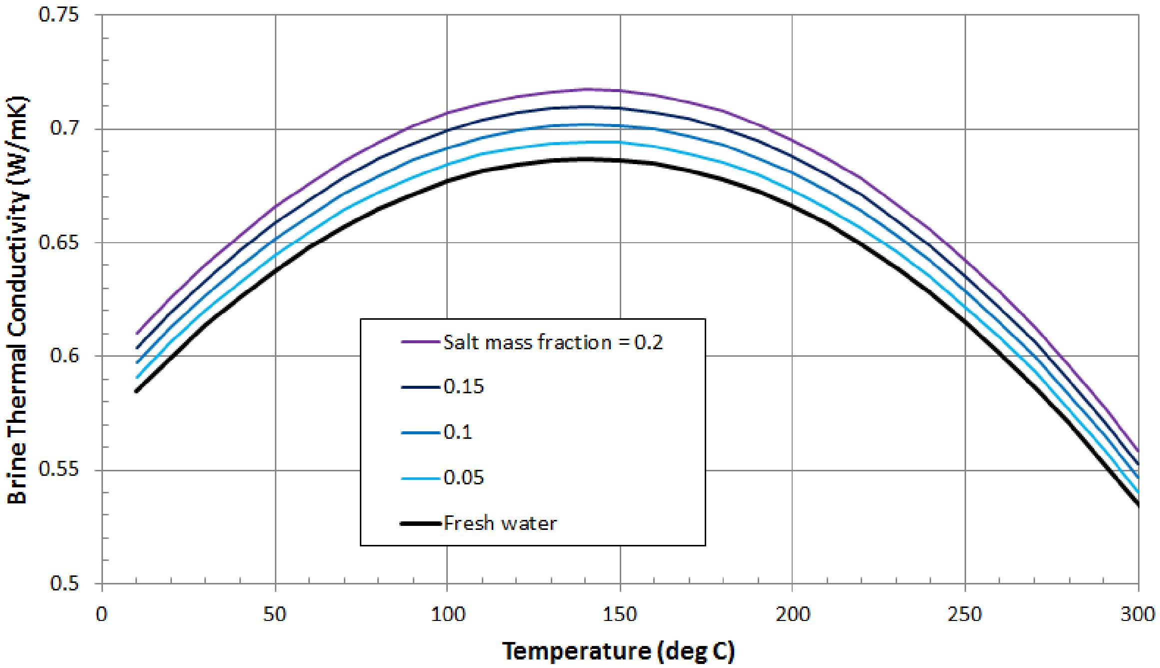

Figure D.3. Brine thermal conductivity versus temperature for baseline pressure P_0 and a range of salinities, calculated from Equations (D.2) and (D.4), used when IE(10) = 1.

The code calculates CO_2 thermal conductivity as a function of temperature and CO_2 density, based on a formulation by Scalabrin et al. (2006). The formulation covers the entire range of pressures and temperatures relevant for ECO2N V2.0, but there is a problem using it near the critical point ($T_c = 31^oC$, $P_c = 73.8$ bars), where the thermal conductivity increases dramatically. Scalabrin based his formulation on the density dependence of Span and Wagner (1996) rather than the Altunin (1975) dependence used in TOUGH2/ECO2N. The values of T_c and P_c are very similar for the two formulations, but the density at the critical point ρ_c differs significantly (ρ_c = 467.6 kg/m^3 for Scalabrin and 571.2 kg/m^3 for Altunin). Scalabrin includes a separate term in his equations for the near-critical-point enhancement, with expressions involving ($T - T_c$) and ($\rho - \rho_c$) in the denominator. If this term is implemented in TOUGH2 (where the density is calculated according Altunin), then the peak in thermal conductivity does not occur at P_c, as shown in Figure D.4, but at the pressure for which Altunin's correlations yield Span and Wagner's value of ρ_c. An attempt was made to modify Scalabrin's formulation by employing Altunin's value of ρ_c, but this was not successful. Instead, the near-critical-point enhancement term is simply omitted, leaving a thermal conductivity that smoothly increases with pressure as it crosses the critical point, as shown in Figure D.4. Figure D.5 compares this simplified expression with the full Scalabrin form, for the complete range of T and P of ECO2N V2.0. Note that only in a small region near the critical point do the two formulations produce different results. Because ECO2N simulations typically avoid the critical point, this approximation is expected to be useful for the majority of applications.

Note that the effect of water vapor incorporated into the CO_2-rich phase is not included in the calculation of CO_2 thermal conductivity. This is quite acceptable for temperatures below 100°C, given the small amount of water vapor present under those conditions, but needs to be evaluated for higher temperatures, where more water vapor exists. Generally, the thermal conductivity of water vapor (0.016 – 0.0188 W/(m K)) is similar to the thermal conductivity of gas-like CO_2 (Figure D.5), so the present approach of treating any water vapor present as CO_2 should be reasonable under those conditions.

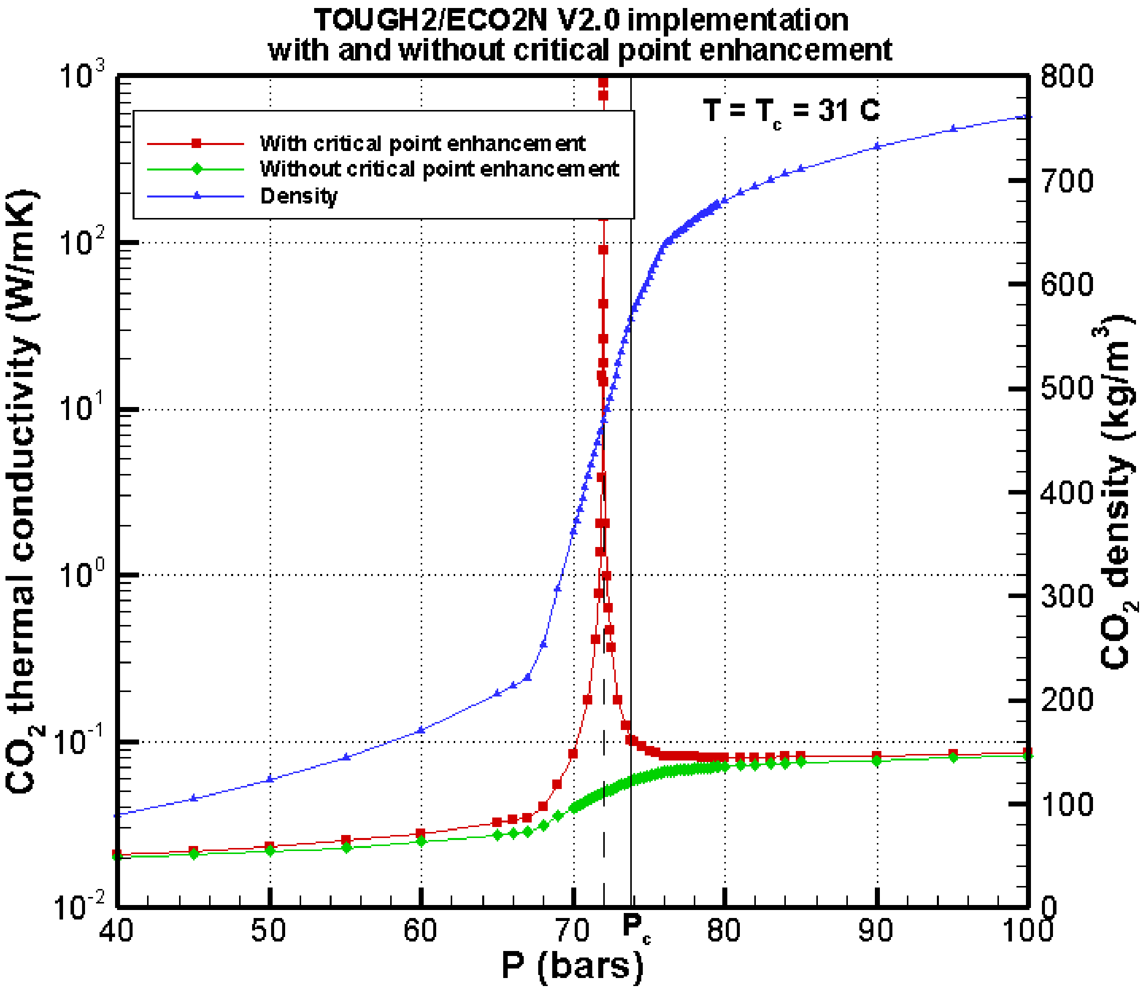

Figure D.4. TOUGH calculation of CO_2 thermal conductivity, for $T = T_c$ and a range of pressures on either side of critical pressure P_c, using the Scalabrin et al. (2006) formulation. If near-critical-point enhancement is included, a peak in thermal conductivity occurs at the wrong pressure (red symbols). Therefore, we omit this term, yielding a smoothly increasing thermal conductivity (green symbols), which is employed when IE(10) = 1. The density calculated by TOUGH using Altunin's correlations is also shown (blue symbols).

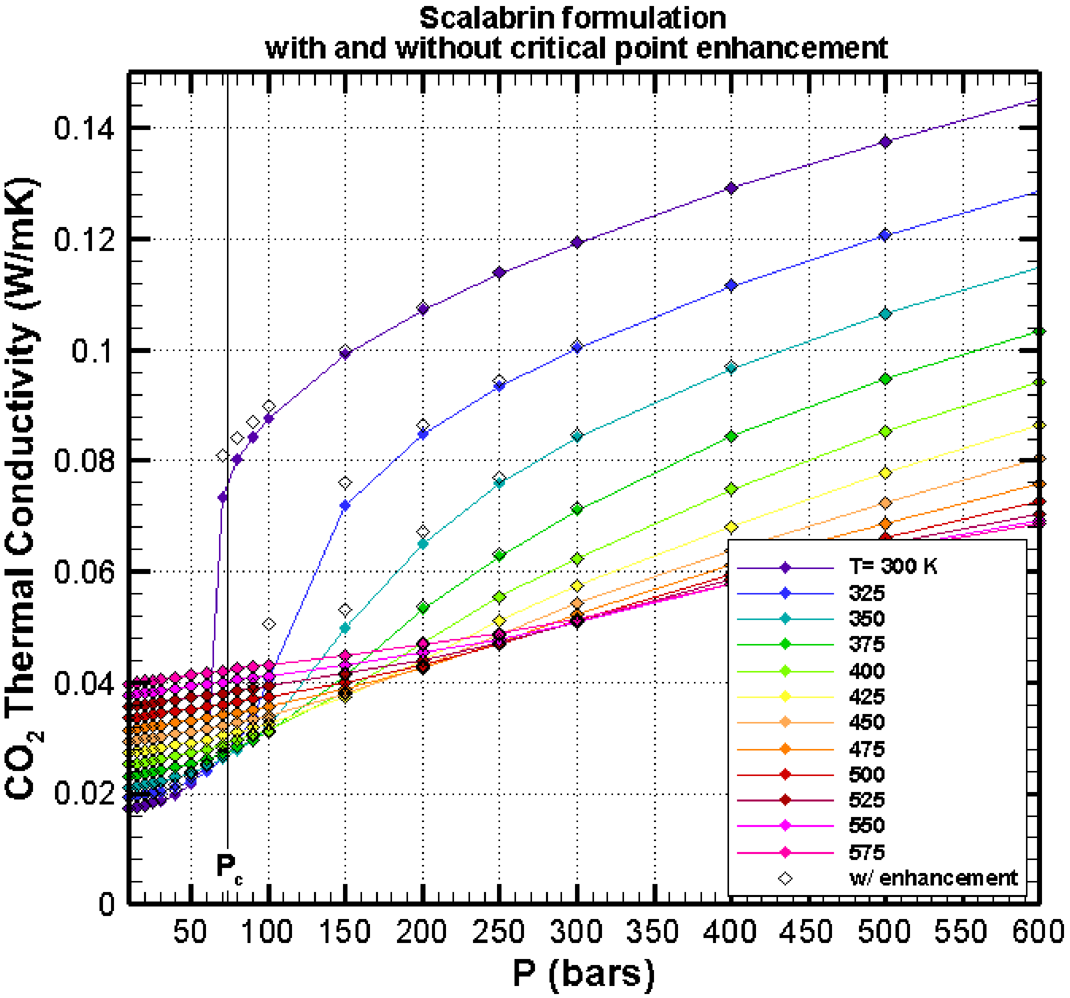

Figure D.5. CO_2 thermal conductivity as a function of temperature and pressure. Colored symbols show the Scalabrin formulation without the near-critical-point enhancement, as it is employed in TOUGH2 when IE(10)=1. The open symbols include the near-critical-point enhancement.

After the code calculates the effective thermal conductivities for brine-saturated rock and CO_2-saturated rock at the prevailing (T,P) conditions, as described above, it combines these terms using liquid saturation to determine the effective thermal conductivity of the grid block, using the usual algorithm (square root or linear dependence) based on MOP(10).

IE(10)=2 Calculate grid-block thermal conductivity using a simple approximation for CDRY

As a simpler alternative to IE(10) = 1, we provide the option to retain the usual meaning of CWET and CDRY as representing fluid-saturated rock, but enable the conductivity of CO_2-saturated rock to be a variable, reflecting the wide range of properties CO_2 can take. Specifically, for material number m, the code uses CWET from the ROCKS block as in standard TOUGH2 to represent the thermal conductivity of brine-saturated rock. The parameter CDRY is the thermal conductivity of gaseous (low density) CO_2-saturated rock, and the parameter FE(11 + m – 1) from the SELEC block is the thermal conductivity of liquid (high density) CO_2-saturated rock. The code calculates the thermal conductivity of CO_2-saturated rock, denoted CDRY1, as being linearly dependent on the CO_2 density ρ of the grid block, according to the equation

$$\text{CDRY1} = \text{CDRY} + [(\rho - \rho_g)/(\rho_l - \rho_g)]\ (\text{FE}(11 + m - 1) - \text{CDRY})$$

where $\rho_g = 0.73$ kg/m^3 and $\rho_l = 1116.94$ kg/m^3 are the minimum and maximum values of CO_2 density, respectively, for ECO2N V2.0 . If the FE(11 + m – 1) value for any material is left blank, then the CWET value for that material is used in its place. Remember to set IE(1), which identifies how many additional lines to read in the SELEC block, to a large enough number to accommodate FE(11 + m – 1) values for all material types. For example, if there are 10 materials, FE(11) through FE(20) will be used. FE(11) - FE(16) are on the second additional SELEC line, and FE(17) - FE(20) are on the third additional SELEC line, so IE(1) = 3.

The code then combines CWET and CDRY1 using liquid saturation to determine the effective thermal conductivity of the grid block, using the usual algorithm (square root or linear dependence) based on MOP(10).

Some typical values of CWET and CDRY are provided in Table D.1. Although the non-wetting fluid is air rather than CO_2 in the table entries, the thermal conductivities of air and gas-like CO_2 are similar, making these CDRY values a reasonable starting point for using IE(10) = 2.

References

Altunin, V.V. *Thermophysical properties of carbon dioxide*, Publishing House of Standards, 551 pp., Moscow, 1975 (in Russian).

Birkholzer, J.T. and S. Mukhopadhyay, Drift-scale coupled processes (DST and THC seepage) models, Report to USDOE/OCRWM, doi:10.2172/837686, 2004.

DeMarsily, G., *Quantitative Hydrogeology*, Academic Press, 1986.

Engineering Toolbox, Thermal conductivities of some common materials and gases, www.EngineeringToolbox.com, 2015.

Hashin, Z. and H. Shtrikman, A variational approach to the theory of the effective magnetic permeability of multiphase materials, *J. Appl. Phys*., 33, 3125-3131, 1962.

Kappelmeyer, O. and R. Haenel, *Geothermics with special reference to application*, Geopublication Associates, Berlin, 1974.

Powell, R.W., Thermal conductivities and expansion coefficients of water and ice, *Advances in Physics*, 7(26), 276-297, 1958.

Railsback, L.B., Heat flow, geothermal gradient, and the thermal conductivity of sedimentary rocks, Petroleum geoscience and subsurface geology website, Department of Geology, University of Georgia, 2011.

Scalabrin, G., P. Marchi, F. Finezzo, and R. Span, A reference multiparameter thermal conductivity equation for carbon dioxide with an optimized functional form, *J. Phys. Chem. Ref. Data*., 35(4), 1549-1575, 2006.

Span, R. and W.Wagner, A new equation of state for carbon dioxide covering the fluid region from the triple-point temperature to 1100 K at pressures up to 800 MPa, *J. Phys. Chem. Ref. Data*., 25(6), 1509-1596, 1996.

Sharqawy, M.H., New correlations for seawater and pure water thermal conductivity at different temperatures and salinities, *Desalination*, 313, 97-104, 2013.

Zimmerman, R.W., Thermal conductivity of fluid saturated rocks, *J. of Petroleum Sci. and Eng*., 3, 219-227, 1989.